

**IN RE: OIL SPILL BY THE OIL RIG "DEEPWATER HORIZON" IN
THE GULF OF MEXICO, ON APRIL 20, 2010**

UNITED STATES DISTRICT COURT
EASTERN DISTRICT OF LOUISIANA
MDL NO. 2179, SECTION J
JUDGE BARBIER; MAGISTRATE JUDGE SHUSHAN

**Expert Report of
Michael Zaldivar, PhD**

Quantification of Flow Rate during Slug Flow

May 1, 2013

11683
Exhibit No. _____
Worldwide Court Reporters, Inc.

CONFIDENTIAL

XMZX411-000001

TREX 011683.0001

[This page intentionally left blank]

Contents

1	Introduction	5
2	Qualifications	6
3	Background	7
4	Executive Summary.....	9
5	Overview of Multiphase Flow and Slugging.....	11
5.1	Multiphase Flow Patterns	11
5.2	Slug Flow	13
5.3	Multiphase Flow Modeling.....	13
6	Analysis	15
6.1	Determination of Flow Pattern	15
6.2	Characterizing Slugging Behavior.....	16
6.3	Link to Riser Motion	17
6.4	Slug Mechanism	17
6.5	Timing of Kink Leaks	22
7	Modeling	26
8	Results	29
8.1	Riser End Flow Rate.....	29
8.2	Kink Leak Flow Rate.....	30
8.3	Sensitivities.....	30
8.4	Other Work.....	31
9	Summary and Conclusions	32

Table of Figures

Figure 1 – Diagram of the DWH riser at the Macondo well site.....	7
Figure 2 – Light and dark colored fluid discharged from Riser End.....	7
Figure 3 – Two holes on the Kink on April 28 (left) and three holes on the Kink on May 19 (right)	8
Figure 4 – Diagram of horizontal flow patterns.....	12
Figure 5 – Diagram of vertical flow patterns	12
Figure 6 – Illustration of tendencies of gas and liquid in multiphase flow in upward and downward inclined pipes.....	13
Figure 7 – Video capture of different colored fluids being discharged from the Riser End (arrow indicates trajectory)	15
Figure 8 – Intensity (brightness) chart of a portion of the video of discharge at Riser End	17
Figure 9 – Progression of riser position with time.....	18
Figure 10 – Oil accumulating in the upstream section of the buoyant loop at its highest position in cycle	18
Figure 11 – Weight of the oil slug causes the buoyant loop to sink.....	19
Figure 12 – Oil slug passes through the buoyant loop in its settled position.....	19
Figure 13 – Stratified flow establishes behind the oil slug.....	20
Figure 14 – Buoyant loop begins moving up	20
Figure 15 – Illustration of angles variations of a hill.....	21
Figure 16 – The second oil slug formed on May 13 due to the steep inclinations.....	22
Figure 17 – Riser Kink annotated with labels for each hole in riser	23
Figure 18 – Kink on May 16 showing only holes B and C leaking.	24
Figure 19 – Kink on May 19 showing only holes B, C and E leaking.	24
Figure 20 – Schematic of the riser showing model boundaries for the no kink model ...	27
Figure 21 – Schematic of the riser showing model boundaries for the kink model.....	27



1 Introduction

This report has been prepared by Dr. Michael Zaldivar, principal at evoleap, LLC (evoleap). BP retained evoleap to provide expert opinions in connection with the *Deepwater Horizon* (DWH) drilling rig incident on April 20, 2010. Specifically I was asked evaluate whether a flow pattern, known as “slug flow”, occurred from May 13 to May 20, 2010, and if it did, what conclusions could be drawn about the flow rate during that period.

Slug flow describes a flow pattern of alternating flows of gas and oil. There is robust video evidence of this alternating flow pattern during this period. This report details the analysis that I used to conclude that the flow pattern during May 13 to May 20, 2010 was slug flow. Further, this report provides my analysis of the flow rates associated with the slug flow during the period from May 13 to 20, 2010.

2 Qualifications

I graduated with a Bachelor of Science in Chemical Engineering from the University of Houston in 1997, and a Master of Science and Doctorate in Chemical Engineering from the University of Michigan in 2002.

I started my career in the oil and gas industry in 2002 with Multiphase Solutions Inc. (MSi)¹ as a flow assurance engineer performing multiphase thermo-hydraulic simulations using OLGA, a multiphase flow simulation tool commonly used for the design and operation of subsea pipelines. After several years with MSi, I transitioned within MSi to developing and building production management systems. These systems, often referred to as online Flow Assurance systems, attach thermo-hydraulic models to field data to advise operations with respect to Flow Assurance issues.

More recently, at Kongsberg Oil & Gas Technology (Kongsberg), I managed the Americas operations of the LedaFlow business unit. LedaFlow, like OLGA, is a commercially-available flow simulator for multiphase pipelines. In that role, I led two teams: (a) a team responsible for the technical support and testing of LedaFlow and (b) a team responsible for further developing LedaFlow. Additionally during my time at Kongsberg, I served on the Technical Advisory Committee for LedaFlow and as Product Manager of LedaFlow.

During my career, I have investigated slug flow in numerous pipeline systems around the world. In engineering projects, I have studied many types of slug flow phenomena including terrain-induced, hydrodynamic, pigging and ramp-up slug flow. These studies focused on ensuring that pipelines being designed did not experience slugging during operations or, if slugging was unavoidable, that they had appropriate handling facilities. For online flow assurance systems, I have designed models and intelligent systems to interpret those model results in order to predict slugging and therefore provide an early warning of slugging to field operators. I have designed flow assurance systems in gas-condensate fields in the Asia-Pacific region and black oil fields in the Gulf of Mexico. More recently, in my role as LedaFlow Manager, I have supported many LedaFlow users building models to be used in slugging studies.

A list of my project experience is included in Appendix A.

¹ MSi has been renamed as MSi Kenny.

3 Background

After the DWH drilling rig sank on April 22, 2010, the riser that connected the DWH wellhead equipment to the drilling rig fell to the seafloor, and a kink formed just above the lower marine riser package (LMRP)². A diagram of the fallen DWH riser during the period relevant to this report (i.e., May 13 to May 20) is shown in Figure 1.

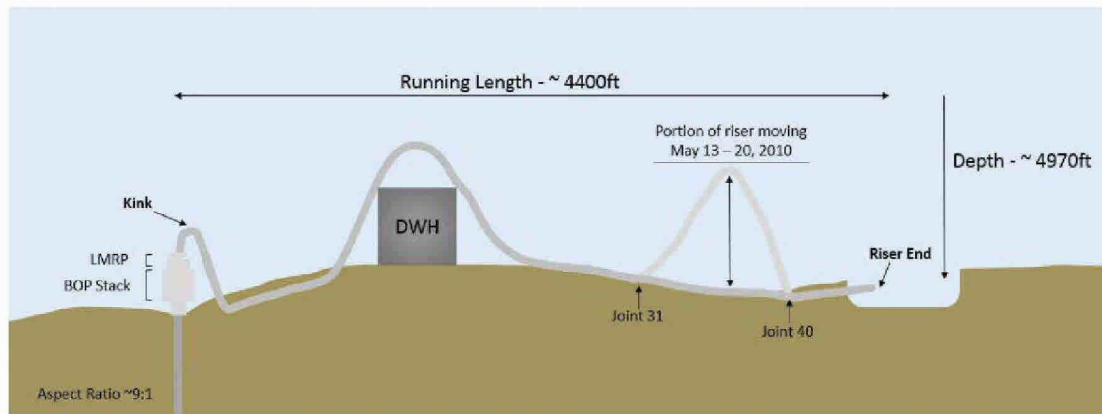


Figure 1 – Diagram of the DWH riser at the Macondo well site.

After the riser collapsed, oil and gas were released into the Gulf of Mexico from two main locations, the end of the riser (Riser End) and the kink that formed above the BOP/LMRP (Kink). From May 13 to May 20, the discharge at the Riser End was observed to repeatedly alternate between a dark-colored fluid and a light-colored fluid (shown in Figure 2).³



Figure 2 – Light and dark colored fluid discharged from Riser End

² BP-HZN-2179MDL04877807.

³ Deposition of Lars Herbst, Vol. 1, October 10, 2012, 208:20-211:11; MDL Dep. Ex. 9183, at p 66,68,140.

On April 28, 2010, two holes appeared on the Kink.⁴ On May 19, 2010, a third hole appeared on the Kink (shown in Figure 3).⁵



Figure 3 – Two holes on the Kink on April 28 (left) and three holes on the Kink on May 19 (right)

Remotely operated vehicles (ROVs) were used to perform various actions near the wellhead and spill site.⁶ Some of these ROVs were deployed to obtain video footage of the oil and gas plumes at various release points. As a result, there are a number of videos showing the plume of oil and gas released at the Riser End and at the Kink. Other ROVs were used to perform surveys of the fallen DWH riser. These riser surveys systematically recorded the spatial position of the riser. I relied upon ROV video footage from the DWH riser surveys as well as video footage of the oil and gas plumes at the Riser End in forming the conclusions presented in this report.

⁴ BP-HZN-2179MDL03676655.

⁵ SNL093-017659.

⁶ BP-HZN-2179MDL02172464.

4 Executive Summary

During the *Deepwater Horizon* response, United States government officials⁷ and members of the Flow Rate Technical Group Plume Team⁸ noted that in May 2010 there was slug flow at the end of the *Deepwater Horizon* riser. Slug flow is a pattern of flow that is characterized by alternate flows of liquid and gas. Slug flow is a common problem in the oil and gas industry and is studied during the design and operation of multiphase pipelines.

Based on a review and analysis of plume videos, there is clear evidence of slug flow, i.e., alternating oil-dominant flow (appearing as a dark, almost black, plume) and gas-dominant flow (appearing as a light, almost white, plume), from the end of the DWH riser. This phenomenon was observed between May 13 and May 20, 2010. If slug flow were not present, the plume would have appeared as a uniform mixture of oil and gas, as can be observed from ROV video footage after May 20, 2010.

Multiple riser inspections⁹ from ROV riser surveys also show that a part of the riser (the buoyant loop) was moving in a vertical oscillating motion, i.e., the buoyant loop was moving between resting on the sea floor and floating above the sea floor.

Relying on ROV video footage from May 16, the vertical oscillating motion of the riser can be linked to the slug flow that was observed at the Riser End. On this date, an ROV (XLX36) was tracking the motion of the riser as part of a riser survey, while at the same time another ROV (Milenium86) was monitoring the end of the plume. The May 16 plume video, together with the May 16 riser survey video, show that the riser motion and the observed slugging had the same period:¹⁰ 183 seconds. From this direct link and subsequent analysis, I concluded that the motion of the buoyant loop was the cause of the slug flow that was observed at the Riser End. Consequently, when the buoyant loop finally settled to the sea floor (i.e., ceased oscillating) on May 21, slug flow was no longer observed at the Riser End.

The characteristics of the slug flow at the Riser End changed over time; similarly, the period and range of motion of the riser also changed over time. This created a unique signature in the pattern of slug flow observed at the outlet. The signature of the slug flow, riser motion, and the flow through the riser are intricately linked. Knowing the signature and riser motion from the ROV footage, I was able to calculate the flow rate through the riser.

⁷ IMS172-037049; Deposition of Lars Herbst, Vol. 1, October 10, 2012, 208:20-211:11; Deposition of Adm. Thad Allen, Vol. 1, September 24, 2012, 330:23-333:10.

⁸ MDL Dep. Ex. 9183 at 10, 66, 68, 110, 135, 140, 145, 146, 150.

⁹ BP-HZN-2179MDL04996577.

¹⁰ The period is the duration of one cycle of the vertical oscillating motion of the riser.

Using LedaFlow, a commercially available software tool that simulates multiphase flow in pipelines and risers, I constructed a model of the riser with a moving buoyant loop that matched the oscillations observed on the ROV videos. Using this model, I varied the flow rate through the riser until the unique pattern of slug flow observed on the ROV videos was matched. This allowed me to calculate the flow rate at the Riser End. I used this same software to calculate a flow rate for the Kink leaks to arrive at a total daily flow rate for the period from May 13 to May 20, 2010.

By matching the unique signature of the observed slugging, I conclude that the flow rate through the Riser End could not have exceeded 31,000 stbpd (stock tank barrels per day). Additionally, I conclude that the maximum total flow rate (through the Kink leaks and Riser End) could not have exceeded 35,900 stbpd during the same period. The best calculated total flow rate for the Kink leaks and Riser End is 30,000 stbpd. The range of possible total flow rates for the Kink leaks and Riser End is between 24,900 stbpd and 35,900 stbpd.

5 Overview of Multiphase Flow and Slugging

Hydrocarbon reservoirs typically contain a fluid that is a mixture of various hydrocarbon compounds. The reservoir fluid exits the reservoir at high pressures and temperatures and gradually reduces in pressure and temperature as it transits to the surface. Eventually the fluid enters into a multiphase region where liquid and gas phases coexist.

In the oil and gas industry, multiphase flow is a term that indicates the presence of multiple phases (e.g., water, oil, gas) flowing through a pipeline. In the context of this work, the MC252 reservoir fluid is a two-phase fluid composed of hydrocarbon liquid (oil) and its associated gas phase.

5.1 Multiphase Flow Patterns

The simultaneous flow of gas and liquid in a pipe can be distributed in a wide variety of spatial configurations, usually referred to as flow patterns (or flow regimes). Key parameters used to determine flow patterns include:

- gas and liquid flow rates
- pipe diameter and angle of inclination
- fluid properties (such as gas and liquid volume fractions, density, viscosity, surface tension)

Figure 4 and Figure 5 show common flow patterns that are possible in gas-liquid two-phase systems for horizontal and vertical pipes.

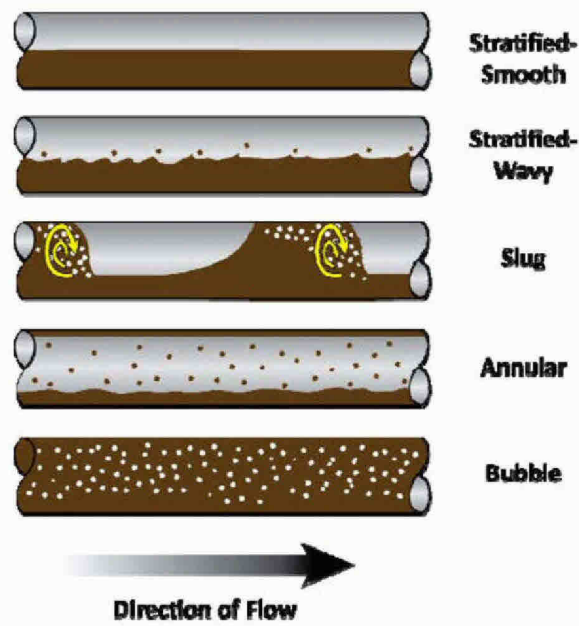


Figure 4 – Diagram of horizontal flow patterns¹¹

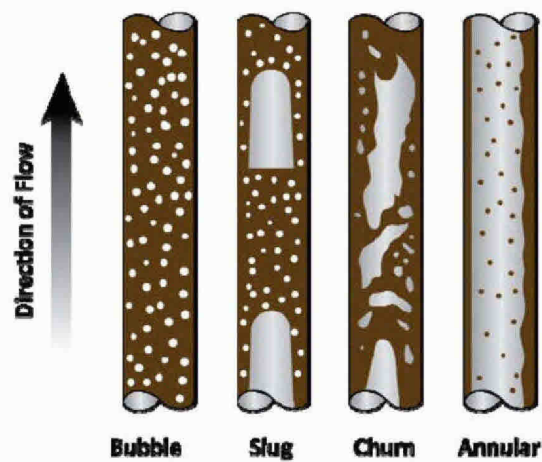


Figure 5 – Diagram of vertical flow patterns¹²

¹¹ The horizontal flow patterns presented are common flow patterns included in Shoham, O. (2006): Mechanistic Modeling of Gas-Liquid Two-Phase Flow in Pipes. Society of Petroleum Engineers.

¹² The vertical flow patterns presented are common flow patterns included in Shoham, O. (2006): Mechanistic Modeling of Gas-Liquid Two-Phase Flow in Pipes. Society of Petroleum Engineers.

The evolution of flow patterns shown in Figure 4 and Figure 5 is a complex phenomenon. For purposes of the analysis contained in this report, the following general principles are useful:

- in an upwardly inclined pipe, gas flows upward more readily than oil because it is the less dense phase
- conversely, in a downwardly inclined pipe, oil will naturally flow downward more readily than gas because it is the more dense phase
- depending on the angle of upward inclination of the pipe, gas will have to move proportionally faster in order to impart enough energy to the oil phase to move the oil up against the force of gravity

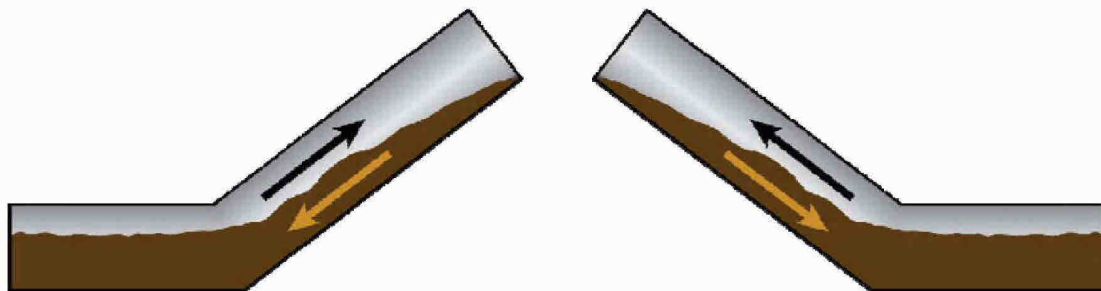


Figure 6 – Illustration of tendencies of gas and liquid in multiphase flow in upward and downward inclined pipes

5.2 Slug Flow

Slug flow is an intermittent multiphase flow pattern that is characterized by alternating flow of oil and gas. Slug Flow is a well-known phenomenon in the oil and gas industry, and has been studied for decades.¹³ Flow assurance engineers analyze the potential for slug flow in the design and operation of multiphase pipelines because it can have large negative effects on the operational efficiency of the receiving facilities. Through the use of modeling tools, like LedaFlow and OLGA, production pipelines and facilities are designed to avoid or mitigate slug flow.

When a pipeline is in slug flow, slugs of liquid (oil) are separated by predominantly gas pockets. In a horizontal or near horizontal pipeline, the liquid slug fills the entire cross-sectional area of the pipe, whereas the gas region has a stratified liquid layer (see Figure 4) flowing along the bottom of the pipe.¹⁴

5.3 Multiphase Flow Modeling

Several commercial software tools are available to analyze multiphase flow in pipelines. In this work, I used LedaFlow as the primary multiphase pipeline simulator. LedaFlow is

¹³ G.E. Alves, "Cocurrent Liquid-Gas Flow in a Pipeline Contractor," Chem. Eng. Progress, 50, pp 449-456, 1954.; G.W. Govier, and K. Aziz, "The Flow of Complex Mixtures in Pipes," Van Nostrand Reinhold, New York, 1972.

¹⁴ Shoham, O. (2006): Mechanistic Modeling of Gas-Liquid Two-Phase Flow in Pipes. Society of Petroleum Engineers.

a commercially available multiphase flow simulator from Kongsberg Oil & Gas Technologies. LedaFlow is a product that was developed through more than 10 years of collaboration between ConocoPhillips, Total and SINTEF. Apart from being a multiphase simulator, LedaFlow allows users to interact with running simulations via a programming interface. Using this interface, I was able to move the elevation of the buoyant loop during the simulations.

I used MultiFlash (a standard industry software program) to generate thermodynamic properties of fluids. Multiphase simulators need to calculate the properties of the fluid, such as density, at different temperature and pressure conditions. Using MultiFlash, I generated a PVT table¹⁵ of these properties and used that table as an input to LedaFlow.

OLGA was used as a benchmark for the LedaFlow models. OLGA is another multiphase pipeline simulator, and has been commercially available for over 30 years. However, OLGA was not able to incorporate the motion of the riser into the models. Therefore I only used OLGA as a point of comparison for the LedaFlow model predictions. For this comparison, I used a version of my model without the motion of the buoyant loop incorporated so that I could directly compare OLGA and LedaFlow results. The benchmarking cases and results are described in Appendix B.

More detailed descriptions of all of the commercial software tools that were used in this work are included in Appendix C.

¹⁵ A PVT table is a file that contains the required fluid properties necessary to perform pipeline simulations. A PVT table is generated by calculating the fluid properties such as viscosity, density, gas mass fraction, enthalpy, specific heat capacity, surface tension, and others over a range of pressures and temperatures which span the operating conditions of the riser.

6 Analysis

As part of this work, I reviewed documents and ROV videos. Appendix D has a list of all documents and materials I considered in forming my opinions and conclusions about the existence of slug flow at the Riser End from May 13 to May 20, 2010, and the associated flow rates during slugging.

6.1 Determination of Flow Pattern

I reviewed over 300 videos showing the plumes of oil and gas released at the Riser End. The earliest video that I reviewed was from April 22, 2010 and the latest video that I reviewed was from May 26, 2010. During May 13 to May 20, 2010, the discharge at the Riser End was observed to repeatedly alternate between a dark-colored fluid and a light-colored fluid (see Figure 7). The US Government’s FRTG Plume Team observed this same alternating pattern and found that it “confirms the ‘slug flow’ regime.”¹⁶



Figure 7 – Video capture of different colored fluids being discharged from the Riser End (arrow indicates trajectory)

I performed an independent evaluation of the ROV video footage to determine whether the observed alternating pattern of dark-colored fluid and light-colored fluid was in fact slug flow. The fact that the flow alternated between light and dark-colored fluid was plainly visible. As noted in Section 5.2, slug flow is an intermittent flow pattern characterized by alternating flows of oil and gas. The only additional analysis required to confirm slug flow was to confirm that the light-colored fluid was in fact gas-dominated and that the dark-colored fluid was in fact oil-dominated.

To do that, I assessed the trajectory of the dark and light discharge (identified by the arrows in Figure 7). The light-colored fluid takes a more vertical path whereas the dark-colored fluid takes a more horizontal path by comparison. The difference in trajectory is caused by the density of the fluid. The less dense the fluid, the more vertical its

¹⁶ MDL Dep. Ex. 9183, p 150.

trajectory. The gas phase of the MC252 reservoir fluid has a lower density than the oil phase¹⁷. Hence, I concluded that the dark-colored fluid observed at the Riser End was oil dominated and the light-colored fluid was gas dominated.

Based on analysis and review of all the available information, I concluded that the flow pattern observed at the Riser End from May 13 to May 20 was slug flow. Videos of the plume at the Riser End before May 13 and after May 20 did not exhibit the cyclic alternating behavior and therefore slug flow did not occur during these periods¹⁸.

6.2 Characterizing Slug Flow Behavior

The slugging at the Riser End had some unique characteristics that changed with time. These characteristics are explained in this section. The existence of these unique characteristics enabled me ultimately to identify the daily flow rate for the May 13 to May 20 period. This aspect of my work is explained in Section 8.1.

Members of the Flow Rate Technical Group (FRTG) Plume Team calculated the period of alternating oil and gas flow at the Riser End by analyzing the brightness level of the ROV video.¹⁹ The Plume Team found the period to be very regular and equal to approximately 200 seconds (on May 14)¹⁹.

Using a stop watch to mark the start and end of a repeating cycle, I also calculated the period of slug flow on various days from May 13 to May 20. My analysis indicates that the period of slug flow decreased as the days progressed from May 13 until May 20, after which slug flow could not be observed. My analysis of the slug flow timing is documented in Appendix E.

Within one period of the riser motion, the slug flow on May 13 consisted of two sets of gas-dominated and oil-dominated flows. This can be readily observed in ROV videos of the Riser End plume.²⁰ As confirmation, Figure 8 shows the brightness chart from the Plume Calculation Team report and it is evident that the repeating pattern consists of two peaks and two troughs. I refer to this pattern as *double peak behavior*. This pattern can be seen from May 13 through May 15, 2010.

¹⁷ Multiflash Fluid Definition File ("CL68379-DEC-EOS20120322.MFL") provided by Dr. C. Whitson.

¹⁸ On May 12, ROV videos showed three instances of light-colored fluid being released from the Riser End over one and half hours. These intermittent flows did not exhibit the same regularity as the alternating flows between May 13 and May 20.

¹⁹ MDL Dep. Ex. 9183 at 148.

²⁰ BP-HZN-2179MDL04569966.

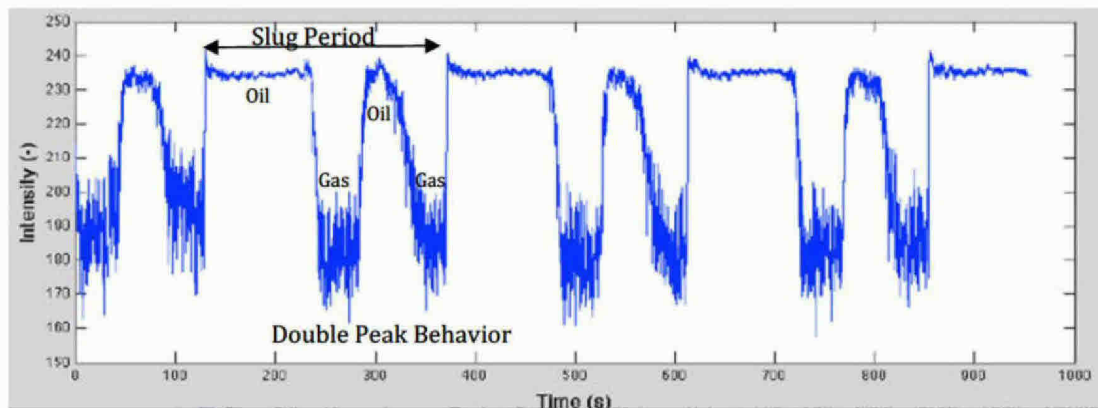


Figure 8 – Intensity (brightness) chart of a portion of the video of discharge at Riser End²¹

Starting May 16, the slug flow consisted of only one gas-dominated and one oil-dominated flow per period. I refer to this pattern as *single peak behavior*. This pattern continued until May 20 when slug flow ceased.

The double peak behavior on May 13 and single peak behavior on May 16 are important features of the unique signature that I used in calculating the flow rate between May 13 and May 20, 2010. As mentioned above, May 13 and May 16 are not the only dates that exhibited these particular behaviors, but these are the dates that detailed ROV riser inspection surveys were performed.

6.3 Link to Riser Motion

On May 16, ROVs were simultaneously monitoring the Riser End and performing a survey of the riser that included the motion of the buoyant loop. Analysis of these videos revealed that the periods of the riser motion and slugging were identical. Because of this direct link between riser motion and slugging, I was able to conclude that the riser motion is the mechanism behind slug formation. Further confirmation comes from subsequent analysis and the fact that once the buoyant loop finally settled on the sea floor, slug flow was no longer observed from the Riser End.

6.4 Slug Mechanism

Prior to May 13, the vertical oscillating motion of the riser was not observed. As shown in Figure 9, ROV surveys on May 4 and May 8 showed that the riser was floating higher than on May 13 (see Figure 9). Eventually, as the buoyant part of the riser sank to the sea floor it began the cyclic motion. Once the cyclic motion began, the buoyant loop moved between resting on the sea floor and floating above the sea floor (the maximum height of the buoyant loop decreased over time).

²¹ MDL Dep. Ex. 9183 at 67.

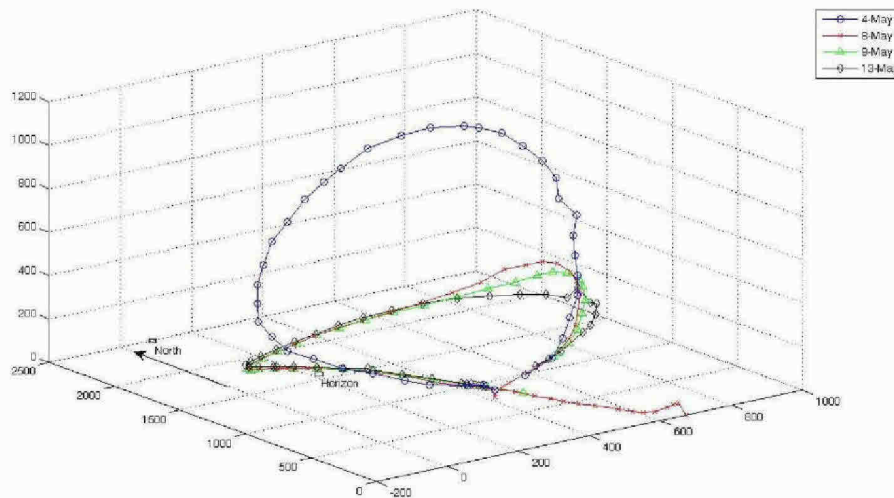


Figure 9 – Progression of riser position with time²²

When the buoyant loop was in its highest position during a cycle, oil was accumulating on the upstream section of the buoyant loop (the part of riser between the start of the buoyant loop and its midpoint) and predominantly gas was flowing over the top of the buoyant loop. Oil, being the denser phase, has a harder time climbing the buoyant loop against the force of gravity. The predominantly gas flow was the source of an observed gas-dominated flow at the Riser End.

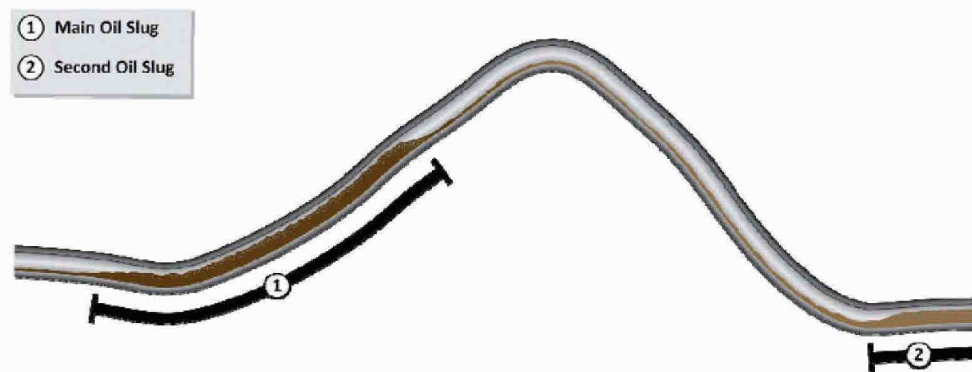


Figure 10 – Oil accumulating in the upstream section of the buoyant loop at its highest position in cycle

As the oil accumulation grew at the upstream section of the buoyant loop (labeled in Figure 10), the weight of the oil caused the loop to sink towards the seafloor.

²² BP-HZN-2179MDL04996568

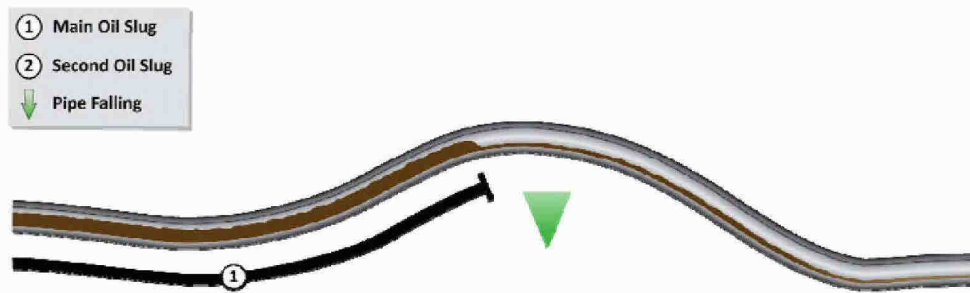


Figure 11 – Weight of the oil slug causes the buoyant loop to sink

As the buoyant loop sank to the seafloor, the oil that had accumulated in the upstream section of the buoyant loop, no longer impeded by gravity, began to flow over the top of the loop and travel towards the end of the riser. At this stage, the flow over the top of the buoyant loop was predominantly oil. This predominantly oil flow, or *oil slug*, was the source of the main oil-dominated flow at the Riser End.

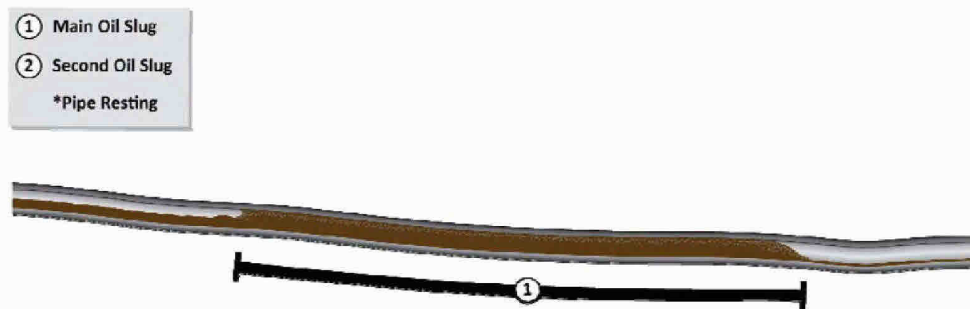


Figure 12 – Oil slug passes through the buoyant loop in its settled position

As the oil slug moved through the buoyant loop, a stratified flow pattern (flow pattern characterized by gas on top and oil on bottom) was established behind the oil slug. The position of the riser at this point (on the sea floor) was the same as the final settled position, and thus, the flow entering the buoyant loop resembled the flow pattern observed after May 20.

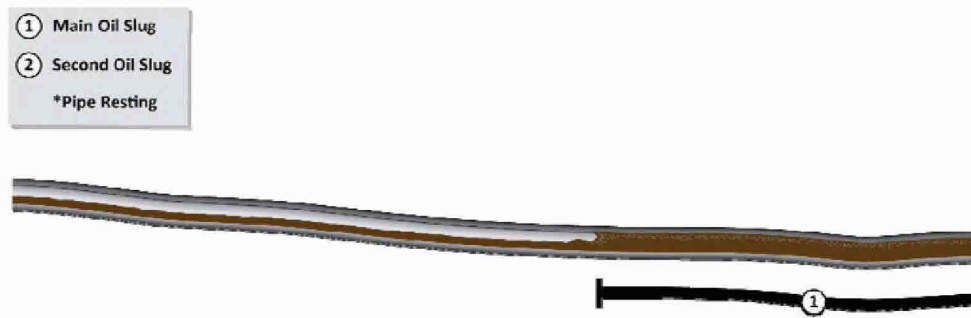


Figure 13 – Stratified flow establishes behind the oil slug

Once the end of the oil slug passed the midpoint of the buoyant loop, the loop once again began to rise. At this stage, the upstream section of the buoyant loop was considerably lighter (more buoyant) because it was filled with more gas than was present in the oil slug.

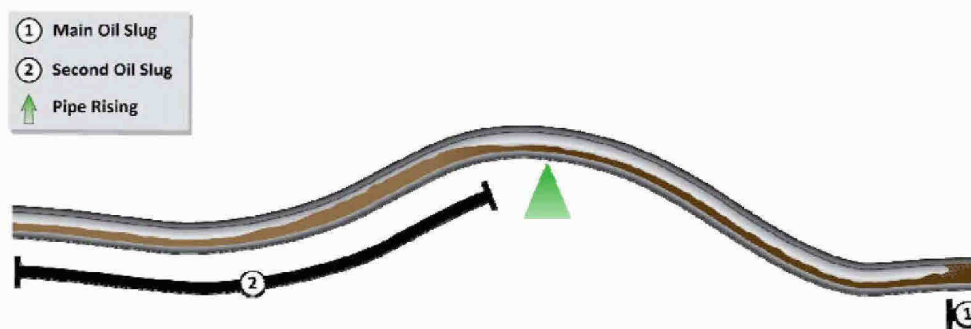


Figure 14 – Buoyant loop begins moving up

The double peak behavior observed on May 13, 2010 results from a phenomenon created by the dynamic motion of the buoyant loop. The double peak was created by the oil and gas that followed the main oil-dominated flow, which was just described. The formation of the second peak proceeded as follows:

1. In multiphase flow, oil (because it is heavier than gas) flowing upward would be slowed by gravity more when the angle of incline is at its greatest (position 1 on Figure 15) compared to where the angle of incline is less (e.g., positions 2 and 3 on Figure 15). The same principle applies to the oil and gas flow through the buoyant loop when the oscillations reached their highest peak.

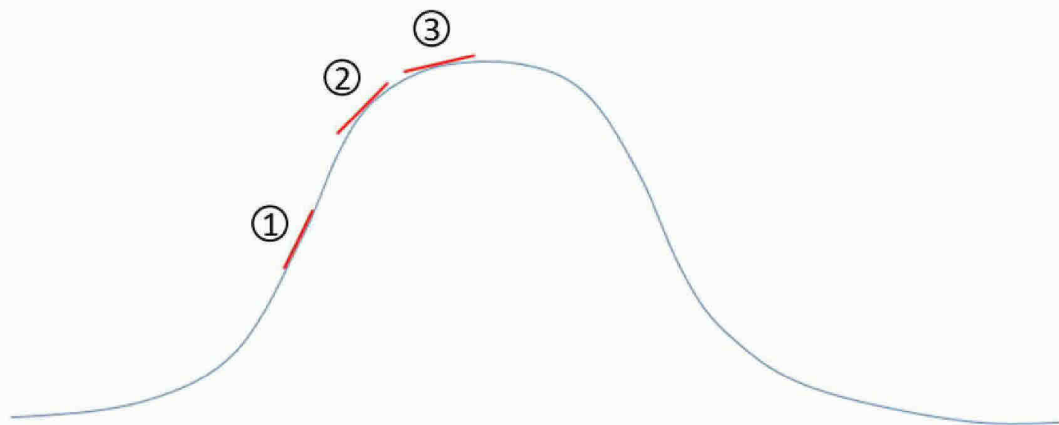


Figure 15 – Illustration of angles variations of a hill

2. As the gas pocket moved through the buoyant loop, the riser began to lift from the sea bed. At this point, the oil upstream of the peak in the buoyant loop (i.e., in the illustration at Figure 14, the oil labeled) would tend to move more slowly toward the peak. The continued upward motion of the riser would further slow the oil that was flowing towards the top of the buoyant loop.
3. When the buoyant loop was at relatively shallow inclinations, the oil slowed, but continued to flow past the top of the buoyant loop. At the steeper inclinations present in parts of the buoyant loop from May 13 to May 15 (but no longer present after May 16), however, the oil flow was nearly stopped.
4. This dynamic explains the double peak phenomenon in the slug flow observed from May 13 to May 15. During this period, the buoyant loop would reach its steepest inclinations at a time that coincided with the presence of a stratified oil and gas flow. As the riser transitioned from the position shown in Figure 14 to the position shown in Figure 16, the stratified oil layer closest to the peak was flowing through a less steep section of the buoyant loop, and flowed over the peak. However, the oil at the steepest part of the buoyant loop was sufficiently slowed by gravity to allow a gas pocket to form above it. This is illustrated in Figure 16 below: the stratified flow shown in Figure 14 has, in Figure 16, split into two oil slugs separated by a gas pocket.

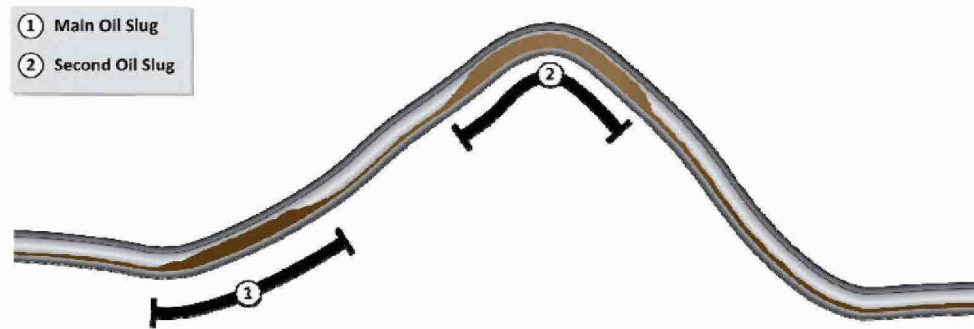


Figure 16 – The second oil slug formed on May 13 due to the steep inclinations

5. This resulted in an overall flow pattern of an oil slug, followed by predominantly gas flow, followed by oil and gas mixture (stratified flow), followed by the second predominantly gas flow, as seen in Figure 16.

By May 16, the buoyant loop was at a shallower inclination, and the second predominantly gas flow was replaced by a gradual transition from oil and gas mixture to the next oil slug. Therefore, it is the range of angles present and dynamic motion of the riser on May 13 that created the double peak behavior. This distinctive combination of riser motion and slug flow behavior is what allows me to predict the range of flow rate that could coexist with the observed phenomena.

6.5 Timing of Kink Leaks

A detailed inspection of the damaged riser after it was retrieved from the seafloor revealed six different leaks were present at the kink (see Figure 17).²³ I reviewed ROV footage of the kink leaks between May 13 and May 20 to identify which leaks were present during the timeframe of interest.



Figure 17 – Riser Kink annotated with labels for each hole in riser²³

From May 13 – May 18, only two of the six leaks, “B” and “C”, were leaking as shown in Figure 18.

²³ BP-HZN-2179MDL04824968-5017, at BP-HZN-2179MDL04824983.

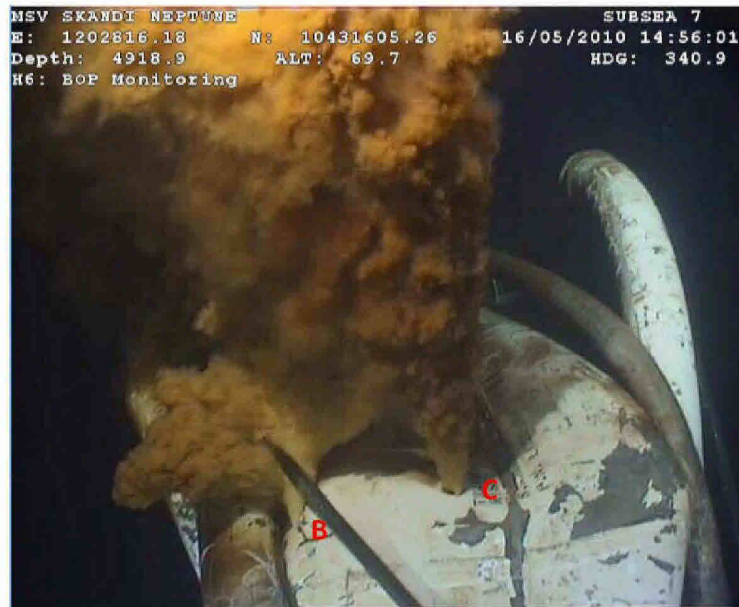


Figure 18 – Kink on May 16 showing only holes B and C leaking²⁴.

Starting May 19, leak “E” and potentially “D” was also observed to be leaking as shown in Figure 19. Since leaks “D” and “E” were very close to each other it was difficult to identify whether one or both of them were leaking.



Figure 19 – Kink on May 19 showing only holes B, C and E leaking.²⁵

²⁴ BP-HZN-2179MDL04569966.

²⁵ BP-HZN-2179MDL04569964.



Based upon my extensive review of ROV video footage, no other leaks were present prior to May 20, 2010.

7 Modeling

I calculated the range of flow rates from the DWH riser in two parts. First, I calculated the flow rate at the Riser End and then, I calculated the flow rate at the Kink leak and Riser End together. I split the problem into two parts because the initial focus of this investigation was slug flow at the Riser End. Because the leaks at the Kink have no impact on slug flow at the Riser End, they were not modeled initially.

To quantify the flow rate through the Riser End, I created a detailed model of the riser, which included the motion of the riser. This model was used to calculate the flow rate at which the simulated slugging matched the characteristics of the slug flow in video footage from ROVs (discussed in Section 6.2).

To quantify the flow rate through the kink holes, I extended the riser model to include the kinked section of the riser. In order to calculate the flow rate through the holes in the kinked section, I included the following additional parameters in the model:

- a. Geometry of the kink leak holes²⁶
- b. Pressure boundary before the kink holes
- c. Fluid temperature before the kink holes
- d. Location of the kink holes along the kink
- e. Hydrostatic pressure outside the kink holes

Accordingly, I prepared two models to quantify the flow rate through the DWH riser. One model starts at the first riser joint, i.e., just beyond the kinked section of the riser and extends to the Riser End (referred to as the “No-Kink Model”). The other model starts from just above the BOP/LMRP and extends to the Riser End (referred to as the “Kink Model”) and includes the Kink.

The No-Kink model has a flow rate boundary at its inlet. A flow rate boundary was chosen because it allowed the flow rate in the riser to be varied directly. Had a pressure boundary (which was also unknown) been chosen, this would have required varying the pressure to indirectly vary the flow rate through the riser. Since the goal was to vary the flow rate through the riser and identify flow rates that matched the unique signature of the observed slug flow (for a discussion of the unique signature, see Section 8.1), having a flow rate boundary is a more direct means of achieving this goal. At the outlet, a constant pressure boundary, set equal to the hydrostatic pressure at the Riser End, was used. The flow rate boundary was used to set the flow rate through the riser. Figure 20 shows a schematic of the No-Kink model.

²⁶ I received area and perimeter measurements for the three holes from Dr. Srdjan Nestic.

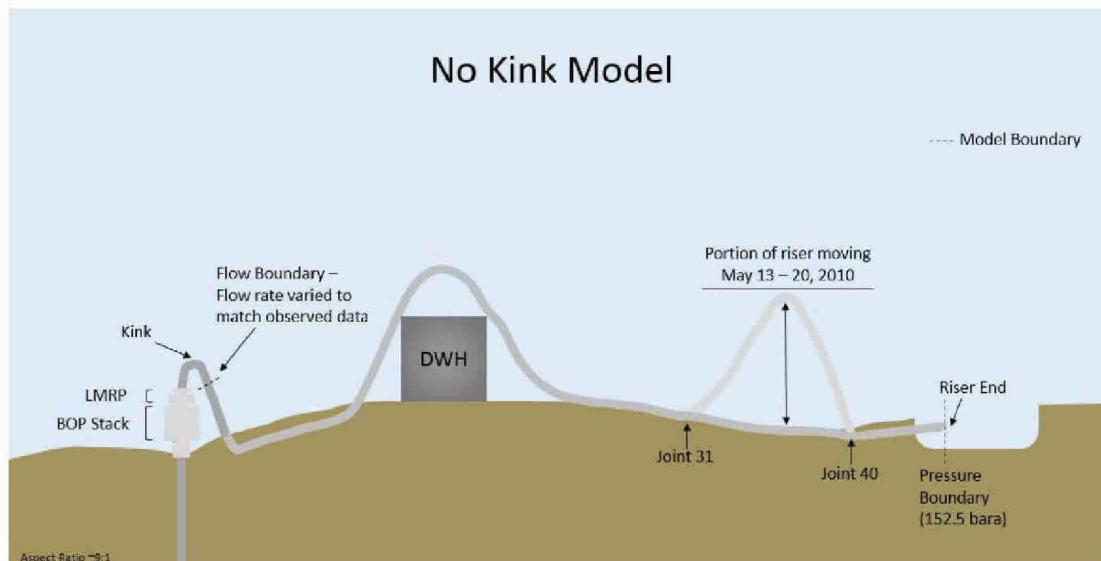


Figure 20 – Schematic of the riser showing model boundaries for the no kink model

In contrast, the Kink Model starts with a pressure boundary before the Kink. This pressure boundary is based on pressure measurements obtained from a pressure gauge installed on the mud boost line (PT-M). The kinked section is modeled as a pipe of reduced diameter with a valve near the location of the throat of the kink. Though no valve existed at this location, I introduced a valve into the model to more accurately model resistances through the kink. The valve (resistance) was adjusted to achieve different flow rates through the riser. I knew that the resistance was adjusted correctly when I was able to match the unique signature of the observed slug flow. The rest of the Kink Model is the same as the No-Kink Model. Figure 21 shows a schematic of the Kink Model.

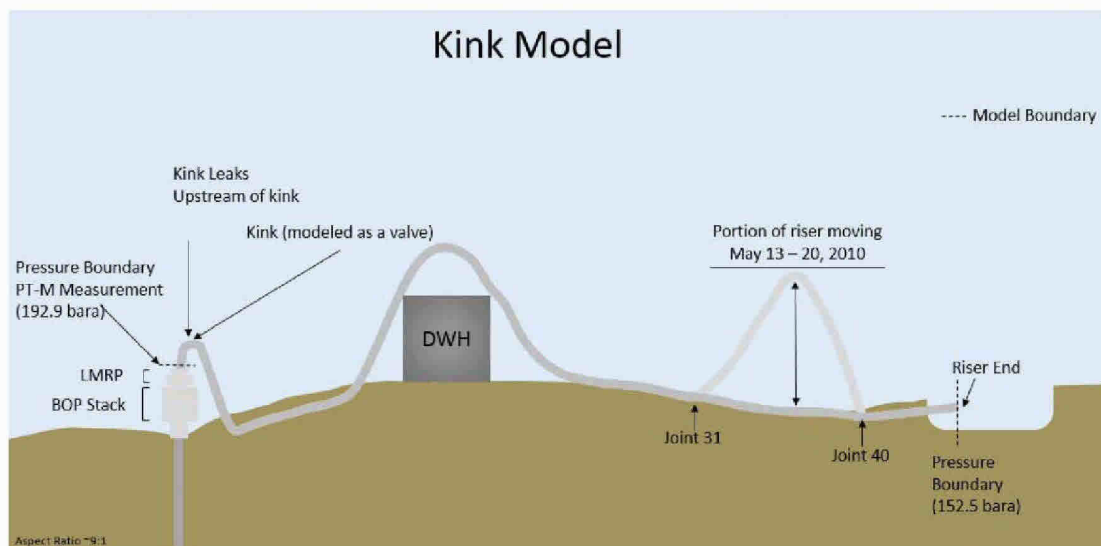


Figure 21 – Schematic of the riser showing model boundaries for the kink model

I did not include the wellbore, BOP or LMRP in either model. Adding these additional components to the model would not have affected the calculated flow rate through the riser. Starting at the reservoir and modeling the flow through the well bore would have yielded a calculated value for the pressure, and temperature above the BOP. But since I already had measurements for both these quantities, I did not need to model more equipment and unnecessarily increase simulation complexity.

For a detailed description of the inputs used in the models, refer to Appendix F.

8 Results

8.1 Riser End Flow Rate

As noted from Section 6.2, the slugging at the Riser End exhibited unique characteristics that changed over time. From May 13 to May 15, ROV videos showed double peak behavior while after May 16, they showed only single peak behavior. I used this unique signature to calculate flow rates through the Riser End. Specifically, I matched the slug flow characteristics to the ROV video footage on May 13 and May 16. To do this, I ran two sets of simulations. One set used the motion characteristics of the riser on May 13 and the other set used the motion characteristics of the riser on May 16. Within each set of simulations, I varied the flow rate through the riser over the same range. The range of flow rates that I used for each set of simulations was ~12,000 stbpd to ~60,000 stbpd.

I only performed simulations for observed behavior on May 13 and May 16 because those are the two days on which I was able to obtain detailed measurements of the riser movement from ROV footage. Both the XLX-37 survey on May 13 and XLX-36 survey on May 16 spanned every riser joint in the buoyant loop. This provided me with measurements of the depths of the buoyant loop at the settled position and the peak position, and the duration of the buoyant loop's oscillatory motion. These measurements were used to model the riser motion in the simulations.

Through these two sets of simulations, I was able to establish a range of flow rates, which I refer to as the *range of qualifying flow rates*. By this I mean that I first identified the range of flow rates that would match the slug characteristics for both May 13 and May 16. Thus, only those flow rates that exhibited double peak behavior on May 13 could be in the range of qualifying flow rates. Further, among the flow rates that qualified on May 13, only those that exhibited single peak behavior on May 16 could be part of the range of qualifying flow rates.

As an example, using the base case for the No-Kink Model (detailed in Appendix G), I obtained double-peak behavior on May 13 between 17,700 stbpd and 41,000 stbpd. For the same case, on May 16, single-peak behavior was only present from 11,700 stbpd to 28,300 stbpd. Based on this, the range of qualifying flow rates is between 17,700 stbpd and 28,300 stbpd.

I was able to refine these bounds by calculating the density of the fluid in the buoyant loop. Since the buoyant loop eventually settled to the seafloor, the density of the flow in the settled position, i.e., in stratified flow, was enough to hold the buoyant loop down. Therefore, during slug flow, the buoyant loop must experience a fluid density lower than the density in stratified flow in order for it to be in motion. Using this additional criterion, the lower bound of qualifying flow rates for the base case was increased to 21,200 stbpd, resulting in a range of qualifying flow rates of 21,200 stbpd to 28,300 stbpd.

Based on this analysis and sensitivity studies which are described later in Section 8.3, the calculated flow rate at the Riser End is 25,100 stbpd.

For a detailed discussion of how the range of qualifying flow rates was determined, see Appendix G.

8.2 Kink Leak Flow Rate

To calculate the flow rate through the Kink leak, I extended the model used to estimate flow from the Riser End to include the kinked section of the riser (refer to Section 7 for a description of the Kink Model). In these simulations, I varied the unknown resistance through the Kink to produce different flow rates through the riser. As described in Section 8.1, qualifying simulations exhibited double peak behavior on May 13 and single peak behavior on May 16. From those qualifying simulations, I chose the simulation with the maximum Kink leak flow rate.

I consider this the maximum Kink leak flow rate for the following reasons. First, I selected an upstream pressure from PT-M that was higher than other reported values for that gauge. A higher pressure results in a higher calculated kink leak flow rate. Second, I relied upon measurements of the holes that were made when they were in their final state (that is, after the kinked section of the riser had been retrieved). I note that the actual sizes of the holes on any day between May 13 and May 20 could have been smaller than the final state when the riser was removed on June 3, 2010. Additionally my model includes leaks from all three leak holes for the entire period whereas the third hole did not appear until May 19. Thus, by using the hole sizes in their final state, using all three holes when only two were present until May 19, and a conservative measurement of the pressure, I calculated the maximum possible flow rate for the three holes composing the Kink leak during the May 13 to May 20 period. This maximum Kink leak flow rate is 4900 stbpd.

8.3 Sensitivities

Some of the model inputs are not known to the same degree of certainty as others. To address uncertainties in the inputs, I ran several sensitivity studies. The same general procedure was performed for each of the sensitivity studies I performed:

- Vary one model input to address its uncertainty
- Run simulations using the May 13 and May 16 riser motion characteristics described in Appendix F-5.
- Determine the range of acceptable flow rates as described in Section 8.1

As an example, the roughness of the riser pipe was not known. To address this uncertainty, I varied the roughness from that of a smooth pipe to 100 times the roughness of a smooth pipe. Detailed discussion of all such sensitivity studies are included in Appendix G.

These sensitivity studies allowed me to quantify the uncertainty in the calculated flow rate through the riser (which includes both the Kink and Riser End) and consequently provide a range of possible flow rates through the riser.

In addition to the sensitivity studies, comparison of LedaFlow models to OLGA models also allowed me to estimate a model uncertainty of $\pm 5\%$ (see Appendix B).

Based on these sensitivity studies and the estimated model uncertainty, I determined that the total flow rate from the Kink and Riser End was between 24,900 stbpd and 35,900 stbpd.

8.4 Other Work

The flow rates I calculated to match the observed slug flow from May 13 to May 20, 2010 presented in this report are based on models that included the riser motion. I also considered whether other mechanisms of slug formation could have caused the observed slug flow. Based upon these other models, I have eliminated the common possible mechanisms for the formation of slugs observed between May 13 and May 20. The results of these other models, and my analysis of these results, are documented in Appendix H.

9 Summary and Conclusions

The end of the DWH riser exhibited slugging behavior between May 13 and May 20, 2010. This behavior was documented in ROV video footage, and noted by members of the FRTG Plume Team and by United States officials. I verified that this flow pattern is slug flow through my review of ROV videos of the flow from the riser end plume. A portion of the riser moved in a vertical oscillating motion between May 13 and May 20. The range and period of the motion decayed over time until the riser stopped moving on the May 21, 2010. On May 16, 2010, ROVs simultaneously monitoring the plume and the buoyant loop illustrated that the slug period and riser motion period were the same. This led to the investigation and confirmation that the observed slug flow was indeed caused by the riser movement.

Two detailed models of the riser were constructed in LedaFlow, one starting just above the BOP/LMRP which included the kink, and one starting after the kink at the first riser joint. Using these models, I was able to simulate the dynamic motion of the riser and establish the flow rate through the riser that would match the characteristics of the observed slug flow. Specifically, on May 13, the slug flow exhibited two gas-dominant and two oil-dominant flows in alternating fashion within one slugging period (double peak behavior). This particular pattern of flow could only occur within a very narrow range of flow rates as it related to how fast the gas pushed the oil slugs. Moreover, the double peak behavior was not observed on May 16 when the range of riser motion was smaller. This phenomenon further limits the possible flow rates through the riser.

By simulating motion characteristics on both May 13 and May 16, the best calculated flow rate through the riser end is 25,100 stbpd. I also calculated an estimate for the flow rate through the kink leaks using simulation models. Combining these two flow rates the best calculated flow rate through the Kink and Riser End is 30,000 stbpd. These flow rates occurred from May 13 to May 20 when slug flow was observed at the Riser End.

There were some uncertainties in the input data to the models. Even with these uncertainties, the maximum estimated total flow rate through the DWH riser between May 13 and May 20, 2010 is bounded between 24,900 stbpd and 35,900 stbpd.


* * * *



The opinions I have expressed in this report are based on my education, training, and experience. My qualifications and experience are described in Section 2 of this report, as supplemented by Appendix A. In forming my opinions, I have considered the materials listed in Appendix D and the results of the simulations that have been provided along with this report. I have not previously testified at trial or by deposition.

I am a principal and employee of evoleap, LLC ("evoleap"). For my time working on this matter, and the time of my colleague, evoleap is compensated at an hourly rate of \$315. For my time testifying on this matter, evoleap is compensated at an hourly rate of \$550. In addition, evoleap receives commissions from Kongsberg Oil & Gas, Inc. ("Kongsberg") for sales of LedaFlow software licenses. For the sale of LedaFlow software licenses used in this matter, evoleap has invoiced Kongsberg \$22,362. None of this compensation is in any way related to the outcome of this case.

Respectfully submitted,



Michael Zaldivar, PhD

05/01/2013

Date

Appendix A - Project Experience

Lucius Depressurization Analysis – Anadarko (GOM)

Model Scope	<ul style="list-style-type: none"> Dual flowline system with risers
Key Contribution	<ul style="list-style-type: none"> Technical Lead Model configuration LedaFlow Simulations and comparison to K2 Field data Report and Presentation to Customer
Key Issues	<ul style="list-style-type: none"> Depressurization procedure and Hydrate Mitigation strategy After hydrate plug, how much gas lift is needed to lift liquid in risers Detailed look at differences in gas/liquid slip relationship for OLGA and LedaFlow in highly inclined flows

Petronius Benchmarking Study – Chevron (GOM)

Model Scope	<ul style="list-style-type: none"> Dry Tree Wells
Key Contribution	<ul style="list-style-type: none"> Technical Lead Model configuration LedaFlow Simulations and comparison to field data Report and Presentation to Customer
Key Issues	<ul style="list-style-type: none"> Benchmarking study to validate LedaFlow against fiber optic cable data. Comparison to OLGA

Holly 3 Drain System Analysis – BG

Model Scope	<ul style="list-style-type: none"> Drain System
Key Contribution	<ul style="list-style-type: none"> Technical Lead Model configuration LedaFlow Simulations Report and Presentation to Customer
Key Issues	<ul style="list-style-type: none"> Confirmation of drain system pipe pressure rating Analysis of pressure spikes resulting from gas by-pass event during level control failure

Belanak LPG Surge Analysis – ConocoPhillips (Indonesia)

Model Scope	<ul style="list-style-type: none"> LPG Export Lines
--------------------	--

Key Contribution	<ul style="list-style-type: none"> • Technical Lead • Model configuration • OLGA Simulations • Report and Presentation to Customer
Key Issues	<ul style="list-style-type: none"> • HIPPS analysis during block valve failure

Belanak LPG FPSO HYSYS Dynamic Model Analysis – ConocoPhillips (Indonesia)

Model Scope	<p>Complete subsea network including:</p> <ul style="list-style-type: none"> • 48 wells (as point sources) • 2 flowlines <p>Integrated model with complete process model of FPSO (Floating Production Storage and Offloading) including:</p> <ul style="list-style-type: none"> • HP and LP separators • Vapor Recovery Unit (VRU) • Amine Contactor • De-ethanizer • De-propanizer • De-butanizer • Compression Trains
Key Contribution	<ul style="list-style-type: none"> • Technical Lead • Build and Configure hi-fidelity models • HYSYS & OLGA Simulations • Worked with ConocoPhillips engineers daily to validate model and leverage model to support decisions and validate design
Key Issues	<ul style="list-style-type: none"> • One of the first built FPSO. Consequently, many studies were performed looking at interaction between subsea and facilities. • Coupled OLGA to HYSYS to look at the impact of terrain slugs on the FPSO facilities

BAB Hydraulic Analysis – JGC and SKEC (UAE)

Model Scope	<ul style="list-style-type: none"> • Infield flowline/trunkline network • Slug catcher
Key Contribution	<ul style="list-style-type: none"> • Model configuration • OLGA Simulations • Report and Presentation to Customer
Key Issues	<ul style="list-style-type: none"> • Validate current slug catcher design during steady state, turn down, pigging and restart operations • Onshore pipeline that exhibited terrain slugging during turn down operations.

Theddlethrope Gas Terminal – ConocoPhillips (UK)

Model Scope	<ul style="list-style-type: none"> Gas blending facility
Key Contribution	<ul style="list-style-type: none"> Model design Design of automatic field-data reconciliation algorithm
Key Issues	<ul style="list-style-type: none"> Data reconciliation algorithm accounting for transportation lag Gas quality management during pigging events on pipelines with high quality gas

Pluto – Woodside (Australia)

Model Scope	<ul style="list-style-type: none"> Five Pluto wells Dual 24" looped deep-water flowlines Riser platform including depressurization and flowline pigging facilities 36" 180 km three-phase export pipeline Onshore facilities including slug catcher, MEG regeneration and storage tanks Offshore lean MEG distribution system
Key Contribution	<ul style="list-style-type: none"> Technical Lead Model design, and build Installation, and commissioning Model validation and benchmarking with design data Model validation and benchmarking with field data
Key Issues	<ul style="list-style-type: none"> Offshore hydrate management strategy Flowline roundtrip pigging with motive gas from reverse-flowing trunkline Pig tracking and management Slug management on 36" trunkline MEG inventory management, especially for turndown scenario

PROMOTS – PCSB (Malaysia)

Model Scope	<ul style="list-style-type: none"> Integrated field modeling of entire gas-condensate production complex of Petronas Carigalli 20+ pipelines, 10+ offshore production platforms, 3 receiving facilities Pigging loop storage system Separation and metering
Key Contribution	<ul style="list-style-type: none"> System design and engineering Installation, and commissioning Model validation and benchmarking against field data
Key Issues	<ul style="list-style-type: none"> Offshore production management Supply assurance Pig tracking Ramp-up and pigging slug management Onshore data integration

K2 Project – ENI (GOM)

Model Scope	<ul style="list-style-type: none"> • 10+ wells • Two dual looped deep-water flowlines • Separation and metering • Dedicated well flow calculation (virtual metering system) • Daily production allocation
Key Contribution	<ul style="list-style-type: none"> • System design and engineering • Installation, and commissioning • Model validation and benchmarking against design data
Key Issues	<ul style="list-style-type: none"> • Offshore hydrate management strategy • Up-to-date cool down time analysis • Pig tracking and management • Calculation of hot oil volume and warm-up time

Shenzi Manifold K – BHP Billiton (GOM)

Model Scope	<ul style="list-style-type: none"> • 20+ wells • Two dual looped deep-water flowlines • Arrival platform including blow-down and round-trip pigging facilities • Separation and metering • Dedicated well flow calculation (virtual metering system) • Daily production allocation
Key Contribution	<ul style="list-style-type: none"> • System design and engineering • Installation, and commissioning • Model validation and benchmarking against design data
Key Issues	<ul style="list-style-type: none"> • Offshore hydrate management strategy • Up-to-date cool down time analysis • Pig tracking and management • Wax management • Calculation of hot oil volume and warm-up time

Kashagan Trunklines and Oil Export pipelines – AGIP KCO (Kazakhstan)

Model Scope	<ul style="list-style-type: none"> • 3 trunklines (oil, sour gas, and fuel gas) and 1 oil export pipeline • Leak detection
Key Contribution	<ul style="list-style-type: none"> • System design and engineering • Model validation and benchmarking against design data • Design and validation of leak detection module
Key Issues	<ul style="list-style-type: none"> • Leak Detection

Qatar Gas Distribution – Qatar Petroleum (Qatar)

Model Scope	<ul style="list-style-type: none"> Onshore gas distribution system Over 40 gas distribution pipelines Over 20 intermediate valve stations and distribution centers in Qatar Over 10 supply points and over 30 offtake points
Key Contribution	<ul style="list-style-type: none"> System design and engineering Design, build, and validate pipeline model and models of valve stations and distribution centers Installation, and commissioning Model validation and benchmarking against field data
Key Issues	<ul style="list-style-type: none"> Leak Detection Gas supply management Calculation of pipeline efficiency Forecast gas supply shortfall scenarios Complex distribution network with multiple flow paths and bidirectional pipelines Line pack management and deliverability forecasting Optimal network routing determination and planning for unplanned supply disruption

Bayu Undan – ConocoPhillips (Australia)

Model Scope	<ul style="list-style-type: none"> One 500+ km subsea gas pipeline
Key Contribution	<ul style="list-style-type: none"> System design and engineering Model testing and validation Installation, and commissioning Model validation and benchmarking against field data
Key Issues	<ul style="list-style-type: none"> Leak Detection

Perseus over Goodwyn – Woodside (Australia)

Model Scope	<ul style="list-style-type: none"> Six subsea wells
Key Contribution	<ul style="list-style-type: none"> System design and engineering Model testing and validation
Key Issues	<ul style="list-style-type: none"> Real-time model-based subsea well flow rate calculation

Angel – Woodside (Australia)

Model Scope	<ul style="list-style-type: none"> Four subsea wells
--------------------	---

Key Contribution	<ul style="list-style-type: none"> • System design and engineering • Model testing and validation
Key Issues	<ul style="list-style-type: none"> • Real-time model-based subsea well flow rate calculation

Carapal Gas Plant HYSYS Dynamic Simulation Study – BG (Trinidad)

Model Scope	<ul style="list-style-type: none"> • One onshore well head • Onshore ~5 km multiphase pipeline to compression facility • Detailed model of separation and compression facility
Key Contribution	<ul style="list-style-type: none"> • Engineering lead on project • Model design, build, test, and validation • Design, execution, and reporting of study
Key Issues	<ul style="list-style-type: none"> • Surge analysis of Carapal compression plant

Onshore Compressor Terminal Integration Project HYSYS Dynamic Simulation Study – BP (UK)

Model Scope	<ul style="list-style-type: none"> • BP Dimlington onshore compression plant • Detailed model of separation and compression facilities
Key Contribution	<ul style="list-style-type: none"> • Engineering lead on project • Model design, build, test, and validation • Design, execution, and reporting of study
Key Issues	<ul style="list-style-type: none"> • Analysis of hot gas bypass requirement on two-stage compressor system

Other Selected Projects:

- Hannay Subsea Tieback Development Study – Talisman (North Sea)
- Kizomba-C Flow Assurance Screening Study – ExxonMobil (West Africa)
- Belanak LPG Vaporization Study – ConocoPhillips (Indonesia)
- Belanak Virtual Pipeline Manager – ConocoPhillips (Indonesia)

LedaFlow Support Cases

While working for Kongsberg, I worked on numerous support cases for customers using LedaFlow. Many of these cases involve slug flow because one of LedaFlow’s key features is its mechanistic (first principles) approach to modeling hydrodynamic slug flow.

Appendix B - Model Benchmarking

Introduction

I used dynamic pipeline models to calculate the flow rate through the DWH riser. These models require detailed inputs that describe the geometry, terrain, pipe wall and insulation materials, fluid properties, and other information about the system being modeled. I used LedaFlow (version 1.2) as the primary dynamic pipeline simulator. To ensure that models are built correctly it is useful to benchmark them against known results from field data, or against other simulation software models.

To benchmark my LedaFlow models, I used another commercially available multiphase simulator called OLGA. I used OLGA 7.2, which was the latest version of OLGA available at the time of my analysis, as well as OLGA 5.3.2, which is the most widely used version in the industry. These software packages are described in more detail in Appendix C. The purpose of this appendix is to explain the steps taken to ensure that the LedaFlow models were built correctly before using them in my analysis to calculate the flow rates through DWH riser. Since these simulation tools are known to have differences between them, benchmarking the models allows these differences to be understood and documented. Additionally benchmarking provides some understanding of the implicit uncertainty in modeling multiphase flow.

The process of generating various inputs required for the models such as the elevation profile of the riser, and heat transfer properties, is explained in other appendices. This appendix focuses on how these inputs, mostly through the use of Excel spreadsheets, were translated into models and how the results of benchmarking simulations were used to validate the models.

Model Input File Generation

OLGA

OLGA has a Graphical User Interface (GUI) which can be used to create model input files (i.e., *opi* files). However, the simulation engine only reads a keyword text-based input file (for OLGA 7, *key*, *genkey* files; for OLGA 5, *inp*, *geninp* files) that is created by the GUI just before a simulation is started. An input file is composed of a list of *statements*.

I created two template input files using the OLGA 5 GUI. One input file, which was the basis of the No-Kink model, had a mass flow rate boundary at the inlet, a pipeline, and a pressure boundary at the outlet. Another input file, which was the basis of the Kink Model, had a pressure boundary at the inlet, a pipeline with the kink leaks and a valve to represent the kink, and a pressure boundary at the outlet.

Statements in the input file dealing with pipeline geometry, heat transfer materials, and descriptions of walls around the pipeline (for heat transfer) were generated directly in Excel. These statements were prepared using formulas that linked directly to the calculation spreadsheets for elevation profile and heat transfer properties described in Appendices F-1 through F-5. The OLGA 7 input files were created by importing and converting the OLGA 5 files (after they were updated with Excel content) from the *inp* format to *key* format.

LedaFlow

LedaFlow has a built-in OLGA input file converter. Once the OLGA 5 files were created, I used the conversion feature in LedaFlow to convert the *inp* file to a LedaFlow script file.

Benchmarking Simulations

The model conversion process has several manual steps which were prone to user error. In order to minimize that possibility, I ran a set of simulations with the same inputs using all three software: LedaFlow v 1.2, OLGA 5, and OLGA 7.

Model

Since OLGA cannot model the oscillating motion of the buoyant loop, I used static profiles for comparison in this benchmarking analysis. Only the No-Kink Model was used for benchmarking as most of the model inputs relate to the riser.

Simulation Matrix

For the purpose of comparison, the flow rate through the system, and inlet temperature were varied. Table 1 lists the parameters and their corresponding values used for benchmarking the models. All variations of flow rate and temperature shown in Table 1 were made for the sole purpose of benchmarking the models.

Table 1 – Simulation Matrix for Benchmarking

Parameter	Values
Mass Flow Rate (kg/s)	18, 45, 72, 120
Inlet Temperature (°C)	65, 80, 95
Elevation Profile	Low, May 13 High Profile

Results

The results are presented as the average root mean square deviation (RMSD) between profile variables calculated by LedaFlow and OLGA (versions 5.3.2.4 and 7.2). The RMSD value is calculated as follows:

$$RMSD = \sqrt{\frac{\sum_{t=1}^n (x_{1,t} - x_{2,t})^2}{n}}$$

Where

$x_{i,t}$ Is the value of profile variable x from software i at the t -th pipeline segment

n is the total number of pipeline segments

The average RMSD for a variable is calculated using the RMSD of that variable across the simulation matrix.

I considered temperature, pressure, liquid holdup,¹ and the liquid mass rate as key variables for comparison. Other variables can be expressed as functions of these key variables and therefore were not presented for the purpose of comparison.

Table 2 – Average RMSD for the No-Kink models

Average RMS Error	Low Profile		High Profile	
	vs. OLGA 7.2	vs. OLGA 5.3.2.4	vs. OLGA 7.2	vs. OLGA 5.3.2.4
LedaFlow 1.2				
Temperature	4.53%	4.59%	4.73%	4.78%
Pressure	0.05%	0.05%	0.09%	0.10%
Liquid Mass Rate	0.37%	0.38%	0.40%	0.41%
Holdup	5.86%	5.44%	6.92%	6.44%

Conclusion

Based on my experience, I expected differences of no greater than 10% between LedaFlow and OLGA. The fact that average differences are less than that is good indication that the model predictions validate one another. The primary difference comes from the heat transfer in the bare pipe of the first two joints. LedaFlow calculates higher heat transfer than OLGA and therefore is consistently lower in temperature.²

All differences are within the realm of expected model differences and serves to quantify “model uncertainty”. Model uncertainty is the expected error in results due to approximations made by one-dimensional models. Based on the results this exercise (Table 2 shows average model differences of less than 7%) and my experience, I conservatively estimate the model uncertainty to be between 5% to 10%.

¹ Holdup is the area of the pipe occupied by liquid at any cross section of the pipe. This is typically expressed as a fraction between 0 and 1.

² Lower temperatures yield a higher calculation for the Riser End flow rate based on the signature matching algorithm described in the main report and further in Appendix G.

Appendix C - Modeling Tools

Several commercially-available tools were used in this investigation. This section includes brief descriptions of each product and its role in this work.

Multiflash

Multiflash is a commercially-available thermodynamic simulator from Infochem Computer Services LTD. Multiflash was used to generate fluid property data needed to perform transient multiphase simulations. Multiflash version 4.2 was used to generate the required fluid properties, or PVT tables. For a more complete description of the software, refer to the product website at: <http://www.infochemuk.com/index.php/product/multiflash>.

Multiphase Flow Simulators

OLGA and LedaFlow are two of the most widely available commercial one-dimensional transient multiphase flow engineering simulators. These simulators simplify the flow to a one-dimensional problem, i.e., the properties of the fluid flow only change along one dimension, namely along the length of the pipeline.

Over the last 40 years, through carefully designed experiments in large-scale multiphase flow loops and by gathering field data from multiphase production pipelines, the relationships required to accurately model multiphase flow as a one-dimensional problem (called closure relationships) have been developed and improved upon considerably. Without these commercial simulators, it would be impossible to develop deepwater fields. The fact that many such subsea developments produce oil and gas reliably is a testament to the accuracy of these simulators.

OLGA

OLGA is a commercially-available multiphase flow simulator from SPT Group, a Schlumberger Company. OLGA has a long history (30+ years) of enabling operating companies to design and develop multiphase production systems. A more complete description of the software is available at: <http://sptgroup.com/en/Products/OLGA/>.

Version 5.3.2.4

This version of OLGA is in my experience the most widely-used version in the industry today. Nearly all of the operating companies that use OLGA, rely on and accept the results from this software version for the design, development and operation of oil and gas fields around the world. This version of OLGA is referenced in this work to provide a basis of what is commonly accepted in the industry.

Version 7.2

This version of OLGA is the latest version of the software that was available during the course of the investigation. This version of the software, released in September 2012, was utilized because it represents the state of the art software from SPT Group for modeling multiphase flow.

LedaFlow 1.2

LedaFlow is a commercially-available multiphase flow simulator from Kongsberg. LedaFlow is a relatively new tool in the market, its first commercial version was made available in June 2011. LedaFlow is a product that was developed through more than 10 years of collaboration between ConocoPhillips, Total and SINTEF. A more complete description of the software is available at: <http://kongsberg.com/en/kogt/offerings/software/ledaflow/>.

Appendix D – Materials Considered

Publicly Available Materials

Add Energy, Appendix W of Deepwater Horizon Accident Investigation Report, "Report - Dynamic Simulations Deepwater Horizon Incident BP," published September 8, 2010.

Bill Lehr, Sky Bristol, and Antonio Possolo, "Oil Budget Calculator - Deepwater Horizon - Technical Documentation," Report to National Incident Command, published November 2010

Cuming Corporation, Technical Note 100-1-A, "Introduction to Syntactic Foam," available at <http://cuming.mosaicmedia.com/wp-content/uploads/2012/06/TN-100-1-A-7-11-12.pdf>

Cuming Corporation, Technical Note 600-1, "Thermal Insulating Properties of Syntactic Foam," available at <http://www.cumingcorp.com/wp-content/uploads/2012/06/TN600-1.pdf>

E.S. Kordyban, T. Ranov, "Mechanism of Slug Formation in Horizontal Two-Phase Flow," J. Fluids Eng. 92(4), 857-864 (Dec 01, 1970).

G.E. Alves, "Cocurrent Liquid-Gas Flow in a Pipeline Contractor," Chem Engng Prog, 50, pp 449-456, 1954.

G.W. Govier, and K. Aziz, "The Flow of Complex Mixtures in Pipes," Van Nostrand Reinhold, New York, 1972.

Jane Lubchenko, Marcia McNutt, Bill Lehr, et al., "BP Deepwater Horizon Oil Budget: What Happened to the Oil?", Report to National Incident Command, published August 3, 2010

R. Belt, "Comparison of Commercial Multiphase Flow Simulators with Experimental and Field Databases", Multiphase Production Technology - June 2011, (available at <http://www.kongsberg.com/en/kogt/offerings/software/ledaflow/ledaflowvalidation/>)

Numerical interpolation program ("SciPy"), available at <http://docs.scipy.org/doc/scipy/reference/tutorial/interpolate.html>

Reddy, C. M. et al., 2011, Composition and fate of gas and oil released to the water column during the Deepwater Horizon oil spill

Shoham, O. (2006): Mechanistic Modeling of Gas-Liquid Two-Phase Flow in Pipes, Society of Petroleum Engineers.

Thomas J. Danielson, "Testing and Qualification of a New Multiphase Flow Simulator", OTC - May 2011, (available at <http://www.kongsberg.com/en/kogt/offerings/software/ledaflow/ledaflowvalidation/>)

Thomas J. Danielson and Kris M. Bansal, "Simulation of Slug Flow in Oil and Gas Pipelines Using a New Transient Simulator", OTC - 2012, (available at <http://www.kongsberg.com/en/kogt/offerings/software/ledaflow/ledaflowvalidation/>)

U.S. Department of Interior, Flow Rate Technical Group, "Assessment of Flow Rate Estimates for the Deepwater Horizon / Macondo Well Oil Spill," published March 10, 2011.

U.S. Geological Survey, "Deepwater Horizon MC252 Gulf Incident Oil Budget - Government Estimates through August 1," published August 2, 2010 (including all Appendices).



W.J. Winters, T.D. Lorenson, and C.K. Paull, eds., Initial report of the gas hydrate and paleoclimate cruise on the RV Marion Dufresne in the Gulf of Mexico, 2–18 July 2002: U.S. Geological Survey Open-File Report 2004–1358 (2007).

Watkins, et al, "Syntactic Foam Thermal Insulation for Ultra-Deepwater Oil and Gas Pipelines", OTC 13134, 2001

Y. Onishi, "Review of 'Deepwater Horizon Release Estimate of Rate by PIV,'" Pacific National Laboratory, PNNL-19525, published June 2010.

MDL Documents

BP-HZN-2179MDL00269156	BP-HZN-2179MDL04908567
BP-HZN-2179MDL00327732	BP-HZN-2179MDL04915723
BP-HZN-2179MDL00333592	BP-HZN-2179MDL04915724
BP-HZN-2179MDL00477088	BP-HZN-2179MDL04915725
BP-HZN-2179MDL02172464	BP-HZN-2179MDL04926107
BP-HZN-2179MDL02562990	BP-HZN-2179MDL04926108
BP-HZN-2179MDL03349164	BP-HZN-2179MDL04927171
BP-HZN-2179MDL03349167	BP-HZN-2179MDL04934351
BP-HZN-2179MDL03676655	BP-HZN-2179MDL04996568
BP-HZN-2179MDL03830472	BP-HZN-2179MDL04996569
BP-HZN-2179MDL04366973	BP-HZN-2179MDL04996569
BP-HZN-2179MDL04802942	BP-HZN-2179MDL04996572
BP-HZN-2179MDL04824968	BP-HZN-2179MDL04996573
BP-HZN-2179MDL04826982	BP-HZN-2179MDL04996573
BP-HZN-2179MDL04830442	BP-HZN-2179MDL04996574
BP-HZN-2179MDL04833555	BP-HZN-2179MDL04996574
BP-HZN-2179MDL04833558	BP-HZN-2179MDL04996575
BP-HZN-2179MDL04833559	BP-HZN-2179MDL04996575
BP-HZN-2179MDL04833560	BP-HZN-2179MDL04996576
BP-HZN-2179MDL04833561	BP-HZN-2179MDL04996576
BP-HZN-2179MDL04833562	BP-HZN-2179MDL04996577
BP-HZN-2179MDL04833563	BP-HZN-2179MDL04996577
BP-HZN-2179MDL04833564	BP-HZN-2179MDL05086932
BP-HZN-2179MDL04833565	BP-HZN-2179MDL05187231
BP-HZN-2179MDL04833566	BP-HZN-2179MDL05698038
BP-HZN-2179MDL04833567	BP-HZN-2179MDL05871047
BP-HZN-2179MDL04833568	BP-HZN-2179MDL05904587
BP-HZN-2179MDL04833569	BP-HZN-2179MDL05904588
BP-HZN-2179MDL04833570	BP-HZN-2179MDL06005992
BP-HZN-2179MDL04833571	BP-HZN-2179MDL06008904
BP-HZN-2179MDL04833572	BP-HZN-2179MDL06010350
BP-HZN-2179MDL04833573	BP-HZN-2179MDL06094683
BP-HZN-2179MDL04833574	BP-HZN-2179MDL06114509
BP-HZN-2179MDL04833575	BP-HZN-2179MDL06314451
BP-HZN-2179MDL04877807	BP-HZN-2179MDL06330450



BP-HZN-2179MDL06599701
BP-HZN-2179MDL06599702
BP-HZN-2179MDL06666023
BP-HZN-2179MDL06742178
BP-HZN-2179MDL06742234
BP-HZN-2179MDL06742608
BP-HZN-2179MDL06742613
BP-HZN-2179MDL06742720
BP-HZN-2179MDL06742721
BP-HZN-2179MDL06742965
BP-HZN-2179MDL06742973
BP-HZN-2179MDL06743166
BP-HZN-2179MDL06743478
BP-HZN-2179MDL06744011
BP-HZN-2179MDL06744773
BP-HZN-2179MDL06744882
BP-HZN-2179MDL06744885
BP-HZN-2179MDL07010149
BP-HZN-2179MDL07014306
BP-HZN-2179MDL07014311
BP-HZN-2179MDL07014314
BP-HZN-2179MDL07129522
BP-HZN-2179MDL07241912
BP-HZN-2179MDL07241913
BP-HZN-2179MDL07241914
BP-HZN-2179MDL07265827
BP-HZN-2179MDL07266155
BP-HZN-2179MDL07266193
BP-HZN-2179MDL07266256
BP-HZN-2179MDL07383106
BP-HZN-2179MDL07447605
BP-HZN-2179MDL075574314-7576801
BP-HZN-2179MDL075576153
BP-HZN-2179MDL075576154
BP-HZN-2179MDL07576153
BP-HZN-2179MDL07576154
BP-HZN-2179MDL07729355
BP-HZN-2179MDL07729356
BP-HZN-2179MDL07729357
BP-HZN-2179MDL07729358
BP-HZN-2179MDL07729359
BP-HZN-2179MDL07729360
BP-HZN-2179MDL07729361
BP-HZN-2179MDL07729362
BP-HZN-2179MDL07729363
BP-HZN-2179MDL07729364
BP-HZN-2179MDL07729365
BP-HZN-2179MDL07729366

BP-HZN-2179MDL07729367
BP-HZN-2179MDL07729368
BP-HZN-2179MDL07729369
BP-HZN-2179MDL07729370
BP-HZN-2179MDL07729371
BP-HZN-2179MDL07729372
BP-HZN-2179MDL07729373
BP-HZN-2179MDL07729374
BP-HZN-2179MDL07729375
BP-HZN-2179MDL07729376
BP-HZN-2179MDL07729377
BP-HZN-2179MDL07729378
BP-HZN-2179MDL07729379
BP-HZN-2179MDL07729380
BP-HZN-2179MDL07729381
BP-HZN-2179MDL07729382
BP-HZN-2179MDL07729383
BP-HZN-2179MDL07729384
BP-HZN-2179MDL07729385
BP-HZN-2179MDL07729386
BP-HZN-2179MDL07729387
BP-HZN-2179MDL07729388
BP-HZN-2179MDL07729389
BP-HZN-2179MDL07729390
BP-HZN-2179MDL07729391
BP-HZN-2179MDL07729392
BP-HZN-2179MDL07729393
BP-HZN-2179MDL07729394
BP-HZN-2179MDL07729395
BP-HZN-2179MDL07729396
BP-HZN-2179MDL07729397
BP-HZN-2179MDL07729398
BP-HZN-2179MDL07729399
BP-HZN-2179MDL07729400
BP-HZN-2179MDL07729401
BP-HZN-2179MDL07729402
BP-HZN-2179MDL07729403
BP-HZN-2179MDL07729404
BP-HZN-2179MDL07729405
BP-HZN-2179MDL07729406
BP-HZN-2179MDL07729407
BP-HZN-2179MDL07729408
BP-HZN-2179MDL07729409
BP-HZN-2179MDL07729410
BP-HZN-2179MDL07729411
BP-HZN-2179MDL07729412
BP-HZN-2179MDL07729413
BP-HZN-2179MDL07729414



BP-HZN-2179MDL07729415
BP-HZN-2179MDL07729416
BP-HZN-2179MDL07729417
BP-HZN-2179MDL07729418
BP-HZN-2179MDL07729419
BP-HZN-2179MDL07729420
BP-HZN-2179MDL07729421
BP-HZN-2179MDL07729422
BP-HZN-2179MDL07729423
BP-HZN-2179MDL07729424
BP-HZN-2179MDL07729425
BP-HZN-2179MDL07729426
BP-HZN-2179MDL07729427
BP-HZN-2179MDL07729428
BP-HZN-2179MDL07729429
BP-HZN-2179MDL07729430
BP-HZN-2179MDL07729431
BP-HZN-2179MDL07729432
BP-HZN-2179MDL07729433
BP-HZN-2179MDL07729434
BP-HZN-2179MDL07729435
BP-HZN-2179MDL07729436
BP-HZN-2179MDL07729437
BP-HZN-2179MDL07729438
BP-HZN-2179MDL07729439
BP-HZN-2179MDL07729440
BP-HZN-2179MDL07729441
BP-HZN-2179MDL07729442
BP-HZN-2179MDL07729443
BP-HZN-2179MDL07729444
BP-HZN-2179MDL07729445
BP-HZN-2179MDL07729446
BP-HZN-2179MDL07729447
BP-HZN-2179MDL07729448
BP-HZN-2179MDL07729449
BP-HZN-2179MDL07729450
BP-HZN-2179MDL07729451
BP-HZN-BLY00000001
BP-HZN-BLY00000201
BP-MDL2179VOL000168-001
BP-MDL2179VOL000168-002
BP-MDL2179VOL000168-003
SNL093-017659
TRN-HCEC-00026904
TRN-INV-00008580
TRN-INV-01544188
TRN-INV-01871788
TRN-INV-01871789

TRN-MDL-01065224
TRN-MDL-01851720



Riser Videos

BP-HZN-2179MDL02349934
BP-HZN-2179MDL00330291
BP-HZN-2179MDL02340771
BP-HZN-2179MDL02341205
BP-HZN-2179MDL02342268
BP-HZN-2179MDL02344485
BP-HZN-2179MDL02346316
BP-HZN-2179MDL02347881
BP-HZN-2179MDL02347971
BP-HZN-2179MDL02348131
BP-HZN-2179MDL02348200
BP-HZN-2179MDL02348245
BP-HZN-2179MDL02348729
BP-HZN-2179MDL02349547
BP-HZN-2179MDL02349731
BP-HZN-2179MDL02349731
BP-HZN-2179MDL02349877
BP-HZN-2179MDL02349934
BP-HZN-2179MDL02350055
BP-HZN-2179MDL02351758
BP-HZN-2179MDL02351831
BP-HZN-2179MDL02353900
BP-HZN-2179MDL02355703
BP-HZN-2179MDL02357799
BP-HZN-2179MDL02364735
BP-HZN-2179MDL02365196
BP-HZN-2179MDL02365566
BP-HZN-2179MDL02367610
BP-HZN-2179MDL02367611
BP-HZN-2179MDL02368421
BP-HZN-2179MDL02369126
BP-HZN-2179MDL02369388
BP-HZN-2179MDL02370865
BP-HZN-2179MDL02372295
BP-HZN-2179MDL02378637
BP-HZN-2179MDL03096420
BP-HZN-2179MDL03096421
BP-HZN-2179MDL03096424
BP-HZN-2179MDL03096425
BP-HZN-2179MDL03096426
BP-HZN-2179MDL03096427
BP-HZN-2179MDL03096428
BP-HZN-2179MDL03096429
BP-HZN-2179MDL03096537
BP-HZN-2179MDL03096552

BP-HZN-2179MDL03096559
BP-HZN-2179MDL03096560
BP-HZN-2179MDL03096561
BP-HZN-2179MDL03096567
BP-HZN-2179MDL03096568
BP-HZN-2179MDL03096570
BP-HZN-2179MDL03096571
BP-HZN-2179MDL03096572
BP-HZN-2179MDL03096573
BP-HZN-2179MDL03096574
BP-HZN-2179MDL03776298
BP-HZN-2179MDL03776299
BP-HZN-2179MDL03776300
BP-HZN-2179MDL04569866
BP-HZN-2179MDL04569867
BP-HZN-2179MDL04569868
BP-HZN-2179MDL04569869
BP-HZN-2179MDL04569870
BP-HZN-2179MDL04569871
BP-HZN-2179MDL04569872
BP-HZN-2179MDL04569874
BP-HZN-2179MDL04569876
BP-HZN-2179MDL04569877
BP-HZN-2179MDL04569878
BP-HZN-2179MDL04569879
BP-HZN-2179MDL04569880
BP-HZN-2179MDL04569881
BP-HZN-2179MDL04569882
BP-HZN-2179MDL04569883
BP-HZN-2179MDL04569884
BP-HZN-2179MDL04569885
BP-HZN-2179MDL04569886
BP-HZN-2179MDL04569887
BP-HZN-2179MDL04569888
BP-HZN-2179MDL04569889
BP-HZN-2179MDL04569890
BP-HZN-2179MDL04569891
BP-HZN-2179MDL04569892
BP-HZN-2179MDL04569893
BP-HZN-2179MDL04569894
BP-HZN-2179MDL04569895
BP-HZN-2179MDL04569896
BP-HZN-2179MDL04569897
BP-HZN-2179MDL04569898
BP-HZN-2179MDL04569899



BP-HZN-2179MDL04569900
BP-HZN-2179MDL04569901
BP-HZN-2179MDL04569902
BP-HZN-2179MDL04569903
BP-HZN-2179MDL04569904
BP-HZN-2179MDL04569905
BP-HZN-2179MDL04569906
BP-HZN-2179MDL04569907
BP-HZN-2179MDL04569908
BP-HZN-2179MDL04569909
BP-HZN-2179MDL04569910
BP-HZN-2179MDL04569911
BP-HZN-2179MDL04569912
BP-HZN-2179MDL04569914
BP-HZN-2179MDL04569915
BP-HZN-2179MDL04569916
BP-HZN-2179MDL04569917
BP-HZN-2179MDL04569918
BP-HZN-2179MDL04569919
BP-HZN-2179MDL04569920
BP-HZN-2179MDL04569921
BP-HZN-2179MDL04569922
BP-HZN-2179MDL04569923
BP-HZN-2179MDL04569924
BP-HZN-2179MDL04569925
BP-HZN-2179MDL04569926
BP-HZN-2179MDL04569927
BP-HZN-2179MDL04569928
BP-HZN-2179MDL04569929
BP-HZN-2179MDL04569930
BP-HZN-2179MDL04569940
BP-HZN-2179MDL04569961
BP-HZN-2179MDL04569964
BP-HZN-2179MDL04569966
BP-HZN-2179MDL04569970 (entire drive)
BP-HZN-2179MDL04569971 (entire drive)
BP-HZN-2179MDL04947818
BP-HZN-2179MDL06004627
BP-HZN-2179MDL06530476
BP-HZN-2179MDL06530477
BP-HZN-2179MDL06530478
BP-HZN-2179MDL06530479
BP-HZN-2179MDL06530480
BP-HZN-2179MDL06530481
BP-HZN-2179MDL06530482
BP-HZN-2179MDL06530483
BP-HZN-2179MDL06530484
BP-HZN-2179MDL06530485

BP-HZN-2179MDL06530486
BP-HZN-2179MDL06530487
BP-HZN-2179MDL06530488
BP-HZN-2179MDL06684389
BP-HZN-2179MDL06684390
BP-HZN-2179MDL06684391
BP-HZN-2179MDL06684392
BP-HZN-2179MDL06684391
BP-HZN-2179MDL06684433
BP-HZN-2179MDL06684442
BP-HZN-2179MDL06684451
BP-HZN-2179MDL06684461
BP-HZN-2179MDL06684462
BP-HZN-2179MDL06684463
BP-HZN-2179MDL07380383
BP-HZN-2179MDL07380384
BP-HZN-2179MDL07380385
BP-HZN-2179MDL07380386
BP-HZN-2179MDL07380387
BP-HZN-2179MDL07380388
BP-HZN-2179MDL07380389
BP-HZN-2179MDL07380390
BP-HZN-2179MDL07380391
BP-HZN-2179MDL07380392
BP-HZN-2179MDL07380393
BP-HZN-2179MDL07380394
BP-HZN-2179MDL07380395
BP-HZN-2179MDL07380396
BP-HZN-2179MDL07380397
BP-HZN-2179MDL07380409
BP-HZN-2179MDL07380456

Other Materials

MDL Deposition Exhibit 9361

MDL Deposition Exhibit 9183

Multiflash Fluid Definition file ("CL68379-DEC-EOS20120322.MFL") provided by Dr. C. Whitson.

Photograph of partial riser joint with buoyancy module. (See p. F-4-2 of report)

Photograph of riser strapped with buoyancy module showing gap between pipe wall and module. (See p. F-4-4 of report)

Appendix E - Slug Timing

Introduction

From my review of ROV video footage at the end of the DWH riser, I observed slugging behavior between May 13, 2010 and May 20, 2010. I timed and recorded the duration of the oil-dominant and gas-dominant slugs that I observed. I performed this review for different days within the May 13 to May 20 time-frame (see Table 1 for a list of days reviewed). I used this information in the analysis of simulation results and to configure the motion of the riser.

This appendix identifies the ROV video footage that I used in the timing analysis and the values that were recorded.

Methodology and Terminology

All the data was recorded through visual observation of videos of riser end plume. Videos from the “Plume Monitoring” and “Chemical Dispersing Ops” folders in the hard drive labeled BOS-007402 (BP-HZN-2179MDL04569966) were reviewed.

The terminology used in the recorded data is defined below:

- Oil Duration: Duration during which the plume is observed to be predominantly dark.
- Transition: Period during which the color of the plume is observed to change rapidly.
- Gas Duration: Duration during which the plume is observed to be predominantly white.

While the oil duration and the transition out of the oil duration are clearly discernible, the start of a gas duration as well as the transition out of the gas duration were less distinct and therefore subject to greater measurement uncertainty.

As discussed and defined in the main report (see Section 6.2) , double peak behavior was observed between May 13 and 16 and the timings of the two alternating periods of oil-dominant and gas-dominant flows have been recorded individually for the period when this behavior was exhibited.

Results

Durations

Table 1 lists the durations of the gas and oil peaks for a number of different videos between May 13 and May 20. Double peak behavior is clearly visible until the morning of May 15. The highlighted row displays the slug timings that were recorded around midnight on May 16. This video was taken simultaneously with the ROV XLX-36 video survey of the moving sections of the riser. Taken together, these videos reveal the slug period is the same as the period of the riser motion cycle.

Table 1 – Summary of recorded timings – all timings are in seconds and based on averages of multiple slugging cycles

Date/Time	Period ¹	Oil Duration 1	Gas Duration 1	Oil Duration 2	Gas Duration 2
5/13 3:00	285	-	-	-	-
5/13 16:00	250	77	28	29	74
5/13 21:40	240	84	30	23	58
5/14 17:30	210	70	36	18	30
5/15 0:30	200	84	38	22	22
5/16 0:00	183	89	56	NA	NA
5/18 0:00	172	68	26	NA	NA
5/19 23:15	165	60	14	NA	NA
5/20 3:42	160	50	8	NA	NA

Period

The overall slugging period is shown in Figure 1. The points in red show the period of the riser motion based on the XLX-37 survey on May 13, and the XLX-36 survey on May 16.

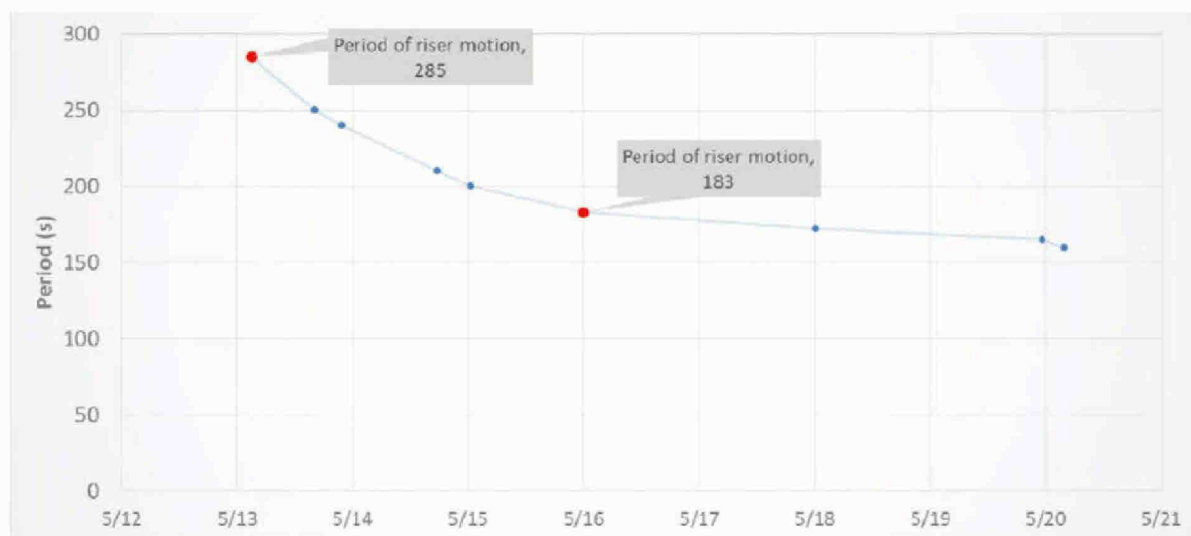


Figure 1 – Slug timings chart showing riser motion period fits the curve well, and reduction in period over time

Conclusions

The analysis provides several insights:

1. Double peak behavior is exhibited from May 13 until the morning of May 15 and is absent after May 16

¹ The duration of the overall repeating pattern of alternating flows.

2. On May 16 the slug period and the period of riser motion were observed simultaneously and were identical.
3. The overall slug flow period is declining over time. The period of the riser motion on May 13 (based on the XLX-37 survey) and May 16 (based on the ROV XLX-36 survey) matches the trend of the overall period of slugging. This validates the May 13 slug flow period that was calculated from the ROV survey data on the same date.

Appendix F – Model Construction

Introduction

Dynamic pipeline simulation models require a number of inputs describing the construction of the pipeline to accurately model the thermo-hydraulic processes.

This appendix, together with other related appendices, documents the inputs, along with their sources, to the Kink and No-Kink models that were used to estimate the flow rate through the DWH riser.

Riser Construction

The riser was primarily constructed in 90 foot sections (called joints) joined together by flanged connections. The *Deepwater Horizon* was carrying an inventory of these 90 foot riser joints which were used to construct the riser.¹ The riser pipe was a steel pipe with 19.5" internal diameter.² Some joints were 7/8" thick while most were 1" thick.¹

Many of the riser joints were covered with a buoyancy material, generically called *syntactic foam*³. For the DWH, syntactic foam buoyancy modules were manufactured by Cuming Corporation (see Appendix F-4). The buoyancy modules were rated for different depths and the depth rating is identifiable by a color-coded strip at the end of each module.⁴ The modules are supplied as two halves which are fastened together around the riser pipe (see Figure 1). The modules, once strapped together, have a hollow cylindrical cross-section with cut-outs to accommodate the auxiliary lines on the outside of the drilling riser. The outer diameter of the buoyancy modules was 52 inches.¹ The modules were 168.5 inches (~14 feet) in length and thus six (6) modules (or twelve halves) were used on each riser joint, exposing 2.875 feet of bare riser pipe on either side of buoyancy module-covered joints. The buoyancy modules that were closest to the DWH vessel were visibly damaged in the ROV survey videos. As the riser fell to the seafloor, some joints also lost entire 168.5-inch sections of buoyancy module exposing more of the 90 foot riser joint to the seawater (see Figure 2 for an example).

¹ TRN-INV-01871789.

² TRN-INV-01871789.

³ Cuming Corporation, Technical Note 100-1-A, "Introduction to Syntactic Foam," available at <http://cuming.mosaicmedia.com/wp-content/uploads/2012/06/TN-100-1-A-7-11-12.pdf>.

⁴ <http://www.cumingcorp.com/c-float-tech-data/>.



Figure 1 - two halves of DWH buoyancy modules⁵



Figure 2 -Riser Joint with 5 of the 6 buoyancy modules⁶

Inputs

The information required to model the various pieces of the DWH riser is tabulated in Table 1 through Table 4.

Table 1 - Summary of riser properties used in the model

Element	Property	Value	Comment/Source
Riser Section: LMRP Top – Joint 1	Geometry	19.5" ID with two 5.5" OD riser pipes	The Hydraulic diameter used was calculated based on this geometry. BP-HZN- 2179MDL00477088

⁵ BP-HZN-2179MDL07729355.

⁶ BP-HZN-2179MDL07729451.

Element	Property	Value	Comment/Source
	Elevation Profile	Estimated	Estimated based on CAD drawings, and ROV footage (see Appendix F-1).
	Leak Sizes	Hole C – 0.41” diameter Holes D+E – 0.41” diameter Hole B – 0.47” diameter	I received the information from Dr. Srdjan Nestic.
	Length	45 ft	Estimated based on Welaptega report and available pup joints on DWH listed in TRN-INV-01871789.
	Roughness	0.0018 inch	Smooth pipe roughness. Sensitivities were performed varying roughness from 0.0018 – 0.18 inches.
Riser Section: Joint 1 to Riser End	Elevation Profile	Calculated	CAD Drawings, ROV Footage (see Appendix F-1)
	Geometry	19.5" ID, with 5.5" and 6.625" concentric riser pipe	BP-HZN-2179MDL04826982. See Appendix F-2 for calculation of hydraulic diameter.
	Length	90 ft	TRN-INV-01871789
	Burial depth between joints 2 and 9	Estimated	CAD Drawings, ROV Footage (see Appendix F-1)
	Burial depth between joints 45 and riser end	Estimated	CAD Drawings, ROV Footage (see Appendix F-1)
	Roughness	0.0018 inch	Smooth pipe roughness. Sensitivities performed varying roughness from 0.0018 – 0.18 inches.

Table 2 – Summary of kink properties used in the model

Element	Property	Value	Source
Kink (Modeled as a Valve)	Opening	Study parameter	Varying this restriction changes the flow rate through the system. Varied to assess slugging characteristics at various flow rates.

Element	Property	Value	Source
	Discharge Coefficient	0.84	Sensitivities were performed from 0.61 – 1.

Table 3 – Summary of fluid properties used in the model

Element	Property	Value	Source
Reservoir Fluid	Composition	CL68379-DEC	Decontaminated sample composition from Core Lab sample 68379. MultiFlash fluid definition file from Dr. Curtis Whitson.
	Temperature (No Kink Model)	80 C	Temperature downstream of LMRP measured at 105 °C after riser cut. Temperature at joint 1 calculated by Kink model is 80-95 °C for flow rate between 1,000 to 35,000 stbpd. Sensitivities performed at 95 C and 65 C.
	Temperature (Kink Model)	105 C	PNAS report ⁷
	Source Flow Rate (No Kink Model)	Study parameter	Varied to assess slugging characteristics at various flow rates.

Table 4 – Summary of properties related to heat transfer used in the model

Element	Property	Value	Source
Seawater	Temperature	4.4 C	NOAA NODC Regional Climatology www.nodc.noaa.gov/cgi-bin/OC5/GOMclimatology/gomregcl.pl
	Outer Heat Transfer Coefficient	1000 W/m ² /K	LedaFlow default. Sensitivity study performed for free convection case and forced convection at 1 m/s seawater velocity.

⁷ Reddy, C. M. et al., 2011, Composition and fate of gas and oil released to the water column during the Deepwater Horizon oil spill.

Element	Property	Value	Source
Soil	Thermal Conductivity	1.4 W/m/K	See Appendix F-3
	Density	1457 kg/m ³	See Appendix F-3
	Heat Capacity	2093 J/kg/K	See Appendix F-3
Carbon Steel	Thermal Conductivity	45.026 W/m/K	See Appendix F-3
	Density	7850 kg/m ³	See Appendix F-3
	Heat Capacity	470 J/kg/K	See Appendix F-3
Buoyancy Module - Black	Thermal Conductivity	0.105 W/m/K	See Appendix F-4
	Density	28.5 lb/ft ³	See Appendix F-4
	Heat Capacity	1280 J/kg/K	See Appendix F-4
Buoyancy Module - Orange	Thermal Conductivity	0.105 W/m/K	See Appendix F-4
	Density	27.93 lb/ft ³	See Appendix F-4
	Heat Capacity	1280 J/kg/K	See Appendix F-4
Buoyancy Module - Yellow	Thermal Conductivity	0.105 W/m/K	See Appendix F-4
	Density	25.44 lb/ft ³	See Appendix F-4
	Heat Capacity	1280 J/kg/K	See Appendix F-4
Buoyancy Module - Green	Thermal Conductivity	0.105 W/m/K	See Appendix F-4
	Density	23.54 lb/ft ³	See Appendix F-4
	Heat Capacity	1280 J/kg/K	See Appendix F-4
Buoyancy Module - Blue	Thermal Conductivity	0.105 W/m/K	See Appendix F-4
	Density	21.99 lb/ft ³	See Appendix F-4
	Heat Capacity	1650 J/kg/K	See Appendix F-4

Fluid Properties

The properties of the fluid were taken from Multiflash fluid definition files provided by Dr. Curtis Whitson. Multiple fluid definition files were provided for 8 fluids (4 bottom-hole samples, 4 decontaminated fluids). For each fluid definition file, the equation of state parameters were identical but the compositions were different. For this work, "CL68379-DEC-EOS20120322.MFL" was used. For the sake of completeness of the work, sensitivities were performed using the other decontaminated sample fluid files.

Using Multiflash, a PVT (pressure, volume, temperature) table was generated. A PVT table is a file that contains the required fluid properties necessary to perform pipeline simulations. A PVT table is generated by calculating the fluid properties such as viscosity, density, gas mass fraction, enthalpy, specific heat capacity, surface tension, and others over a range of pressures and temperatures which span the operating conditions of the riser. A temperature range from -10 to 107.8 °C and a pressure

range of 135 to 320 bar were used to generate the PVT table. The same PVT table was used for all simulations.

Boundary Conditions

The boundary conditions for both Kink and No-Kink models are the same at the Riser End, which is a constant pressure of 152.5 bara. At the inlet the boundary conditions used by the two models are described in Table 5.

Table 5 - Inlet boundary description for Kink and No-Kink models

Model	Inlet Boundary		
	Type	Value	Temperature
Kink	Pressure	600 psig ⁸	80 C ± 15 C
No-Kink	Mass Flow	Study Parameter	80 C ± 15 C

Kink Leaks

In my model, the leak holes are treated as circular holes with hydraulic diameters. I relied upon area and perimeter data I received from Dr. Srdjan Nestic. Specifically, the area and perimeter for each hole can be found in Appendix F-2.

In my model, I placed the kink leaks upstream of the kink valve exposing them to the highest possible pressure, thus yielding the most conservative (highest) estimate of leak flow rate. In reality, the kink leaks are at the throat of the kink where the pressure would have been the lowest (even lower than the pressure downstream). More details can be found in Appendix F-2.

Riser Elevation Profile

The riser elevation profile is an important parameter to modeling the system. Figure 3 shows the profile of the riser after it completely settled to the sea floor, as well as the profile of the buoyant loop at its peak position on May 13 and May 15. The peak of this high position gradually reduced until the riser remained in the low position starting May 21.

⁸ BP-HZN-2179MDL06314451.

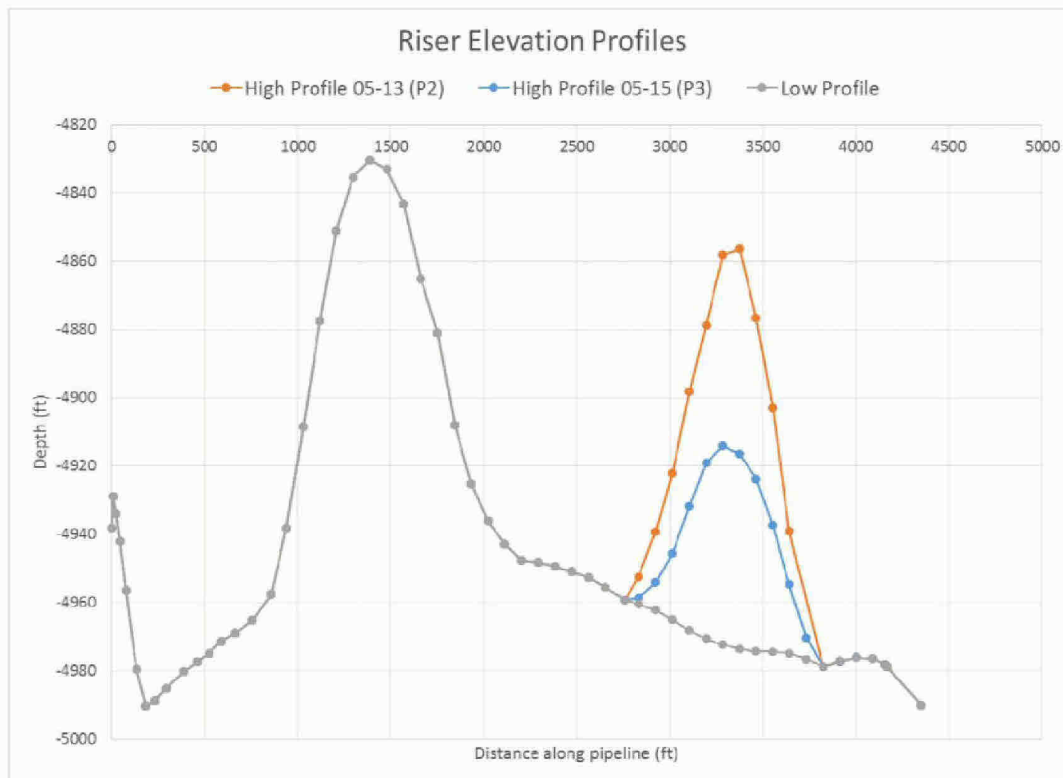


Figure 3 – Riser elevation profiles showing the buoyant Loop on the sea floor (Low), and its peak position on May 13 and May 15

Appendix F-1 contains a detailed discussion of how the riser profile positions were determined. Appendix F-5 contains a detailed discussion of how the riser motion was characterized and used in my models.

Thermal Modeling

A reservoir fluid is at its hottest temperature as it flows out of the reservoir. As the fluid flows upwards, its temperature is lowered by two mechanisms: (a) heat loss to the colder environment and (b) energy loss as the fluid travels up the well and through the riser. To model the first mechanism accurately, a detailed description of the surrounding conditions needs to be provided to the simulator. The second mechanism requires an accurate characterization of the fluid composition and an accurate estimation of the pressure loss.

In the current context, the model starts downstream of the BOP and the flow proceeds through the riser pipe. The model assumes a circular cross-section for the pipe and allows for concentric layers of other materials around the pipe until an effectively infinite heat sink, such as the seawater, is reached. Accurate thermal modeling requires inputs for thickness, thermal conductivity, density, and specific heat capacity of each layer of material around the fluid (starting with the pipe wall itself). A brief description of values used for each layer and how they were determined is given below. For a more detailed discussion including references, please see Appendix F-3.

Seawater

For the seawater, the temperature and convective heat transfer coefficient were included as inputs in the model. Typical values for sea water temperature of 4.4 °C and convective heat transfer coefficient of 1000 W/m²/K were used for this deepwater system. However, a sensitivity of the outer heat transfer coefficient using natural convection (where $H \approx 200$ W/m²/K) and a current velocity of 1 m/s ($H > 2000$ W/m²/K) were also simulated. Refer to Appendix F-3 for more details.

Riser pipe material

The riser pipe is constructed out of carbon steel. The thermal properties used for carbon steel are listed in Table 1. TRN-INV-01871789 lists all the riser joints carried on the DWH vessel. Based on this information, a thickness of 1" was used for the slick sections and the sections covered with black, yellow, and orange color-coded buoyancy modules, while 0.875" was used for sections covered with green and blue buoyancy modules.

Buoyancy Modules

The thermal properties of the various color-coded buoyancy modules are also listed in Table 1. The densities for the modules are listed in TRN-INV-01871789. For a detailed discussion including references to thermal properties for Cuming syntactic foam materials, see Appendix F-4.

Appendix F-1 – Riser Elevation Profile

Introduction

After the DWH drilling rig sank on April 22, 2010, the riser that connected the DWH wellhead equipment to the drilling rig fell to the seafloor. However, the riser did not completely settle on the seafloor until May 21, 2010. Between May 13 and May 20, part of the riser (the buoyant loop) was moving off the sea floor in a vertical oscillatory motion.¹ Once settled, it remained in that position until the riser was removed on June 3, 2010 to allow the installation of the Top Hat.²

In order to calculate the flow rate through the DWH riser during the May 13-20 period using transient pipeline modeling software, an accurate representation of the riser elevation profile was essential. Several ROVs were deployed after the accident in order to assist in the response operations. Among the tasks that the ROVs repeatedly carried out were surveys of the path of the riser. The data from these surveys were also made available in the form of three CAD drawings.³

The data from these surveys were used to construct a complete riser elevation profile that was then used in the simulations. This appendix provides background information, as well as detailed descriptions of the procedure used to extract the riser profile data.

Information Used and Conventions

Description of Elevation Profile

ROV surveys were used to extract Northing, Easting, and Depth coordinates.⁴ From these three-dimensional coordinates, lengths between points were calculated as the square root of the sum of squares of differences between successive coordinates. This calculation gives an L-Z coordinate profile, where L is length along the pipeline and Z is the depth. These calculated values can then be converted to an S-Z coordinate system where $S = \sqrt{L^2 - Z^2}$. This is the information supplied to simulators, i.e., a set of (S,Z) coordinates.

ROV Riser Path Surveys

Details of the source of the ROV riser surveys are listed in Table 1.

Table 1 – ROV Source Footage for Riser Surveys

Date	ROV Name	Start point	End point	Reference(s)
------	----------	-------------	-----------	--------------

¹ BP-HZN-2179MDL04996568.

² BP-HZN-2179MDL04996577.

³ BP-HZN-2179MDL04934351, BP-HZN-2179MDL06094683, BP-HZN-2179MDL05871047.

⁴ The terms easting and northing are geographic Cartesian coordinates for a point. Easting refers to the eastward-measured distance (or the x-coordinate), while northing refers to the northward-measured distance (or the y-coordinate).

May 08, 2010	XLX-10	Kink leak	Riser End	BP-HZN-2179MDL06684392 BP-HZN-2179MDL07380388
May 13, 2010	XLX-37	Joint 10	Joint 43	BP-HZN-2179MDL04569970
May 15-16, 2010	XLX-36	Joint 10	Joint 44	BP-HZN-2179MDL04569970

CAD Drawings

CAD drawings from May 4, May 8, and May 13 2010, were used as verification of the review of the ROV footage. Data for all three dates was extracted from the May 13 Riser Survey CAD file⁵. The ROV paths are embedded in the following layers: POINTS, Survey 051310, and Riser 050810. Only data from the POINTS layer was eventually used directly in the final profile.

Data Format

CSV Files

For the ROV XLX-37 and ROV XLX-36 riser inspection surveys, each video segment, roughly 30 minutes, has accompanying CSV files that list Northing, Easting, Depth, Alt (distance to bottom), and Heading (compass) against absolute clock time as well as relative time into the video segment. No such CSV files were available for the XLX-10 survey.

Visual Information from Various ROVs

The data that were visually available from the ROV footage are illustrated through screen captures of the footage in Figure 1 through Figure 3. While screen captures from XLX-37 and XLX-36 showed all the information available in the CSV files, screen captures from XLX-10 shows only Depth, Alt (distance to bottom), and Heading (compass) information.



Figure 1 – Screen capture of XLX-37 Riser Survey video on May 13, 2010

⁵ BP-HZN-2179MDL05871047.

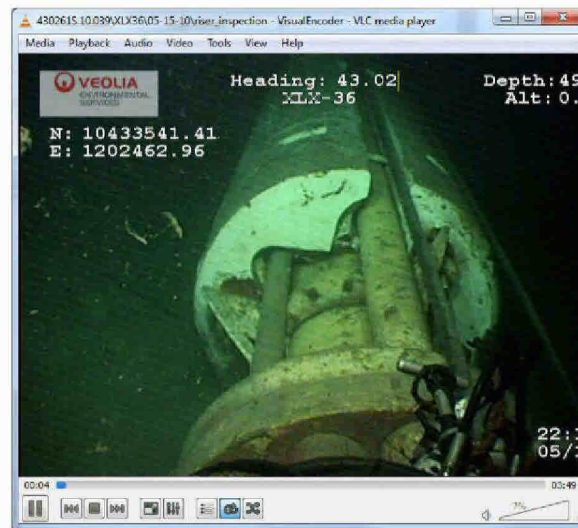


Figure 2 – Screen capture of XLX-36 Riser Survey video on May 15, 2010



Figure 3 – Screen capture of XLX-10 Riser Survey video on May 08, 2010

CAD Drawings

Using a CAD drawing viewer, the coordinates from the various layers of interest were extracted. Each point was represented by its X, Y, and Z coordinates with X corresponding to easting, Y with depth, and Z with northing.

Depth Basis

The data required for the elevation profiles were extracted from multiple ROV data and CAD drawings. However, because each of those sources had a different depth measurement offset, the ROV XLX-37

depth readings were chosen to serve as a common basis. All other depth sources were corrected based on overlapping data between those sources and XLX-37.⁶

Final Profiles

Three profiles were generated out of the review.

1. A profile, referred to as P1, with riser settled on the seafloor based on:
 - a. XLX-10 for the points upstream of joint 10 (the initial section of the riser attached to the BOP)
 - b. a mix of XLX-36 and XLX-37 for points downstream of joint 10 up to joint 44 (this includes the section of the riser with the buoyant loop)
 - c. XLX-10 data for points downstream of joint 44 (the final section of the riser).
2. A profile, referred to as P2, with joints 30-40 (the buoyant loop) at their peak positions as observed on May 13 incorporated into profile P1
3. A profile, referred to as P3, with joints 30-40 at their peak positions as observed on May 15 incorporated into profile P1

The three profiles are illustrated in Figure 4.

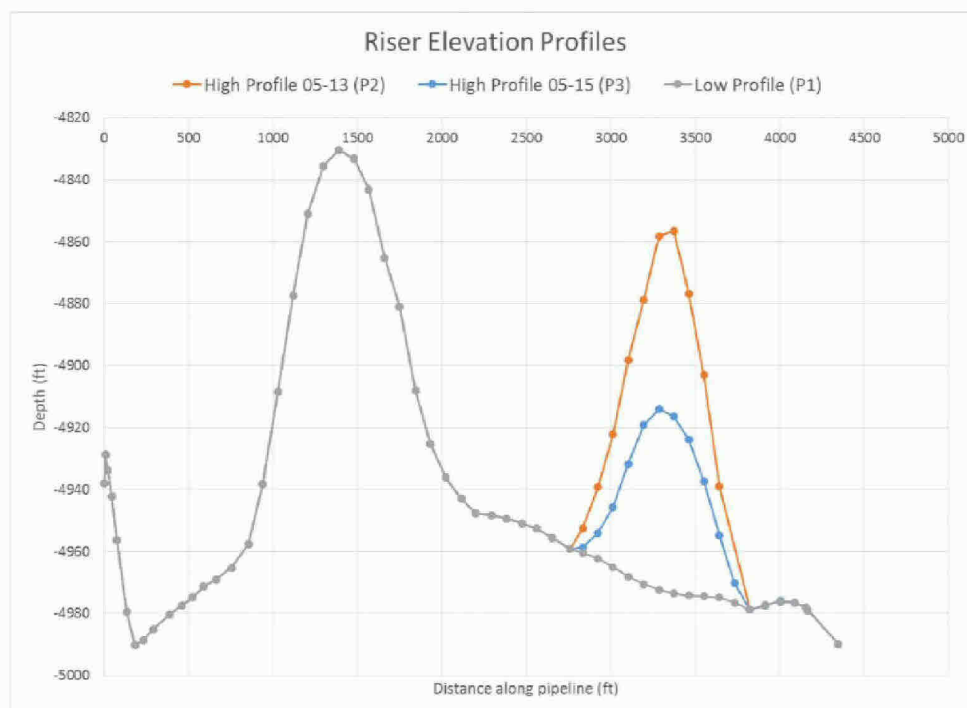


Figure 4 – Elevation profiles P1 (settled position), P2, and P3 (peak positions)

Riser Elevation Procedure

The overall riser elevation was assembled using different processes depending on the available information. Table 2 summarizes the sources of the information. The following sections describe the processes to assemble the elevation profile in greater detail.

⁶ The models do not utilize absolute depth but rather base their calculations on the relative change in elevation.

Table 2 – Source of ROV profile information

Point	Source
Top of BOP Stack	Estimated (see below)
Kink Throat	CAD POINTS ⁷
Upstream of Joint 1	CAD POINTS, XLX-10
Joint 1	CAD POINTS, XLX-10
Between Joint 1 and 2	CAD POINTS, XLX-10
Joint 2	CAD POINTS, XLX-10
Start Burial	CAD POINTS, XLX-10
Buried pipe	CAD POINTS, XLX-10
Buried pipe	CAD POINTS, XLX-10
Buried pipe	CAD POINTS, XLX-10
Buried pipe	CAD POINTS, XLX-10
Buried pipe	CAD POINTS, XLX-10
Buried pipe	CAD POINTS, XLX-10
Buried pipe	CAD POINTS, XLX-10
End Burial	CAD POINTS, XLX-10
Joint 9	CAD POINTS, XLX-10
Joint 10	XLX-10
Joint 11	XLX-10
Joint 12	XLX-10
Joint 13	XLX-10
Joint 14	XLX-10
Joint 15	XLX-10
Joint 16	XLX-10
Joint 17	XLX-10
Joint 18	XLX-37
Joint 19	XLX-37
Joint 20	XLX-37
Joint 21	XLX-37
Joint 22	XLX-37
Joint 23	XLX-36
Joint 24	XLX-37
Joint 25	XLX-36
Joint 26	XLX-36
Joint 27	XLX-36
Joint 28	XLX-36
Joint 29	XLX-36

⁷ All CAD Points in this table were obtained from BP-HZN-2179MDL05871047.

Point	Source
Joint 30	XLX-36
Joint 31	XLX-36 (Low), XLX-37 (High)
Joint 32	XLX-36 (Low), XLX-37 (High)
Joint 33	XLX-36 (Low), XLX-37 (High)
Joint 34	XLX-36 (Low), XLX-37 (High)
Joint 35	XLX-36 (Low), XLX-37 (High)
Joint 36	XLX-36 (Low), XLX-37 (High)
Joint 37	XLX-36 (Low), XLX-37 (High)
Joint 38	XLX-36 (Low), XLX-37 (High)
Joint 39	XLX-36 (Low), XLX-37 (High)
Joint 40	XLX-36 (Low), XLX-37 (High)
Joint 41	XLX-36
Joint 42	XLX-36
Joint 43	XLX-36
Joint 44	XLX-36
Joint 45	XLX-10
~Joint 46	XLX-10
Riser End	XLX-10

ROVs XLX-37 and XLX-36

The two surveys from XLX-37 on May 13 and XLX-36 on May 15 were used to extract data from joints 10 to 44. A total of 30 videos (10 from XLX-37 and 20 from XLX-36) were reviewed. As mentioned before, both these surveys had accompanying CSV files with each video segment. For the purpose of the video review, these CSV files were consolidated into one CSV file for each ROV containing all the data from one entire survey. The following procedure was used to obtain the information necessary for the riser elevation profile:

1. Video review
 - a. Record ROV measurements (Northing, Easting, Depth) when the ROV was at key locations on the riser
 - b. At moving joints, use the time varying coordinates to characterize the motion of the riser
2. Data extraction
 - a. Northing and easting are extracted as the averages for the period that the ROV is parked on the riser.
 - b. For XLX-37 where the data was noisy, depth was calculated as the median value of the period that the ROV was observing a joint. For XLX-36, averages were used.
 - c. For some joints, especially moving joints, depth data is not available due to data freeze or because the ROV does not observe the joint through an entire cycle of motion, thereby missing the peak or the bottom (or both). For these joints, depths were estimated by keeping the length of the joint as close as possible to 90 feet and ensuring that the overall elevation profile was visually smooth.

ROV XLX-10 on May 8

XLX-10 provides the only complete survey of the riser from the kink leaks all the way to the riser end. Unlike XLX-37 and XLX-36, the hard drive that contained XLX-10 videos did not contain CSV files with the corresponding path and depth information. This made it significantly more difficult to perform the reviews. Upon close review, it was found that the CAD POINTS layer contained northing, easting, and depth information corresponding to each point in the video when the ROV was parked at a fixed position. However, the depths in the CAD data did not correspond to the visual observation of depths in the videos. While the part of the riser up to joint 17 had already settled prior to the XLX-10 survey and this configuration did not change, the riser had still not settled to its final position. Similarly, past joint 44, the pipeline had already been buried underground making it unlikely that any change occurred to its position. By comparing the northing and easting information for joints 10 through 17 between the CAD POINTS layer and XLX-37, we were able to confirm that the CAD data for northing and easting matched the XLX-37 data closely. This allowed the extraction of northing and easting from the CAD data for joints upstream of joint 10, which were not available through XLX-37 and XLX-36. However, because of the mismatch of depth data between video visuals and CAD data, the depth data in the CAD data was not used. Instead minimum and maximum observed depth data shown on the videos was recorded and the average of these were taken as the depth. The depth information from XLX-10 was very stable (within ± 1 foot) and therefore there is little uncertainty in this data. XLX-10 depths for joints 10, 11, 14, and 17 were used to estimate the average depth measurement offset in XLX-10 depths in comparison to XLX-37. All other depths (for upstream of joint 10) were corrected by the average offset.

Specific Local Estimations

Kink Throat Location

No ROVs were able to park on the throat of the kink (where the leaks formed) to get a good location estimate. However, XLX-10 parked on a strap on joint 1 which was about 15 feet upstream of the first flanged joint. Later it also straddled the four corners of the base of the BOP. Assuming that the kink is close to the center of the BOP, the points (northing and easting) were plotted along with the plan of the riser. A straight line fit to the riser consisting of the point upstream of joint 1, joint 1, and a point 30 feet downstream of joint 1 was drawn and extrapolated. The point on the intersection of this extrapolated line and a diagonal joining the BOP corners was taken as the northing and easting for the kink throat (see Figure 5).

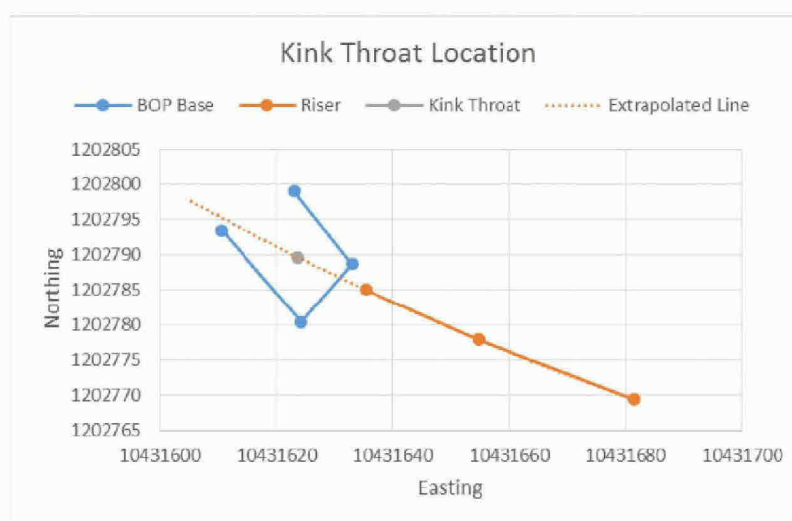


Figure 5 – Estimation of Kink Throat location

Kink Throat Elevation

Once the kink throat location (northing and easting) was estimated, another extrapolation was used to estimate the depth. I assumed that the riser angle did not vary from the last measured angle (between joint 1 and 15 feet upstream of joint 1) to the kink throat. Figure 6 illustrates how this calculation was performed.

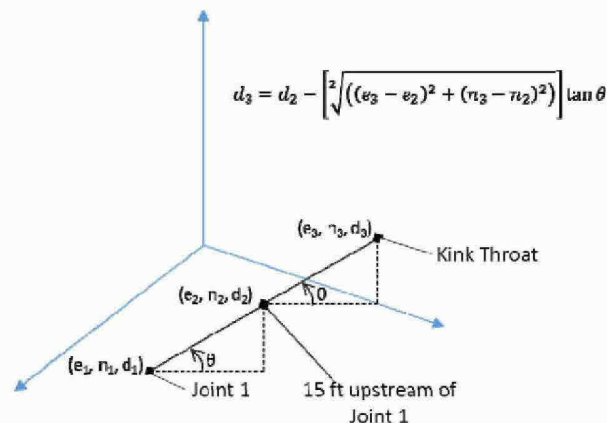


Figure 6 – Estimation of Kink Throat Depth

BOP Top Location

The location of the BOP top was estimated using a length of 45 feet (which is one of the pup joint lengths listed in TRN-INV-01871789) and approximating the BOP to be directly below the kink throat location. In other words, the BOP top northing and easting are the same as that of the kink throat and the depth is estimated such that the length of pipe between BOP top and start of joint 1 is exactly 45 feet.

Burial Depth: Joint 2 - 9

Just downstream of joint 2, the riser pipe goes underground and emerges back out just upstream of joint 9. The precise depth of burial is unknown and affects heat transfer because the fluid is significantly warmer than the surrounding environment at this point. The distance along the ground between joints 1 and 9 was calculated to be 715.1 feet. Based on 90 feet per joint, the actual riser length should be ~720 feet (8 joint X 90 ft / joint). With the riser OD being 21.5", the burial depth could not have been more than 1 foot. Therefore I used a burial depth of 300 mm (~ 1 foot).

Plume Location and Depth

The plume location could not be estimated from any ROV videos. However, the CAD drawing has a specific point marked as the plume location. Thus, the northing and easting points were taken directly from this CAD drawing.

XLX-10 survey goes beyond joint 44 and stops on points along the riser past joint 45 beyond which the riser goes underground. Using joints 43 and 44 to estimate the depth offset, when the ROV was parked directly above the plume its depth is approximately 4980 feet. The plume is approximately 10 feet down in the crater. Using this information the plume depth was estimated at 4990 feet. Sensitivity studies have been performed with the plume depth at + 5 ft from this estimate.

Smoothing

The best estimated profiles were assembled based on all the information above and are illustrated above in Figure 4. These profiles contain sharp angle changes at the location of the joints. A numerical interpolation program⁸ was used to generate a smoother profile so as not to create sharp angle changes which are unrealistic. Smooth riser profiles were generated because it is intuitive, and evident from the videos, that the riser bends along its length and not at the flange locations. The smoothed profiles for P1 and P2 are illustrated in Figure 7. Note that the smoothing procedure ensures that the profile passes through all the known points that are part of the unsmoothed profiles.

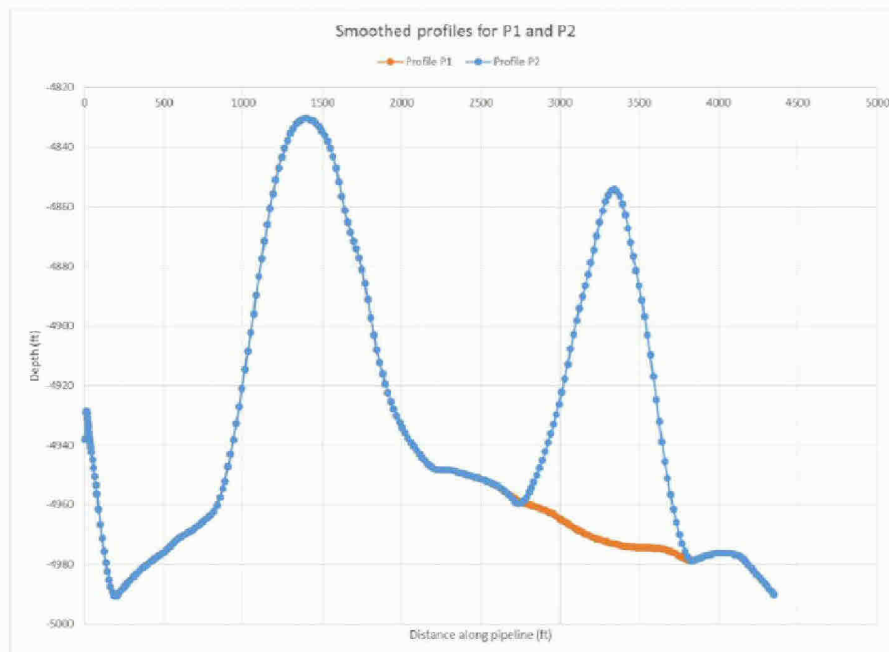


Figure 7 – Smoothed riser profiles for P1 and P2

Uncertainties

There are several uncertainties in the estimation of riser profiles. In this section these uncertainties are discussed.

Kink Location

As described previously, the kink location was estimated using straight line interpolation from available coordinate information. While this estimate may have some uncertainty, for the purpose of this investigation, the kink location has no effect on the estimate of Riser End flow. Moreover, the leak rate through the Kink is a strong function of the leak hole geometry and a weak function of its location (in a 1D model). Therefore this uncertainty has no effect on my conclusions and no sensitivities were performed around this estimate.

⁸ SciPy (<http://docs.scipy.org/doc/scipy/reference/tutorial/interpolate.html>).

XLX-10 Depth Estimates

The XLX-10 depths were visually recorded. The low variability in displayed depths and good match on points where overlapping measurements are available from other ROV surveys make the uncertainty in the estimates fairly low. As a result, no sensitivity is required for this estimate.

XLX-37 May 13 Peak Estimates

Two points from XLX-37 on the moving part of the riser are uncertain. They have been estimated to generate a smooth elevation profile and also meeting the 90 foot riser joint length constraint.

- Joint 35 has two peaks which were quite different from each other. Data for the first peak was a lot noisier than data for the second peak; therefore, the second peak data was used.
- Both joint 39 and 40 have estimated peak depths because, during the survey of joint 39, the ROV data froze. As a result, the measurements have a gap of over four minutes during which the data was frozen. The ROV moved away from joint 39 without capturing the peak position data. When the data comes back, the ROV is at joint 40. However, the start of the data for joint 40 is too high and would only be possible if the pipeline were kinked at joint 39.

Data from the May 15 riser survey shows that the movement is very regular and periodic and the peak depths form a smooth profile. Given this information, the estimates of the depths using the joint length constraint are reasonable estimates.

Appendix F-2 – Riser Geometry

Introduction

This appendix contains information about the actual riser and drill pipe diameters and the calculated hydraulic diameters that were used as model input parameters. A separate appendix (Appendix F-1) covers the riser elevation profile.

Riser Geometry

The riser geometry was largely (excluding the kinked section) taken from the well schematic.¹ The riser tube has an internal diameter of 19.5 inches.

A drill pipe was present in the riser; the outer diameter of that drill pipe varied with depth. Table 1 lists the key transitions of the drill pipe outer diameter.

Table 1 – Key drill pipe running lengths

From	To	Diameter (in)	Length (ft)
Top of LMRP	End of 2 drill pipes	2 drill pipes each is 5.5	22.09
End of 2 drill pipes	Drill Pipe OD Transition	5.5	861.62
Drill Pipe OD Transition	Riser End	6.625	3464.80

After the DWH sank on April 22, 2010, the riser that connected the well to the drilling rig fell to the seafloor and a kink was created just downstream of the lower marine riser package (LMRP). Figure 1 shows the complicated geometry of the kinked section of the riser. The geometry of this kinked section was not well understood until it was removed and analyzed by Welaptega.²

¹ BP-HZN-2179MDL00477088.

² BP-HZN-2179MDL04824968-5017.

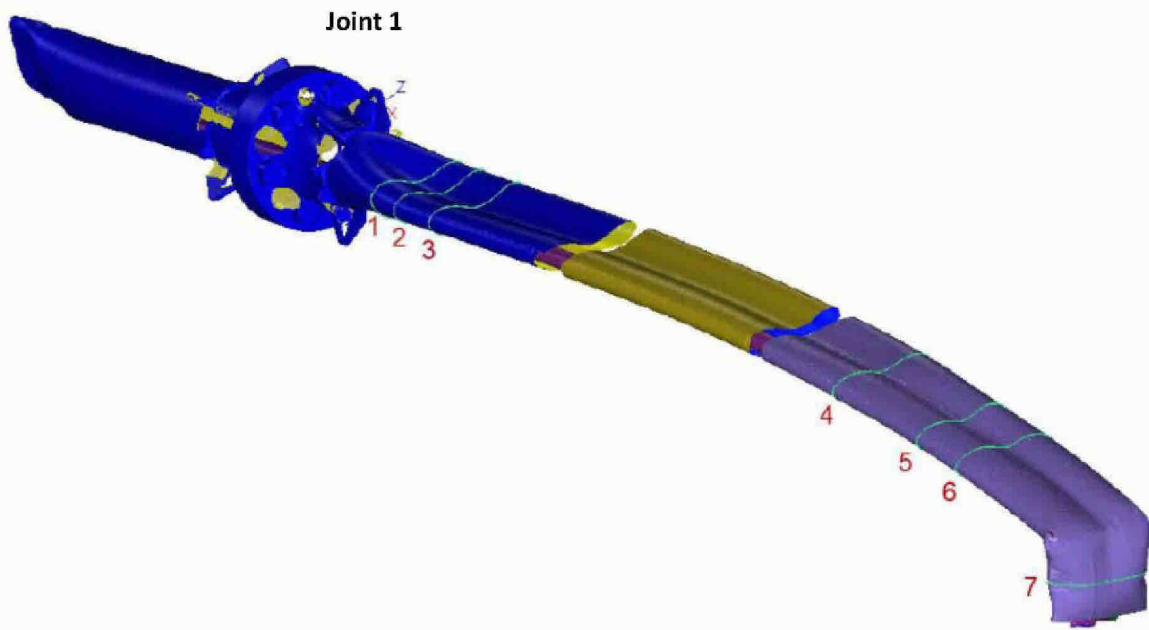


Figure 1 - Kinked section of the riser.

Two drill pipes were lodged in the kinked section.³ Figure 2 shows a photograph of the upstream section the riser that was removed (i.e. the part of the riser just downstream of the top of the LMRP). From the image it is clear that two drill pipes were lodged in the kink.



Figure 2 – Upstream section of the removed riser segment

Figure 3 shows both drill pipes that were inside the kinked section of the riser just downstream of the cut closest to the LMRP. One of the drill pipes stops 138 inches downstream of the cut closest to the LMRP.³

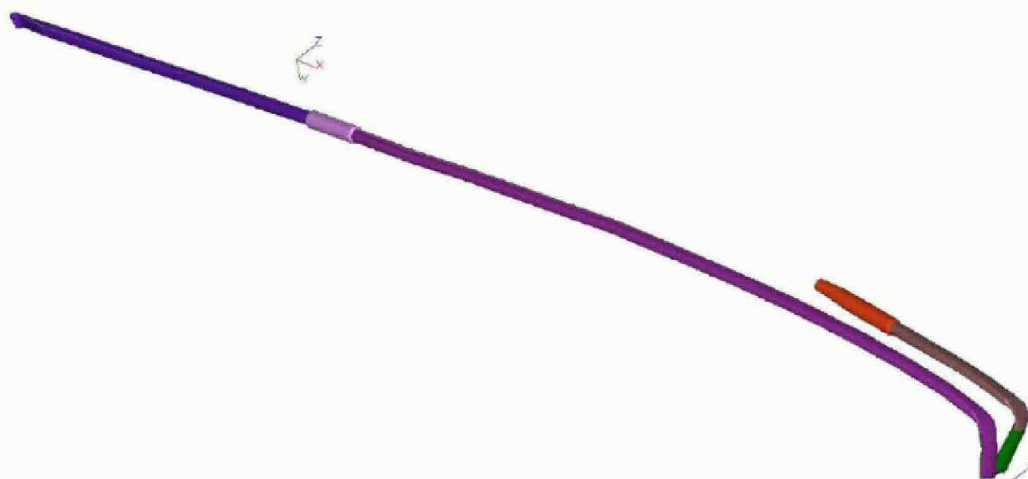


Figure 3 – Drill pipes inside the kinked section of the riser.

³ BP-HZN-2179MDL04824968-5017.

As a conservative assumption an additional 16 inches of riser pipe was added to the Kink model to account for the pipe that remained attached to LMRP after the kinked section was removed.

Hydraulic Diameter

The drill pipe inside the riser was capped at the end of the riser on May 5 and thereafter the flow through the riser pipe was only in the annular portion of the riser.⁴ A hydraulic diameter is a common engineering approach used to model non-circular geometries. Since both OLGA and LedaFlow assume a circular geometry, the following equation was used to calculate the hydraulic diameter of the annular cross section of the riser including the drill pipe(s):

$$d_h = \frac{4A}{P} = \frac{\pi (D^2 - d^2)}{\pi(D + d)} = D - d$$

where

D is the internal diameter of the riser

d is the external diameter of the drill pipe

A is the cross-sectional area available for flow

P is the wetted perimeter (the perimeter of the riser exposed to fluid)

Table 2 lists the hydraulic diameters calculated for various portions of the DWH riser.

Table 2 – Calculated hydraulic diameter used as model parameters

Section	Area (in ²)	Perimeter (in)	d _h (in)
2 5.5" drill pipes	251	96	10.5
5.5" drill pipe	275	78.5	14
6.625 drill pipe	264	82	12.875
Kink	12.9 ⁵	80	4

Kink

To estimate the discharge from the kink leaks, my model was extended to include the kinked section. This introduced an additional uncertainty of how to address the resistance created by the complicated flow path through the kink. To account for the unknown resistances and blockages in the flow path (see Figure 4 for an example), the kink was hydraulically modeled as valve.

While it is recognized that this is a rough approximation, for the purpose of this work, this approximation will have minimal or no impact on the result. This is because the flow rate discharged from the riser end was previously determined independently. For the Kink model, the valve position (or kink resistance) was then adjusted to match the flow rate discharged from the riser end.

⁴ FRTG, "Assessment of Flow Rate of the Deepwater Horizon / Macondo Well Oil Spill" (MDL Dep. Ex. 9005) at 3; BP-HZN-2179MDL02172464

⁵ The smallest cross-sectional area of the kink was used to calculate the hydraulic diameter of the valve that represented the kink resistance. More details are provided in this section.



Figure 4 – Blockage in the kinked section of the riser⁶

Leaks

The leak holes are treated as circular holes with hydraulic diameters (d_h). Since it is not possible to place leaks at the same location of the valve that represents the kink), the leaks were placed upstream of the valve, exposing them to the highest possible pressures. This results in higher estimates of kink leak flow rates. In reality, the kink leaks are at the throat of the kink where the pressure would have been the lowest. Table 3 shows the hydraulic diameters which were calculated based on detailed measurements of the kink holes.⁷ It is unclear from the ROV videos whether Hole D was leaking during the period of my investigation. As a result, I assumed that Hole D was leaking because that assumption provides an even more conservative (higher) estimate of flow rate from leak.

Table 3 – Calculated hydraulic diameter of kink leak holes.

Hole	Area (in ²)	Perimeter (in)	d_h (in)
B	0.175	1.5	0.47
C	0.276	2.7	0.41
D+E	0.276	2.7	0.41

⁶ BP-HZN-2179MDL00269156-259 at 269255.

⁷ Area and perimeter provided to me by Dr. Srdjan Nestic.

Appendix F-3 – Heat Transfer Properties

Introduction

Multiphase simulators require a description of the materials surrounding the fluid as it flows through the pipeline in order to accurately simulate the heat exchanged between the fluid and its environment. This appendix describes how the heat transfer was modeled for the DWH riser pipe. This includes the calculation of effective thermal properties used for the various materials.

Heat Transfer Model

In the simulator used in this work (LedaFlow), the “walls” around the fluid were modeled as concentric layers with varying thermal properties (see Figure 1). In LedaFlow, the WALL (DYNAMIC) option was used. This option accurately models the thermal behavior of the walls, accounting for the storage of heat in each layer.

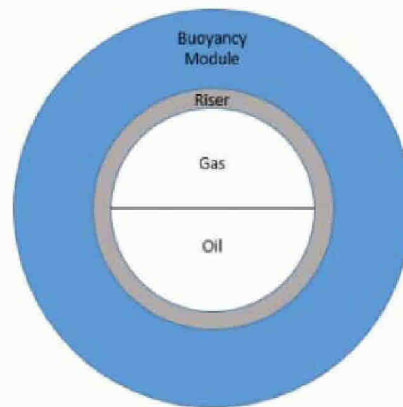


Figure 1 – Example of wall as modeled in multiphase flow simulators.

Materials

The materials and thermal properties used to model heat transfer in the riser are shown in Table 1. These properties were modified to account for various factors which are discussed later in this Appendix.

Table 1 – Unmodified Thermal Properties of Materials

Name	Heat Capacity		Thermal Conductivity		Density	
	SI (J/kg/K)	British (BTU/lb/F)	SI (W/m/K)	British (BTU/hr/ft/F)	SI (kg/m ³)	British (lb/ft ³)
Carbon Steel	470	0.1123	45.03	26.02	7850	490.1
Soil	2000 ¹	0.4777	0.97 ²	0.56	1400 ³	87.4
Buoy-Black ⁴	1280	0.3057	0.105	0.0607	456.5	28.5
Buoy-Orange ⁴	1280	0.3057	0.105	0.0607	447.4	27.9
Buoy-Yellow ⁴	1280	0.3057	0.105	0.0607	407.5	25.4
Buoy-Green ⁴	1280	0.3057	0.105	0.0607	377.1	23.5
Buoy-Blue ⁴	1280	0.3057	0.105	0.0607	352.2	22.0

The modified properties used are shown in Table 2. An explanation of how these properties were derived is provided in this Appendix.

Table 2 – Modified Thermal Properties used in Models

Name	Heat Capacity		Thermal Conductivity		Density	
	SI (J/kg/K)	British (BTU/lb/F)	SI (W/m/K)	British (BTU/hr/ft/F)	SI (kg/m ³)	British (lb/ft ³)
Carbon Steel	470	0.1123	45.03	26.02	7850	490.1
Soil (Joint 2-9)	2000	0.4777	3.83	2.21	1400	87.4
Buoy-Black	1280	0.3057	14.42	8.33	457	28.5
Buoy-Orange	1280	0.3057	14.42	8.33	447	27.9
Buoy-Yellow	1280	0.3057	14.42	8.33	408	25.4
Buoy-Green	1280	0.3057	14.37	8.31	377	23.5
Buoy-Blue	1280	0.3057	14.37	8.31	352	22.0
Buoy-Yellow (1 Missing) ⁵	1280	0.3057	66.52	38.44	408	25.4
Buoy-Blue (1 Missing) ⁵	1280	0.3057	65.29	37.73	352	22.0
Soil (Joint 46)	2000	0.4777	4.23	2.45	1400	87.4
Soil (Joint 46 – Riser End)	2000	0.4777	1.88	1.08	1400	87.4

¹ Default property of “Subsea Silt and Clay” from OLGA 7.2 material library. I chose “Subsea Silt and Clay” because conductivity and density matched well to the values used above.

² Thermal conductivity of sediment recovered from the IMAGES VIII/PAGE 127 gas hydrate and paleoclimate cruise on the RV Marion Dufresne in the Gulf of Mexico, 2–18 July 2002; chapter 7 in Winters, W.J., Lorenson, T.D., and Paull, C.K., eds., 2007, Initial report of the IMAGES VIII/PAGE 127 gas hydrate and paleoclimate cruise on the RV Marion Dufresne in the Gulf of Mexico, 2–18 July 2002: U.S. Geological Survey Open-File Report 2004–1358.

³ Physical properties of sediment obtained during the IMAGES VIII/PAGE 127 gas hydrate and paleoclimate cruise on the RV Marion Dufresne in the Gulf of Mexico, 2–18 July 2002; chapter 4 in Winters, W.J., Lorenson, T.D., and Paull, C.K., eds., 2007, Initial report of the IMAGES VIII/PAGE 127 gas hydrate and paleoclimate cruise on the RV Marion Dufresne in the Gulf of Mexico, 2–18 July 2002: U.S. Geological Survey Open-File Report 2004–1358.

⁴ Properties for the buoyancy modules are described in greater detail in Appendix F-4.

⁵ Each joint is normally covered with 6 buoyancy modules. Properties have been adjusted to account for one missing buoyancy module for Joints 30 and 31 (yellow) and Joint 45 (blue).

Walls

The materials listed in Table 2 were used to construct various model walls along the riser length. The model walls, along with their constituent layers and thicknesses (ϕ), are listed in Table 3. Note that the riser wall material is carbon steel for all of the model walls listed because that is the material used to construct the DWH riser.

Table 3 – Walls used in models

Wall Name	Pipe	Buoyancy Module			Soil			Water
	ϕ (in)	Type	ϕ (in)	Discretized Layers	Type	ϕ (mm)	Discretized Layers	H_{out}^6
BarePipe-2X5.5DP	1							3225
BarePipe-5.5DP	1							1736
Buried-5.5DP	1				Soil (Joint 2-9)	109.5	3	1000
BarePipe-6.625DP	1							2039
Buoyed-Blk	1	Buoy-Black	15.25	7				1000
Buoyed-Org	1	Buoy-Orange	15.25	7				1000
Buoyed-Yel	1	Buoy-Yellow	15.25	7				1000
Buoyed-Grn	0.875	Buoy-Green	15.375	5				1000
Buoyed-Blu	0.875	Buoy-Blue	15.375	5				1000
Buoyed-Yel-1Less	1	Buoy-Yellow (1 missing)	15.25	7				1000
Buoyed-Blu-1Less	0.875	Buoy-Blue (1 missing)	15.375	5				1000
Buried-6.5-8DP-Shallow	1				Soil (Joint 46)	120.7	3	1000
Buried-6.5-8DP-Deep	1				Soil (Joint 46 – Riser End)	2823.8	7	1000

Figure 2 shows a schematic of where specific model walls are used along the elevation profile of the riser. The profile in the high position of May 13 (profile P2) is used for illustration, though the same walls were included in every model.

⁶ The outer heat transfer coefficient of seawater in $W/m^2/K$. In some cases the outer heat transfer coefficient was adjusted. More details about how this was done are covered later in this appendix.

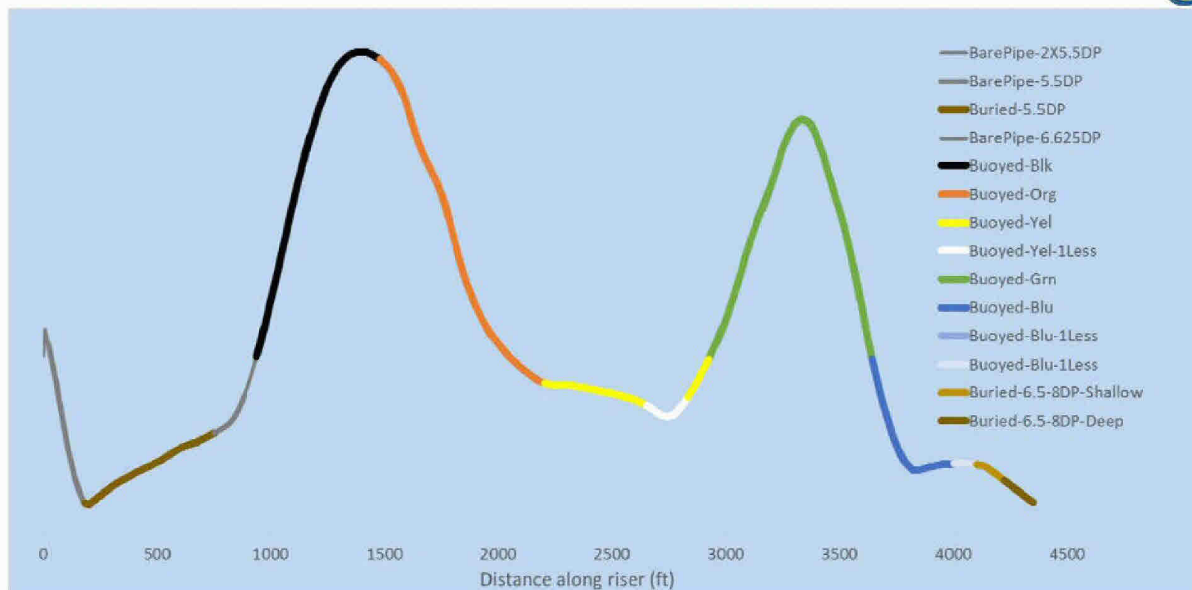


Figure 2 – Schematic showing location of walls along riser elevation profile

Calculation Methodology

Certain parameters used to model the thermal properties of the walls required modification prior to use in the models. This section describes the modifications that were made and the technical basis for making these modifications.

Reasons for Modified Thermal Properties

Pipeline Internal Diameter

As discussed in Appendix F-2, my models use a modified inner diameter to represent the hydraulic diameter of the riser pipe. Use of smaller hydraulic diameters result in reduced area available for heat transfer. To account for this reduced area, different thermal parameters were adjusted depending on the nature of the wall. Generally:

- If the pipe is bare, the outer heat transfer coefficient of seawater was adjusted
- If the pipe has buoyancy modules, the conductivity of the buoyancy module material was adjusted
- If the pipe is buried, the conductivity of the soil was adjusted

These adjustments allowed the model to accurately simulate the heat transfer.

Exposed Pipe near Riser Joint Connections

The riser joints that were covered with buoyancy modules had 2.875 feet of exposed pipe on either side of the buoyancy modules where they were flange-connected to adjacent riser joints (see Figure 3).



Figure 3 – Picture of buoyancy module-covered riser joint showing exposed pipe near the end⁷

Explicitly accounting for these 5.5 feet sections of bare pipe would have significantly increased the number of computational cells and increased the run-time of simulations. Therefore, an adjustment was made to the conductivity of the buoyancy modules such that the overall heat transfer for a 90 foot joint with 5.5 feet of exposed pipe was modeled as a fully covered 90 foot pipe with a modified conductivity for the buoyancy modules.

Additional Exposed Pipe on Joints with One Missing Buoyancy Module

Each joint is covered by six buoyancy modules; each with a length of a 168.5 inches (~14 feet)⁸. From my review of ROV video footage, I could discern that joints 30, 31, and 45 were each missing one buoyancy module. The additional bare pipe is handled in the same manner as the bare pipe at the ends of each joint. I adjusted the thermal conductivity of the buoyancy modules such that overall heat transfer for a 90 foot joint with 19.5 feet of exposed pipe (14 feet from the missing buoyancy module and 5.5 feet from the exposed joint ends) was calculated to be the same as a fully covered 90 foot pipe with the modified conductivity for the buoyancy modules.

Calculation Method

The general formula used in all calculations to modify conductivities is given below.

⁷ BP-HZN-2179MDL07729373.

⁸ TRN-INV-01871789.

$$\frac{1}{\Sigma \left(\frac{d_i \ln \left(1 + \frac{2t}{d_i} \right)}{2k} \right) + \frac{1}{H_{outer}} + \frac{d_{i,soil} \cosh^{-1} \left(\frac{2D_{burial}}{d_{i,soil}} \right)}{2k_{soil}}} D_i$$

$$= \frac{1}{\Sigma \left(\frac{d'_i \ln \left(1 + \frac{2t}{d'_i} \right)}{2k'} \right) + \frac{1}{H'_{outer}} + \frac{d_{i,soil} \cosh^{-1} \left(\frac{2D_{burial}}{d_{i,soil}} \right)}{2k'_{soil}}} D'_i$$

where,

D_i is the actual inner diameter of the riser pipe,

d_i is the inner diameter of a layer based on the actual ID of the riser pipe,

t is the thickness of a layer,

k is the thermal conductivity of a layer,

H_{outer} is the convective heat transfer coefficient of seawater,

$d_{i,soil}$ is the inner diameter of the soil layer,

D_{burial} is the burial depth defined as distance from top of the soil to the centerline of the pipe,

k_{soil} is the thermal conductivity of the soil layer,

all quantities with the accent (') are modified values based on hydraulic diameter of the pipe

Adjustment of Buoyancy Module Conductivity for Exposed Pipe

The buoyancy module conductivity was adjusted for exposed pipe by taking a weighted average of overall heat transfer coefficients (U), weighted by the length of exposed pipe and module-clad pipe, and then back-calculating a conductivity to give the same overall U.

$$\frac{L_{buoy} n_{buoy} U_{buoy} + (L_{joint} - L_{buoy} n_{buoy}) U_{bare}}{L_{joint}} = U_{adj}$$

$$\frac{1}{\frac{D'_i \ln \left(1 + \frac{2t_{pipe}}{D'_i} \right)}{2k_{steel}} + \frac{d'_i \ln \left(1 + \frac{2t_{bouy}}{d'_i} \right)}{2k_{bouy}^{adj}} + \frac{1}{H_{outer}}} = U_{adj}$$

where

$d'_i = D'_i + 2t_{pipe}$ is the inner diameter of the buoyancy module (outer diameter of the riser)

L_{buoy} is the length of a buoyancy module (168.5"),

n_{buoy} is the number of a buoyancy modules,

L_{joint} is the length of a buoyancy module (90 ft),

U_{buoy} is the overall heat transfer coefficient for pipe covered by buoyancy material,

U_{bare} is the overall heat transfer coefficient for a bare joint,

k_{buoy}^{adj} is the adjusted thermal conductivity of buoy,

k_{steel} is the thermal conductivity of steel,

t_{pipe} is the thickness of the riser pipe wall,

t_{pipe} is the thickness of the riser buoy,

The equations are solved for a value of k_{buoy}^{adj} .

Appendix F-4 – Riser Buoyancy Modules

Introduction

The DWH riser pipe was assembled by connecting together 90 foot sections of pipe called riser joints. Some joints were “slick,” (i.e., only pipe), while most had buoyancy modules strapped around them. The buoyancy modules were made of a special light material generically called syntactic foam.¹ Apart from providing buoyancy, the syntactic foam material is also a poor conductor of heat and thus provides thermal insulation to the riser. In this Appendix the source documents used to estimate the thermal properties of the syntactic foam material are documented.

Known Information

The buoyancy modules used on the DWH drilling risers were manufactured by Cuming Corporation (see Figure 1). Figure 2 shows part of a riser joint similar to those used on the DWH. The manufacturer’s label is clearly visible in red next to a purple-colored strip. The color of the strip indicates the depth rating for the module.

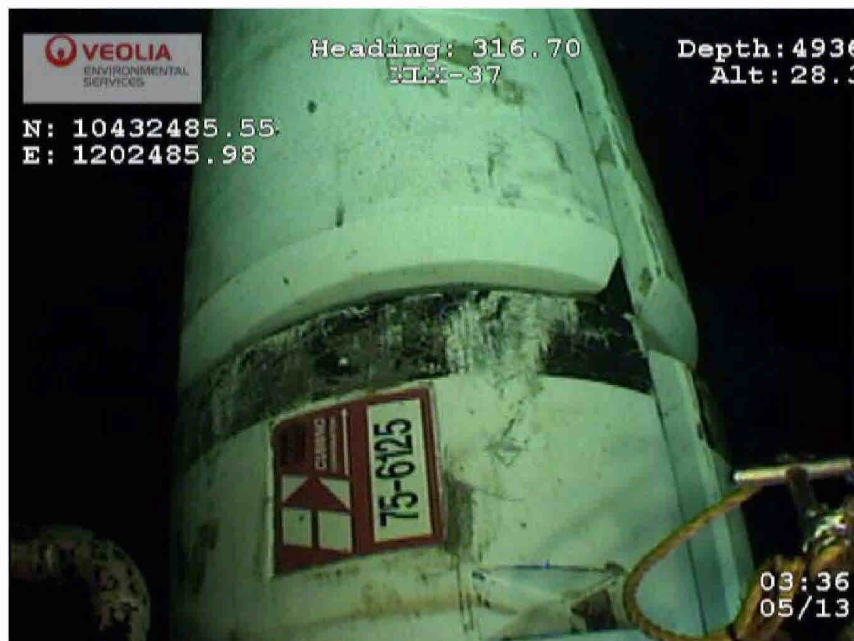


Figure 1 – Screen capture from riser inspection ROV footage showing Cuming Corporation label on buoyancy module²

¹ Cuming Corporation, Technical Note 100-1-A, “Introduction to Syntactic Foam,” available at <http://cuming.mosaicmedia.com/wp-content/uploads/2012/06/TN-100-1-A-7-11-12.pdf>.

² BP-HZN-2179MDL04569970.



Figure 2 –A buoyancy module-covered riser joint similar to those used on Deepwater Horizon³

Figure 3 shows a cross section of the syntactic foam used in Cuming Corp’s C-FLOAT buoyancy modules. The schematic shows that the material is formed by suspending hollow macrospheres made of fiberglass or carbon fiber (for buoyancy) and microspheres made of glass (for thermal insulation and strength) in an epoxy binder medium. The foam thus formed is then covered in a fiberglass skin.

³ Photograph of a partial riser joint with buoyancy module.

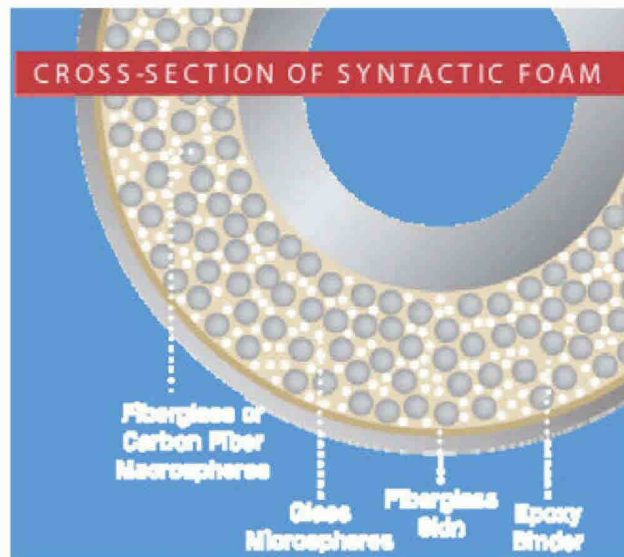


Figure 3 – A cross-section sketch of Cuming Corp’s C-FLOAT product⁴

The relative amounts of macro- and micro-spheres, and the thickness of the walls of the spheres are varied based on the requirements of pressure rating and buoyancy.⁵ Thus the different color-coded modules have varying amounts of suspended macro- and micro-spheres and consequently different densities, heat capacity, and thermal conductivity. Conductivity increases with increasing density (Watkins, 2001).

Densities

The densities of the buoyancy modules are listed in Table 1.⁶

Table 1 – Density of Buoyancy Modules on Riser Joints

Depth Rating	1000	2000	3000	4000	5000	6000
Color Code	Tan	Blue	Green	Yellow	Orange	Black
Diameter (in.)	42	52	52	52	52	52
Density (lb/ft ³)	21.35	21.99	23.54	25.44	27.93	28.50
Density (kg/m ³)	341.99	352.25	377.07	407.51	447.40	456.53

Estimated Quantities

Two other properties that are important for thermal modeling have to be estimated: thermal conductivity and heat capacity. Literature is available on thermal properties of syntactic foams that are used as insulation materials but these are slightly different than the materials used for buoyancy applications. Besides the material used for buoyancy being different from that used for insulation, syntactic foam used for insulation is cast onto the pipe forming a tight bond between the pipe and the binder material, whereas buoyancy modules are strapped on to the riser pipe with cutouts to allow for

⁴ Source: <http://www.cumingcorp.com/c-float-tech-data/>.

⁵ Watkins, et al, “Syntactic Foam Thermal Insulation for Ultra-Deepwater Oil and Gas Pipelines”, OTC 13134, 2001 - a technical note published by Cuming Corp.

⁶ TRN-INV-01871789.

choke, kill, and booster lines around the primary riser pipe. Figure 4 shows a close-up view of the gap between the riser pipe and the buoyancy module.



Figure 4 – Picture of riser strapped with buoyancy module showing gap between pipe wall and module⁷

Based on Figure 4 and Figure 5, a thermal conductivity of 0.105 W/m/K, and a specific heat capacity of 1280 J/kg/K were selected and used in the model. The heat capacity was taken directly from Figure 5 while the thermal conductivity is the average of the semi-rigid and rigid type of syntactic construction. The semi-rigid and rigid type constructions are the type used for buoyancy modules.⁸

⁷ Photograph of riser strapped with buoyancy module showing gap between pipe wall and module.

⁸ Watkins, et al, "Syntactic Foam Thermal Insulation for Ultra-Deepwater Oil and Gas Pipelines", OTC 13134, 2001 - a technical note published by Cuming Corp.

Typical Properties of Syntactic Foam Insulation Materials										
Operating Temperature Range, °C	Maximum Service Depth, meters	Rigid			Semi-Rigid			Flexible		
		Nominal Density, kg/m ³	Thermal Conductivity, W/m-°C	Specific Heat Capacity, J/g-°C	Nominal Density, kg/m ³	Thermal Conductivity, W/m-°C	Specific Heat Capacity, J/g-°C	Nominal Density, kg/m ³	Thermal Conductivity, W/m-°C	Specific Heat Capacity, J/g-°C
<60	—	Use conventional syntactic foam buoyancy materials for temperatures below 60° C.								
60 -	1200	513	0.09	1.25	593	0.10	1.35	673	0.11	1.70
80	2300	609	0.10	1.25	689	0.11	1.35	769	0.12	1.70
80 -	1200	545	0.11	1.25	625	0.12	1.35	705	0.13	1.70
100	2300	641	0.12	1.25	721	0.13	1.35	801	0.14	1.70
>100	—	Ask about new syntactic insulation materials being developed for use above 100° C.								

Note: All Values Are Approximate

Figure 5 – Thermal Properties of Cuming Corp Syntactic Foam Insulation Materials⁹

ULTRA-DEEPWATER SYNTACTIC FOAM INSULATION MATERIALS (Numbers are approximate)

Type of Syntactic Construction	Maximum Service Depth Rating, m (ft)	Maximum Temperature, °C (°F)	Thermal Conductivity, W/m °K (Btu/ft °F hr)	Specific Heat Capacity, J/g °C (Btu/lb °F)
Rigid	1200 (4,000) to 2300 (7,500)	80 (175) to 100 (212)	0.08 (0.04) to 0.12 (0.07)	1.28 (0.30)
Semi-Rigid	1200 (4,000) to 2300 (7,500)	80 (175) to 100 (212)	0.09 (0.05) to 0.13 (0.08)	1.28 (0.30)
Flexible	1200 (4,000) to 2300 (7,500)	80 (175) to 100 (212)	0.10 (0.06) to 0.15 (0.09)	1.28 (0.30)

Figure 6 – Thermal Properties reported by CTO of Cuming in a conference publication¹⁰

Sensitivities

Thermal Properties

Although there is some variation in thermal properties found in cited references, the sensitivity of the model parameters to these numbers is very low. This is shown in Table 2, which lists the change in effective thermal conductivity based on changes to the thermal conductivity of the buoy materials. As can be seen from this table, there is very little change in the adjusted conductivity¹¹ despite large changes in the raw conductivity.

⁹ Technical Note 600-1, Cuming Corp (<http://www.cumingcorp.com/tech-notes/>) - conference publication by the Chief Technical Officer.

¹⁰ Watkins, et al, "Syntactic Foam Thermal Insulation for Ultra-Deepwater Oil and Gas Pipelines", OTC 13134, 2001 - a technical note published by Cuming Corp.

¹¹ See Appendix F-3 for a description of how the conductivities were adjusted.

Table 2 – Sensitivity of effective conductivity to the raw conductivity of syntactic foam

Raw conductivity (W/m/K)	Adjusted conductivity (W/m/K)
0.08	14.3842
0.09	14.3989
0.105	14.4210
0.11	14.4284
0.12	14.4432

The effective conductivity is a very weak function of the conductivity of the syntactic foam. This is to be expected since the heat transfer in each riser joint is dominated by the bare section at the extremities where the riser is in direct contact with the seawater.

Specific heat capacity and density both affect heat storage in the foam and therefore only affect simulations involving temperature transients (such as a cool down simulation). In the current context, specific heat capacity has little to no impact on the results and therefore the sensitivity to this parameter is negligible.

Water Layer

As seen in Figure 5, a gap exists between the buoyancy modules and the pipe wall. Once the riser is submerged the gap fills with water. That layer of water has not been incorporated into the wall layers with buoys. A sensitivity was performed to evaluate the impact. The results can be seen in Table 2.

Table 3 – Sensitivity of water layer on the overall heat transfer coefficient (OHTC) prior to adjustment of thermal properties of buoyancy material.

	OHTC (W/m ² /K) No Water	OHTC (W/m ² /K) Water
Buoyed-Black	0.435	0.429
Buoyed-Orange	0.435	0.429
Buoyed-Yellow	0.435	0.429
Buoyed-Green	0.434	0.433
Buoyed-Blue	0.434	0.433

In this sensitivity water is treated as a conductive layer. As seen from Table 2, there is very little change in the overall heat transfer coefficient (OHTC) with the inclusion of a water layer. Once modified, as describe by the procedures in Appendix F-3, the resulting heat transfer is still dominated by the bare section at the extremities of the riser joint. It is clear that the inclusion of water as a conductive layer does not significantly impact the heat transfer.

In reality, the water would have convected heat away from the pipe at higher rates than modeled. Had this affect been included in the model, the resulting higher rate of heat loss would have lowered the temperature at the outlet. However, sensitivity studies have already been conducted that model the effect of significant changes in the temperature of the fluid. These sensitivity studies covered a wide range of values for the temperature of the inlet and the outer heat transfer coefficient, therefore no additional sensitivity study was performed to assess the impact of the convective water layer.

Appendix F-5 – Riser Motion

Introduction

Between May 13 and May 20, 2010, a section of the DWH riser between joints 31 and 40 (henceforth referred to as *the buoyant loop*) was moving in a vertical oscillating motion. The ROV survey of the riser pipe on May 10 did not reveal this motion, however, parts of the riser had yet to settle fully to the seafloor. ROV footage from May 13 and May 16 revealed this cyclic riser motion. The amplitude of the motion, or the peak position attained by the buoyant loop, was higher on May 13 than on May 16. The riser survey on the morning of May 21 showed that the buoyant loop had stopped moving.¹

In this appendix, a detailed description of the analysis performed on data from ROV surveys in order to characterize the riser motion is provided followed by an explanation of how the motion thus characterized was modeled.

Available Data

The same ROV riser survey data from May 13 and May 16 used to extract the riser elevation profile was also used to characterize the riser motion (See Appendix F-1 – Riser Elevation Profile for a discussion of the data format and the quality of the data from the two surveys).

Motion Characterization Procedure

The ROV XLX-36 survey on May 16 provides insight into the nature of the riser’s motion. Several features of the May 16 survey make it optimal for motion characterization:

- ROV XLX-36 parked on top of every moving joint (ROV XLX-37 observed most moving joints from the side)
- The depth data from XLX-36 is extremely stable and reliable whereas XLX-37 data were both noisy and lagged behind the observed motion
- ROV XLX-36 managed to capture several cycles of motion on some joints

Figure 1 shows the depth chart for joint 33 where XLX-36 spent enough time to capture 7 complete cycles of motion. The blue line shows the measured depth and overlaid orange line shows a data fit using a function of the following form:

$$d_t = \begin{cases} d_{min} + d_{range} \left[0.5 + 0.5 \cdot \sin \left(\frac{2\pi}{t_{end} - t_{start}} \times (t - t_{start}) - \pi \right) \right] & \text{when } t_{start} < \text{mod}(t, T) < t_{end} \\ d_{min} & \text{otherwise} \end{cases}$$

where,

d_t is the depth at time t ,

T is the period for each cycle,

¹ BP-HZN-2179MDL04996577.

t_{start} is the time at which the riser lifts off (relative to start of period),

t_{end} is the time at which the riser touches down (relative to start of period),

d_{min} is the depth of the seafloor,

d_{range} is the height of the peak relative to d_{min}

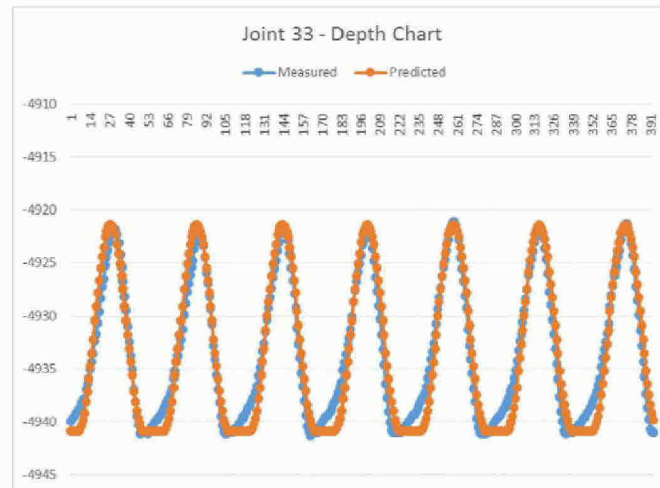


Figure 1 – A representative sample of riser motion data from XLX-36

The functions that describe the motion on May 16 are expected to be representative of the motion on May 13. Even though the peaks the riser reached are not the same on May 16 as on May 13, the observed motion was similar.

Characterization

The sine function used to approximate the motion of the riser does a good job of matching the actual observed riser motion at a given joint. There is insufficient information to estimate the motion of the joints relative to the motion of other joints. However, because the riser is rigid, it seems unlikely that the riser exhibited much, if any, wave action. Thus, I have assumed that all joints reach their peak at the same time. The joints, however, exhibit different amounts of time spent on the ground. On May 13, the joints that have the highest elevations have a zero value for t_{start} and t_{end} is equal to the period T . For joints that have non-zero values for t_{start} and t_{end} , these variables have been set to be symmetric around the peak, i.e., $t_{end} = T - t_{start}$, to enforce synchronized peaking of the joints. Table 1 and Table 2 list the calculated parameters for May 13 and May 16 respectively.

Table 1 – Motion characterization parameters for May 13

Joint #	t_{start}	t_{end}	T
31	40	245	285
32	35	250	285
33	30	255	285
34	10	275	285
35	10	275	285
36	0	285	285
37	0	285	285
38	0	285	285
39	22	262	285
40	35	250	285

Table 2 – Motion characterization parameters for May 16

Joint #	t_{start}	t_{end}	T
31	45	138	183
32	31	152	183
33	22	160	183
34	22	160	183
35	22	160	183
36	22	160	183
37	22	160	183
38	22	160	183
39	28	154	183
40	32	150	183
41	42	140	183

Modeling Riser Motion

Software

Dynamic riser motion is a common phenomenon that occurs in production risers attached to vessels, which are subject to motion due to tides and other meteorological phenomena. LedaFlow (see Appendix C) for a description of this software) is driven through a scripting interface (QtScript) that allows users significant access to vary simulation parameters during the running of a simulation. Using that scripting interface, the existing version of LedaFlow (v 1.2) allows one to simulate the motion of the riser with the functional form described earlier.


Methodology

In this section the procedure for describing the riser motion, and the modeling of that motion during simulations are explained.


Description of Riser Motion

In order to describe the riser motion, first two models were built using LedaFlow, one using the low elevation profile and one using the peak elevation profile. Kongsberg (that company that provides LedaFlow) provided a set of scripts in QtScript and Python² that used these two models to generate a text-based configuration file, describing the motion of the riser, called movingmesh.txt. The moving mesh file (movingmesh.txt) has two parts to it as shown in Figure 2. The first six columns of data are generated by the scripts provided by Kongsberg. Each row corresponds with a point on the mesh.³ The first four columns are the mesh points for the low profile and the length of pipe between consecutive mesh points. The fifth and sixth columns list the angle between successive pipe segments in the low and high configuration. The next six columns are user input parameters that describe the motion. The function column specifies the function, a sine function as described earlier, and a hyperbolic tangent function that was not used for this work.⁴ The last two parameters r_up, and r_down are only used for the hyperbolic tangent function.

i	A	B	C	D	E	F	G	H	I	J	K	L
	X	Y	Z	Length	Alpha_low	Alpha_high	Function	Period	t_start	t_end	r_up	r_down
344	852.7154	0	-1512.04443	2.76444	-0.01618	0.12875	1	285	40	245	10	10
345	855.47944	0	-1512.09183	2.76444	-0.01715	0.13843	1	285	39.5	245.5	10	10
346	858.24348	0	-1512.13923	2.76444	-0.01715	0.13843	1	285	39	246	10	10
347	861.00743	0	-1512.19004	2.76444	-0.01838	0.14784	1	285	38.5	246.5	10	10
348	863.77143	0	-1512.24085	2.76444	-0.01838	0.14784	1	285	38	247	10	10
349	866.53525	0	-1512.29949	2.76444	-0.02121	0.1556	1	285	37.5	247.5	10	10
350	869.29907	0	-1512.35813	2.76444	-0.02121	0.1556	1	285	37	248	10	10
351	872.0627	0	-1512.42534	2.76444	-0.02431	0.16308	1	285	36.5	248.5	10	10
352	874.82632	0	-1512.49255	2.76444	-0.02431	0.16308	1	285	36	249	10	10
353	877.59139	0	-1512.56064	2.70608	-0.02738	0.17049	1	285	35.5	249.5	10	10
354	880.23645	0	-1512.64073	2.70608	-0.02738	0.17049	1	285	35	250	10	10



Script-generated



User inputs

Figure 2 – Columns in movingmesh.txt file used to describe riser motion

Moving the Riser during Simulation

Using the scripts provided by Kongsberg, the motion is not executed while the simulation calculations are in progress. The simulation is run for a period of one second, then the elevation profile is adjusted in accordance with the motion of the riser, and then the simulation is restarted with the new elevation profile and advanced for the next second. This procedure is repeated in a loop for the duration of the simulation (3-4 hours in the context of the current work). Figure 3 shows a snippet of the script with this simulation loop.

² A programming language.

³ The “mesh” is representation of the riser using discrete elements, “cells”, as a representation of the riser. LedaFlow calculates the behavior of multiphase flow for each cell in the mesh.

⁴ A hyperbolic tangent function was explored as a possible fit to the motion of the riser. It did not accurately characterize the motion of the riser and was therefore not used.

```

// =====
// Simulation loop
// =====
var tt = 0.0;
var cycles = timeAdvance/moveDt;
var progress = 0.0;
for( cycle=0; cycle<cycles; cycle++) {

    // set time advance (one interval)
    t.mycase.setTimeAdvance(moveDt);

    // Move that mesh
    mm.moveMesh(meshCoord, tt);
    t.mesh(pipeName).setCoord(meshCoord);

    // run until the next update
    t.calculate();

    // sacrifice superficial velocity such that we can plot the dynamic riser profile
    t.derivedVars(pipeName).last();
    t.derivedVars(pipeName).setSupVel(meshCoord);

    // Override case status and progress percentage.
    tt = tt + moveDt;
    progress = tt/timeAdvance;
    t.status.setStatus("Running");
    t.status.setProgress(progress);
    print ("Progress: " + 100.0*progress + "%");
}
t.status.setStatus("Completed");

```

Figure 3 – A snippet of the runtime script for executing dynamic riser motion simulations

Notes

Physics

By moving the riser elevation profile through the script, the redistribution of liquids in the riser, is captured. However, in reality there is also an acceleration that is experienced by the fluids. This effect is not captured. However, the maximum absolute value of the acceleration from the riser surveys is very small, less than $1.5 \times 10^{-2} \text{ m/s}^2$, as compared to gravity (9.81 m/s^2) and therefore this effect is unlikely to have produced any substantive change in the results.

Recording of Elevation Profile with Time

Since the core LedaFlow software does not expect elevation profile changes with time, the storage allocated for the variable was not designed to record changes with time. Therefore, the superficial bubble velocity variable storage space is being used in the script to store the elevation profile as it changes with time. This is acceptable for this work in that the superficial bubble velocity is not important to the studied phenomenon.

Appendix G – Simulation Results

Introduction

In the main report I present the calculated best estimated flow rate for flow through the Riser End and the total flow through the Kink and Riser End. I also present the uncertainty range for these calculated flow rates. To calculate best estimated flow rate and associated uncertainty ranges, I constructed a model that simulated the oscillating movement of the buoyant loop. This appendix describes in greater technical detail the manner in which I calculated these flow rates and uncertainty ranges.

As part of my work, I also evaluated other mechanisms of slug formation. The results of those evaluations are documented in Appendix H. Other simulation work included benchmarking the LedaFlow models, the results for these simulations are documented in Appendix B.

Calculating Flow Rate Range

As I described in the body of the main report, I ran two sets of simulations to calculate flow rates through the Riser End. For one set of simulations, I used the motion characteristics of the buoyant loop on May 13 which produced a double peak behavior for the slug flow. For the other set of simulations, I used the motion characteristics of the buoyant loop on May 16 which produced a single peak behavior for the slug flow. I varied the flow rate through the riser over a wide range of flow rates for both sets of simulations. The range I used was from ~12,000 to ~60,000 stbpd.

As I further explained, the observed slug flow on May 13 exhibited double peak behavior (see Section 6.2). Though both May 14 and May 15 also exhibited double peak behavior, May 13 was used as the basis of this work because there was also a detailed riser survey on that day. That survey was the first to systematically document the cyclical oscillation of the buoyant loop.

On May 16, the observed slug flow exhibited single peak behavior. Single peak behavior occurred from May 16 through May 20. I used May 16 as basis of this this work because there was a detailed riser survey on that day. Thus, as with May 13, May 16 is a date with a robust set of data documenting the oscillation of the buoyant loop.

As stated above, the flow rate was varied through the riser using the same range of flow rates for the two sets of simulations. To qualify as a possible flow rate, the simulation using the May 13 riser motion had to exhibit double peak behavior and the simulation using the May 16 riser motion had to exhibit single peak behavior.

Figure 1 shows a representative double peak behavior. A large number of simulations were run during this investigation. To analyze those simulations, I developed an algorithm to systematically identify and characterize double peak behavior.

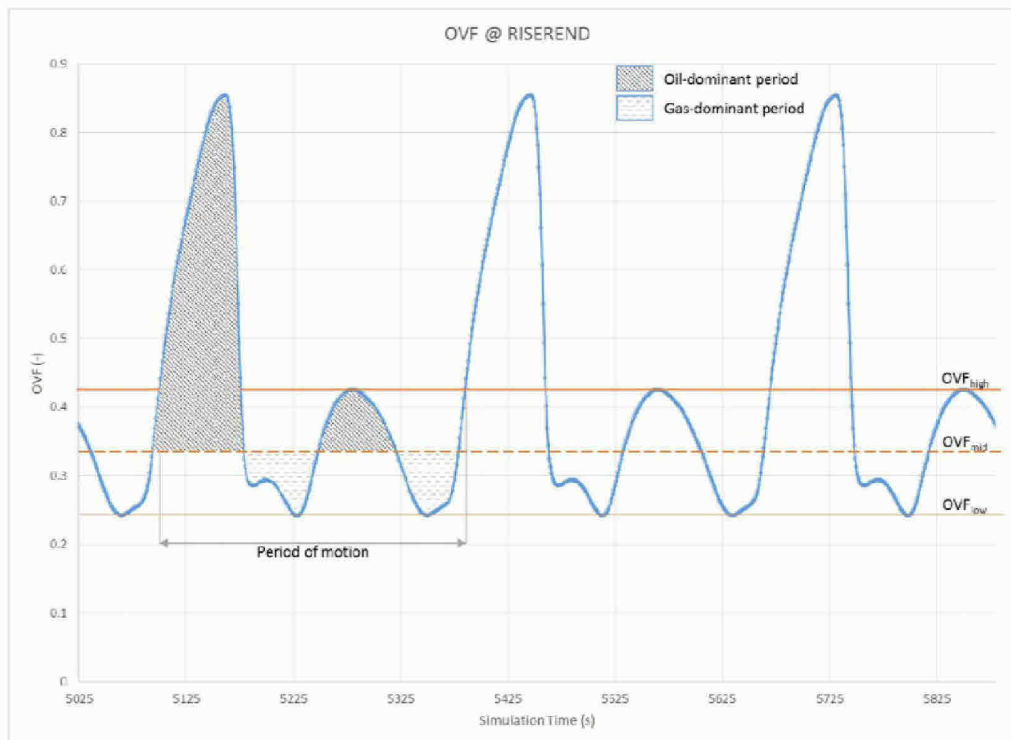


Figure 1 – Calculation of slug characteristics from trend of oil volume fraction

Identifying Double Peak Behavior

To computationally identify double peak behavior for each simulation, I employed the following algorithm:

1. Export trend¹ of gas volume flow rate (QG) and oil volume flow rate (QO) at riser end. A trend can be thought of as a data series structured as a collection of <time, value> pairs.
2. Calculate oil volume rate fraction (OVF) at riser end as

$$OVF = \frac{|QO|}{|QO| + |QG|}$$

This will result in a computed trend variable.

3. Ignore the first one hour of the computed OVF trend data² to allow for simulation to stabilize
4. Calculate two thresholds for OVF, an OVF_{low} and an OVF_{high} . Initially, set OVF_{low} to the lowest OVF during the entire simulation, and OVF_{high} to the highest OVF during the entire simulation. Then,
 - a. Pick all points in the OVF trend that are below OVF_{low} and group them into sets of points that are contiguous in time. This will result in a collection of sets of trend points. By this I mean each member of the collection will be a set of trend points (<time, value>)

¹ A trend is a variable as a function of time.

² In some simulations, two hours of simulation were allowed for stabilization. During this period, the riser was held fixed. All of the data with the riser in a fixed position were ignored.

- pairs) that are contiguous in time. To illustrate this, see Figure 2. Sets T1 and T2 represent two members of this collection.
- Similar to step (a), pick all points in the OVF trend that are above OVF_{high} and group them into sets of points that are contiguous in time. In Figure 2, sets P1 and P2 will be members of the resulting collection.
 - Combine the two collections from steps (a) and (b) and order by the first time in each set
 - Ensure that the resulting ordered collection from step (c) has two sets of alternating oil-dominant ($OVF > OVF_{high}$) and gas-dominant ($OVF < OVF_{low}$) flow periods in any given time span equal to the period of riser motion. In Figure 2, within the time span denoted by the "Period of motion" label, the ordered set looks like (P1, T1, P2, T2). Thus, this trend exhibits double-peak behavior.

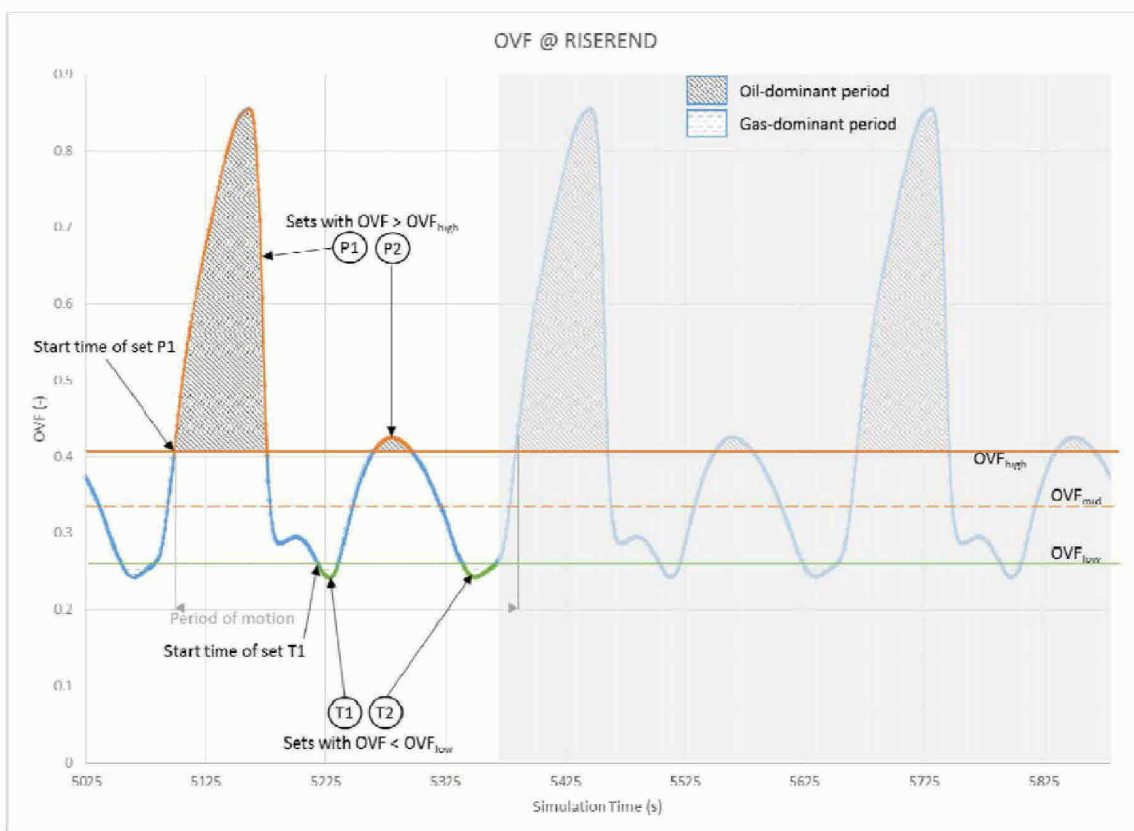


Figure 2 – Illustration of algorithm for identifying double-peak behavior

Example Analysis

Plots of the oil volume rate fraction at the Riser End as a function of time are shown in the figures below. The plot on the left shows simulation results using May 13 motion characteristics, and the plot on the right shows simulation results using May 16 motion characteristics. Higher oil volume rate fractions are representative of the darker fluid, which is oil-dominant. All plots shown below are from the simulations using an assumed inlet temperature of 176 °F. For reference, the oil volume rate fraction at steady state (once the riser has settled) is between 0.40-0.47 (varies with flow rate).

The plots for ~27,000 stbpd, shown in Figure 3, exhibit clear double peak behavior on the left and single peak on the right. Thus, this flow rate is within the range of qualifying flow rates because it matches both the double peak behavior on May 13 and the single peak behavior on May 16. Additionally, the range in the OVF is ~0.28-0.86 on May 13, and ~0.1-0.86 on May 16. These large ranges are qualitatively consistent with the observed oil-dominant and gas-dominant flows.

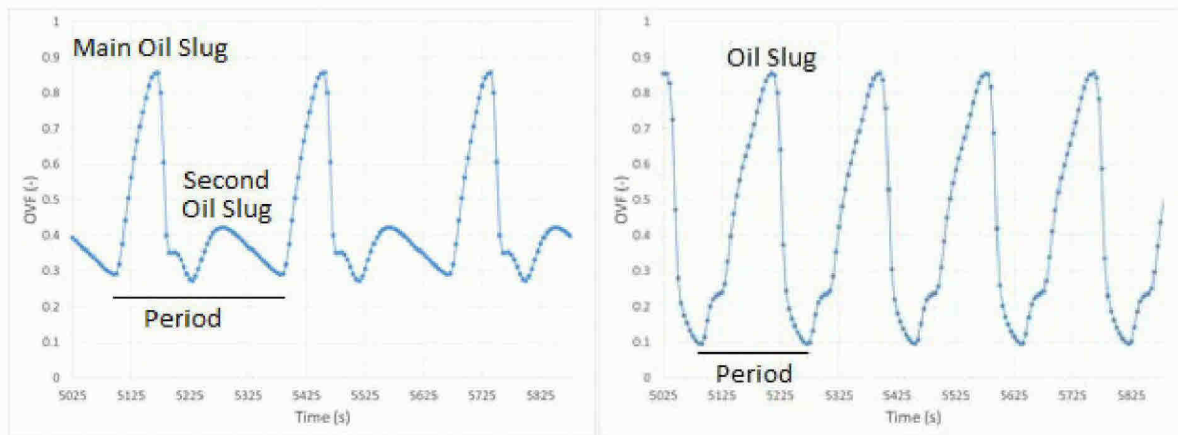


Figure 3 - Plot of oil volume rate fraction at the Riser End for 27100 stbpd on May 13 (Left) and May 16 (right)

It is important to note that Figure 3 (left) shows the OVF of the second peak is consistent with the OVF range once the riser has settled. If true, the second peak should look similar to the stratified flow present after May 20. Figure 4 compares the second peak on May 14 with stratified flow on May 23 (when the riser had settled to the sea floor and there was no slugging observed at the Riser End). From the two images it is apparent there is a good qualitative agreement; both images show approximately the same amount of gas (white) at the top of the pipe.



Figure 4 - comparison of second peak on 5/14 (Left) with stabilized stratified flow on 5/23 (right)³.

³ BP-HZN-2179MDL04569966.

At a much higher rate of ~40,000 bpd, shown in Figure 5, the plots reveal a more complicated slug flow behavior which does not match the May 13 and May 16 behavior. The results from May 13 do not exhibit the double peak behavior while the results from May 16 exhibit double peak behavior (discussed further in the next section) when they should be showing single peak behavior. For these reasons, this is not a qualifying flow rate for the May 13 to May 20 slugging period.

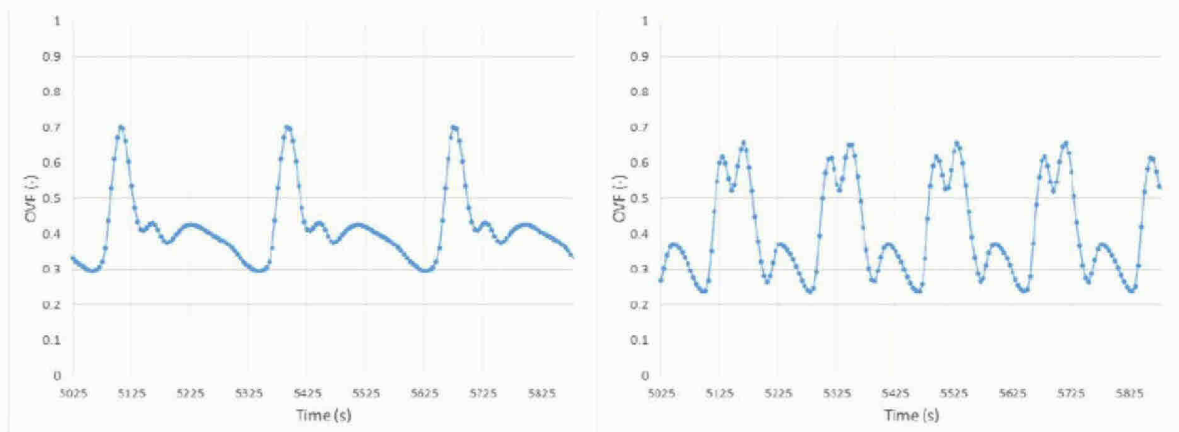


Figure 5 - Plot of oil volume rate fraction at the Riser End for 40000 bpd on May 13 (Left) and May 16 (right).

Charts for simulations using a flow rate of 11,800 stbpd shown in Figure 6 clearly do not match the double peak behavior for May 13. Since double peak behavior is not present on May 13 this flow rate is also not a qualifying flow rate for the May 13 to May 20 slugging period.

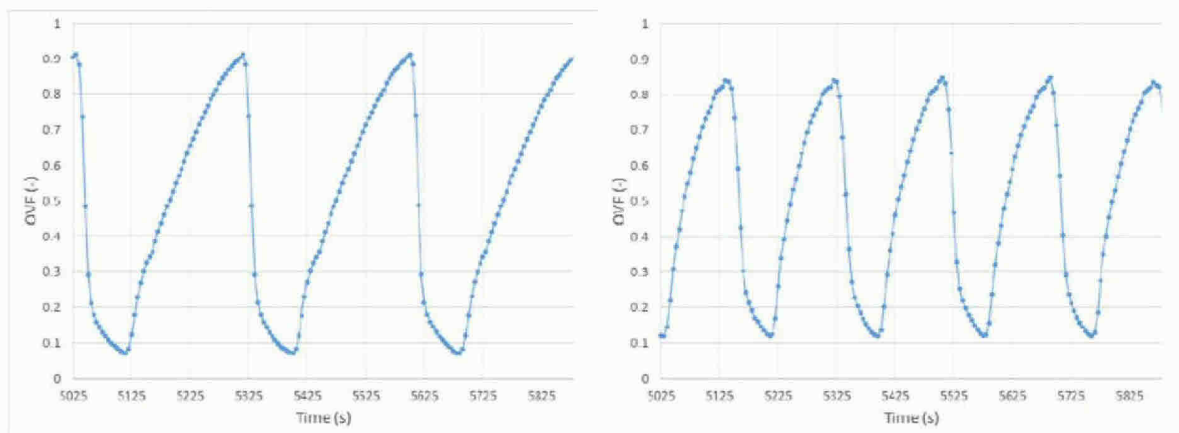


Figure 6 - Plot of oil volume rate fraction at the Riser End for 11800 bpd on May 13 (Left) and May 16 (right)

Upper Bound - Implications of Simulating a Double Peak on May 16

The mechanism behind double peak behavior observed on May 13 is explained in the main report. At very high simulated flow rates (over ~30,000 stbpd) the model produces a double peak for May 16. However, the mechanism responsible for the simulated double peak behavior is not the same as the mechanism that actually caused the observed double peak behavior. As further explained below, the

flow rates that produce the simulated double peak behavior on May 16 provide an upper bound on the flow rate range for May 13 to May 20, 2010.

On May 16, the loop spent close to 45 seconds in the settled position (based on analysis of ROV observations, see Appendix F-5) before starting to rise up. This allowed for stratified flow to establish behind the main oil slug. When the loop started to rise, the oil in the downstream section of the riser accelerated toward the end of the buoyant loop. For qualifying flow rates, this accelerated oil volume catches up with the main oil slug and leaves the Riser End as one slug (single peak behavior). However, at higher flow rates, the accelerated volume is not able to catch up with the main oil slug, which is moving faster because of the higher flow rates, and leaves the Riser End as a separate second oil slug, thus producing the double peak behavior. This process is illustrated in Figure 7.

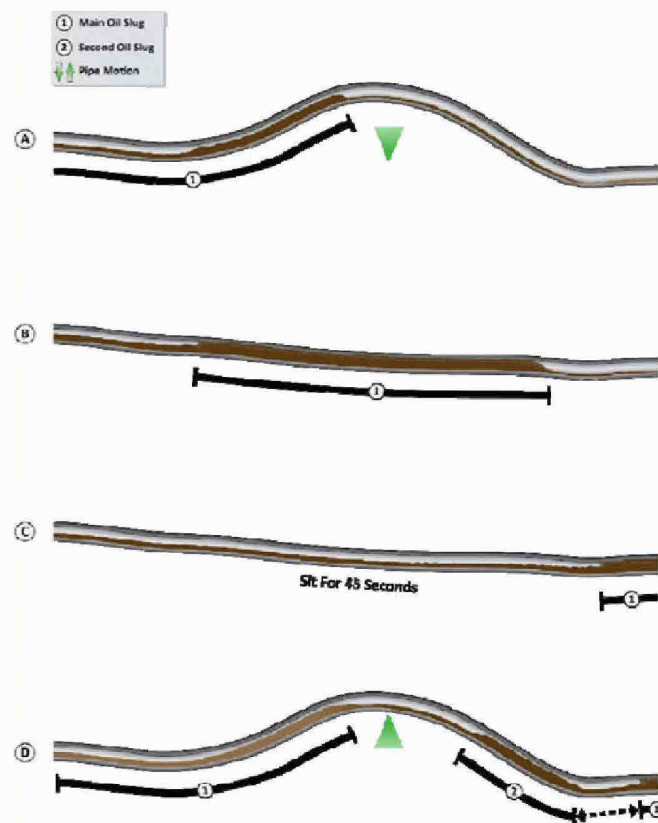


Figure 7 - simulated double peak behavior on May 16

The high flow rate double peak produced in simulations for May 16 serves as the upper bound for determining qualifying flow rates because this behavior is not consistent with the observed single peak behavior on May 16.

Lower Bound - Density

The method I used to bound the minimum flow rate relied on the average fluid density of the buoyant loop. Since the buoyant loop settled on the seafloor and stayed in that position after May 20, I know that the average fluid density of the buoyant loop during motion must go below the average steady

state density with the loop in the settled position. At very low flow rates (rates less than 20,000 stbpd), this condition was not met. By looking at the minimum density during motion and ensuring that it went below the steady state density without motion (with the loop in the settled position), I ruled out flow rates that were too low.

Riser End Flow Rate Sensitivity

The technical basis and results regarding flow rate sensitivities are documented below. None of the sensitivities discussed below show a large impact on the range of qualifying flow rates.

Temperature

For both the Kink and No-Kink models, the inlet temperature of the fluid is uncertain. The most relevant temperature data available is that of the fluid just downstream of the LMRP (measured after the riser was cut). This temperature was 221 °F⁴ but this measurement was made after the riser was severed from the LMRP on June 3. There is no temperature measurement of the flowing fluid at the wellhead from May 13 to May 20, 2010.

The temperature measured after the riser was cut was taken at a later date at a higher estimated flow rate than the rates I am predicting over the dates considered. At the flow rates I have calculated, the fluid would have spent more time in the well bore and would therefore have lost more heat to the surroundings.

Additionally, for the No Kink model, with a model boundary starting at Joint 1 (downstream of the kinked section), the temperature of the fluid would have dropped further due to the heat lost to the environment and Joule-Thompson effect across the kinked section. Thus, the temperatures I assumed for my temperature sensitivity analysis are all lower than the flowing temperature of 221 °F that was measured on June 3.

To address uncertainty in flowing temperature before June 3, I ran three sets of simulations, each at a different temperature. The temperatures I used were 149, 176, and 203 °F. I chose 203 °F as the upper limit of my temperature sensitivity based on the results of the Kink Model simulations. In those simulations, I used the measured 221°F temperature at the model boundary (roughly the same location as the measurement) and let the model estimate the temperature drop across the kinked section.

For the lower bound, I used 149 °F. This value is estimated from temperature measurements which were taken on the outside wall of the kinked section⁵ and past the kinked section. The average of all of those measurements is 146 °F. Although a significant temperature drop across the riser wall is more realistic, I used a very small temperature difference of 3 °F across the pipe to estimate the internal fluid temperature. It is extremely unlikely that the fluid temperature was as low as this assumed lower bound temperature. Therefore it provides a conservative lower temperature for use in determining the potential sensitivity of the flow estimates to temperature uncertainties.

⁴ Reddy, C. M. et al., "Composition and fate of gas and oil released to the water column during the Deepwater Horizon oil spill", 2011.

⁵ BP-HZN-2179MDL05698038.

Through simulation results, I determined the sensitivity of the range of qualifying flow rates to the temperature of the fluid. Generally, higher temperatures resulted in lower estimates of the flow rate. I used 176 °F as the inlet temperature for my base case.

Table 1 lists the estimated flow rate ranges from the inlet temperature sensitivity cases. In spite of using a wide range of temperatures, the effect on the flow rate estimates is low.

Table 1 – Sensitivity to inlet temperature

Model/ Sensitivity Parameter	Value	Best Estimated Flow Rate (STBPD)	Minimum Flow Rate (STBPD)	Maximum Flow Rate (STBPD)
Base Case	176 °F	25400	21300	28400
Base + lower bound Inlet Temperature	149 °F		22500	29600
Base + Upper bound Inlet Temperature	203 °F		21300	27200

Outer Heat Transfer

The convective outer heat transfer coefficient (OHTC) of seawater varies with the velocity of water. OHTC is a measure of how easily the heat emanating from the riser is transferred to the surrounding seawater. The OHTC for natural convection (i.e., without any currents) was calculated to be around 200 W/m²/K. With a 1 m/s current velocity, the OHTC was calculated at around 2500 W/m²/K. I ran three different cases varying the OHTC based on: (1) natural convection, (2) forced convection at 1 m/s current velocity, and (3) a value in the middle of 1000 W/m²/K. The base case results use an OHTC of 1000 W/m²/K.

Results from the sensitivity cases are presented in Table 2. These results indicate that the sensitivity of the flow rate estimates to the outer heat transfer coefficient (OHTC) is low.

Table 2 – Sensitivity to outer heat transfer coefficient

Model/ Sensitivity Parameter	Value	Best Estimated Flow Rate (STBPD)	Minimum Flow Rate (STBPD)	Maximum Flow Rate (STBPD)
Base Case	~1000 W/m ² /K	25400	21300	28400
Base + Natural Convection	~200 W/m ² /K		26000	28400
Base + Forced Convection (1 m/s)	~ 2500 W/m ² /K		23600	29600

Riser End Depth

Since the riser end depth was estimated visually, a sensitivity to a higher riser end position was evaluated. I used a depth of -4990 feet in the base case. Results using -4985 feet are reported in Table 3. For a discussion of how these depths were determined, see Appendix F-1. The effect of the riser end position on the estimated flow rates is insignificant.

Table 3 – Sensitivity to depth of the Riser End plume

Model/ Sensitivity Parameter	Value	Best Estimated Flow Rate (STBPD)	Minimum Flow Rate (STBPD)	Maximum Flow Rate (STBPD)
Base Case	-4990 ft	24800	21300	28400
Base + Riser End Depth	-4985 ft		23600	28400

Roughness

The roughness of the riser pipe was unknown. I used a roughness of 0.0018 in (standard smooth pipe) for the base case. However, the riser pipe was likely rougher due to expected normal wear from use as well as the nature of the DWH incident. I performed sensitivity studies at 10 and 100 times the smooth pipe roughness and the results are reported in Table 4. The flow rate estimates were not very sensitive to riser pipe roughness.

Table 4 – Sensitivity to the roughness of riser pipe

Model/ Sensitivity Parameter	Value	Best Estimated Flow Rate (STBPD)	Minimum Flow Rate (STBPD)	Maximum Flow Rate (STBPD)
Base Case	0.0018 in	24800	21300	28400
Base + 10 times Roughness	0.018 in		26000	27200
Base + 100 times Roughness	0.18 in		24800	26000

Kink Discharge Coefficient

An additional sensitivity was performed using the Kink Model to assess the sensitivity to the discharge coefficient of the Kink valve. As noted in the main report, the Kink is modeled as a valve. Though no valve existed at this location, a valve was introduced in the model to account for the unknown resistances through the kink. The valve (resistance) was adjusted to achieve different flow rates through the riser.

The discharge coefficient of the valve affects the energy recovery through the valve. The lower the discharge coefficient, the less energy is recovered and consequently the lower the temperature exiting the kink. I performed a sensitivity over a wide range of discharge coefficients 0.5 to 1. The flow rate estimates were not very sensitive to variation of discharge coefficient.

Table 5 – Results from Kink model base case and various sensitivity studies

Model/ Sensitivity Parameter	Value	Best Estimated Flow Rate (STBPD)	Minimum Flow Rate (STBPD)	Maximum Flow Rate (STBPD)
Base + Kink Discharge Coefficient	0.5	25000	21100	26700
Base + Kink Discharge Coefficient	0.61		21900	26700
Base + Kink Discharge Coefficient	0.84		22300	28900
Base + Kink Discharge Coefficient	1.0		23400	28100

Best Estimated Flow Rate

For each sensitivity a best estimated flow rate was calculated as the average of the minimum qualifying rate and the maximum qualifying rate. The overall best estimated flow rate is calculated as the average of those averages.

Based on all the sensitivity studies, the best estimated flow rate through the Riser End is 25,100 stbpd and the range of qualifying flow rates including all the sensitivities is from 21,100 stbpd to 29,500 stbpd.

Kink Leak Flow Rate Sensitivity

The maximum estimated kink leak flow rate is 4,900 stbpd. As described in the main report, this value is considered a maximum because the kink leak was modeled conservatively. In particular, I selected an upstream pressure from PT-M that was higher than other reported values for that gauge. I relied upon measurements of the holes that were made when they were in their final state (that is, after the kinked section of the riser had been retrieved). Additionally my model includes leaks from all three leak holes for the entire period whereas the third hole did not appear until May 19. Thus, by using the hole sizes in their final state, using all three holes when only two were present until May 19, and a conservative measurement of the pressure, I calculated the maximum possible flow rate the Kink leaks during the May 13 to May 20 period.

The other variable that has an effect is the inlet temperature. I have used an inlet temperature of 105 °C.⁶ Table 6 shows the density variation with respect to the temperature above the LMRP. The leak mass flow rate will vary as the square of the density based on the simplified equations for flow through an orifice given below.

⁶ Reddy, C. M. et al., “Composition and fate of gas and oil released to the water column during the Deepwater Horizon oil spill”, 2011.

$$\dot{Q} = C \sqrt{\frac{\Delta P}{\rho}}$$

$$\dot{m} = \rho \dot{Q}$$

where,

\dot{Q} is the volume flow rate through the orifice,

C is a constant that is a function of the discharge coefficient and the area of the orifice,

ΔP is the pressure drop across the orifice,

ρ is the net fluid density, and

\dot{m} is the mass flow rate through the orifice.

Based on this relationship, even at a temperature as low as 75 °C, the increase in flow through the leaks is only 5.5% or 270 stbpd. This volume rate is insignificant in comparison to using all three holes (at their final size) for the entire period when only two holes were present until May 19.

Table 6 – Density of fluid at different temperatures and boundary pressure above LMRP

Pressure (bar)	Temperature (C)	Density (kg/m3)
192.9	105	359.385
192.9	100	365.639
192.9	95	372.102
192.9	90	378.779
192.9	85	385.681
192.9	80	392.814
192.9	75	400.189

Because my calculation is already very conservative (high), I did not perform any other sensitivity analysis on the Kink leak flow rate.

Model Uncertainty

Through the benchmarking exercise documented in Appendix B, I estimated that the model has an uncertainty in the range of 10%, or $\pm 5\%$. Adding this to the sensitivities performed here, I estimate that the total flow rate through the DWH riser from May 13 to May 20, 2010 was between 24,900 stbpd and 35,900 stbpd.

Appendix H -Slug Initiation

Introduction

After establishing the flow pattern observed at the end of the DWH riser between May 13 and May 20, 2010 was slug flow, I sought to establish the range of flow rates where slug flow was possible. Because slug flow is usually initiated by the terrain (terrain-induced slug flow) or by hydrodynamics (slugs initiated by the difference in the relative velocity of the gas to the liquid), I began my investigation by looking at these two mechanisms. This appendix describes the simulations that I performed to test if either terrain-induced or hydrodynamic slugging was the cause of the observed slug flow.

Background

After the DWH drilling rig sank on April 22, 2010, the riser that connected the DWH wellhead equipment to the drilling rig fell to the seafloor. However, the riser did not completely settle to the seafloor until May 21, 2010. Rather, a section of the riser remained buoyant, creating a loop suspended in the water (the buoyant loop, see Figure 1).¹ Between May 13 and May 20, 2010, the buoyant loop was oscillating vertically, moving between resting on the seafloor and suspended in the water. During the same period slug flow was observed at the Riser End. Taken together, it initially appeared that the riser motion and slug flow were likely linked. However, it was not obvious to me that the riser motion was the cause of the observed slug flow until later in my investigation.

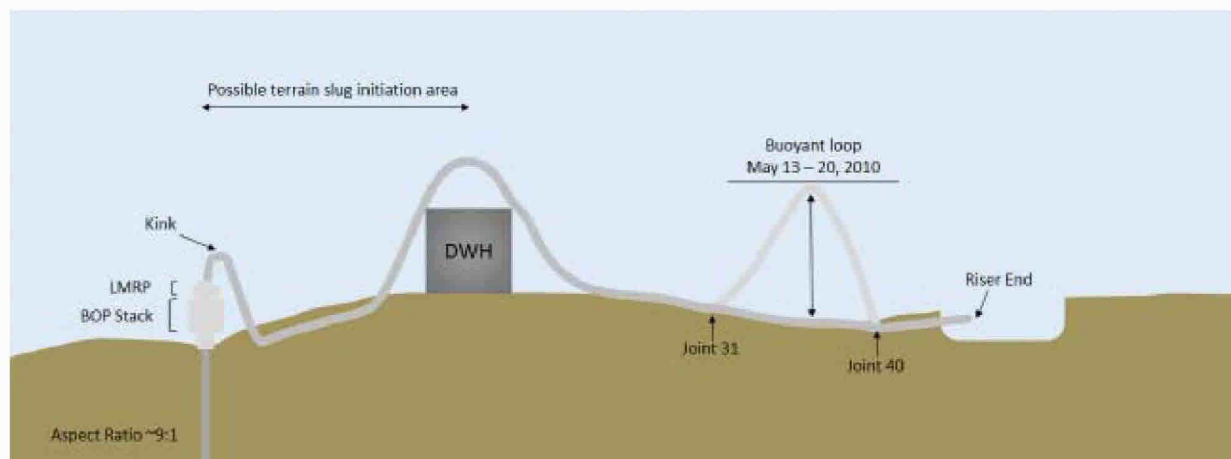


Figure 1 – Schematic of DWH riser showing possible terrain slug initiation area and the buoyant Loop

Initially, I evaluated whether the section of the riser that settled on the DWH rig was initiating terrain slugs (see Figure 1) and whether those terrain slugs were responsible for the riser motion and the observed slug flow. This analysis assumed that the riser motion was a result of slug flow (and not the cause), and therefore the early models did not include riser motion.

¹ BP-HZN-2179MDL04996577

Interpretation of Results

To evaluate the different mechanisms of slug initiation, I ran multiple simulations over a range of flow rates. In order to visualize which simulations predicted slug flow and the flow rate boundary at which slug flow no longer occurs, an OVF² (oil rate volume fraction) Bifurcation Map³ was used. On an OVF Bifurcation Map, the maximum and minimum OVF at the Riser End are plotted on the y-axis against the flow rate through the riser on the x-axis. The slugging phenomenon can be observed on the OVF Bifurcation Map in areas where the maximum OVF is greater than the minimum OVF. If, on the other hand, no slugging is present, the outlet flow rate has a steady volume fraction and therefore the minimum and maximum OVF will be the same.

As an example, Figure 2 is the OVF Bifurcation map for the No Kink model hydrodynamic slugging analysis. From this figure, it is clear that slugging can occur at flow rates less than ~22,000 stbpd, because the maximum OVF for those flow rates is greater than the minimum OVF. However, at flow rates greater than ~22,000 stbpd, the maximum OVF converges with the minimum OVF, indicating slug flow is no longer possible.

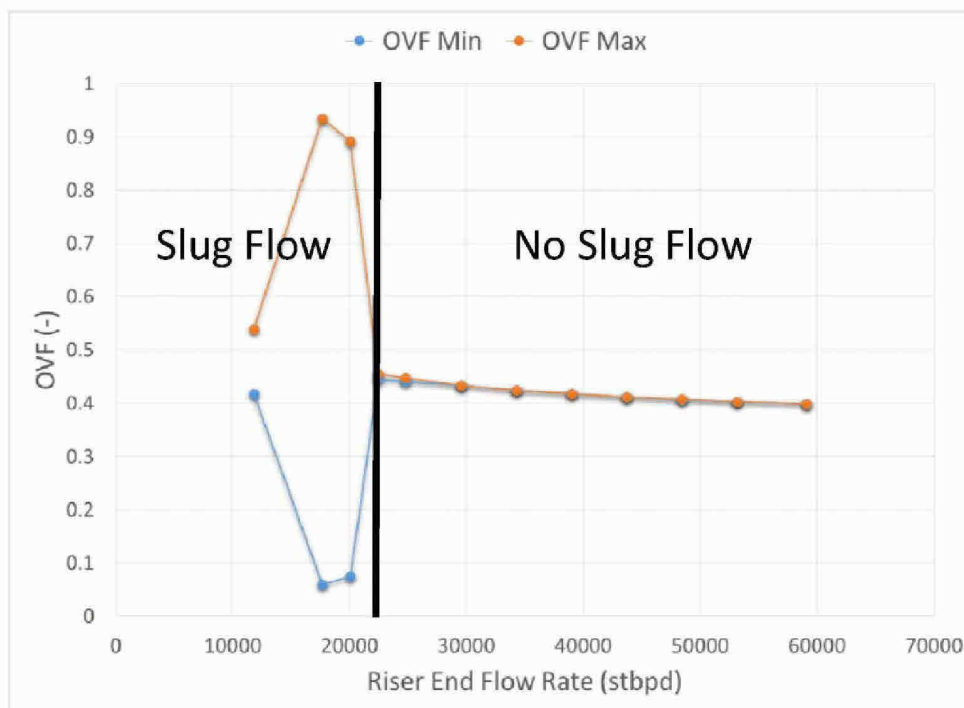


Figure 2 – An example of an OVF Bifurcation Map quickly showing where slugging exists

After I determined the range of flow rates where slug flow could occur, I investigated the slug flow characteristics in more detail. As an example, I looked at the trend of the OVF (shown in Figure 3) to see

² OVF is defined in Appendix G.

³ The OVF Bifurcation Map does not provide insight into the nature (such as duration of oil-dominated flow) or frequency of slugging; the OVF Bifurcation Map was analyzed as a starting point to narrow down the range of flow rates to investigate in more detail.

if the slugging exhibited the correct period and signature as observed in the ROV videos of the Riser End plume. In the example shown, the OVF goes through large variations (between ~ 0.15 and ~ 0.85), which would have been observed as gas and oil dominant flows. However, it is clear that these dominant flow periods do not occur with the same regularity as the dominant flows observed in the ROV video footage of the Riser End plume. Because the observed slug period displayed on the ROV videos (detailed in Appendix E) were very uniform whereas the calculated slug period (calculated as the time between two peaks in Figure 3) is much more variable. Thus, I concluded that the simulated slug period does not match the observed slug flow.

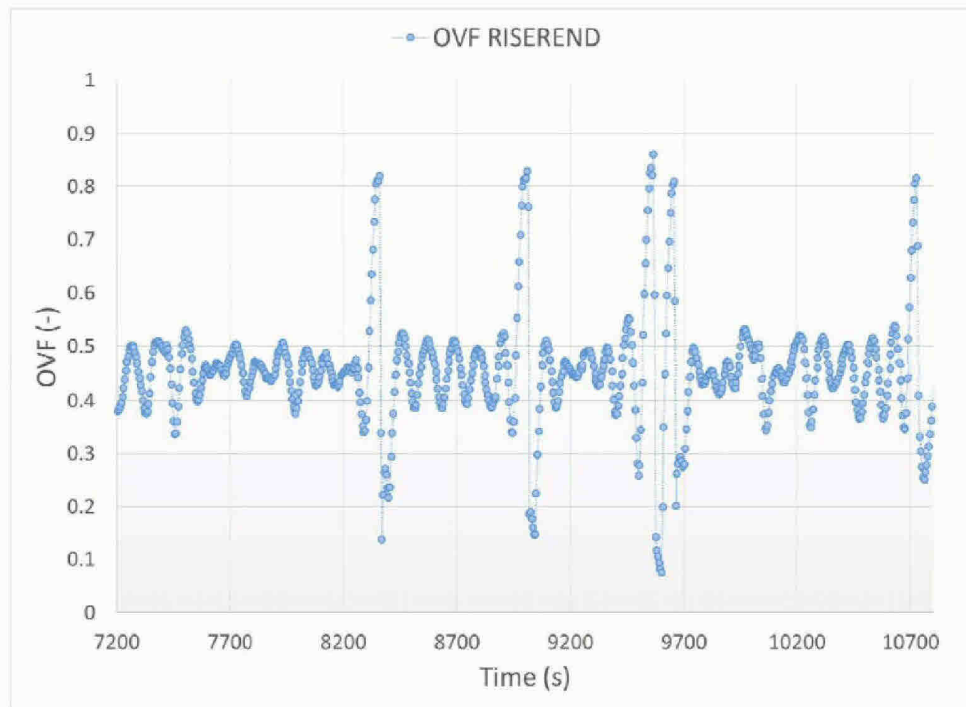


Figure 3 - Trend of OVF at the end of the riser for ~ 20000 stbpd flow rate through Riser End

Terrain Slugging

Figure 4 shows the elevation profile of the riser in its settled position as well as the peak positions based on riser surveys on May 13 and May 16. The initial “hill” in the terrain is caused by the fact that the DWH riser climbed over the DWH rig that had settled on the seafloor. The profile of the riser leading up to this hill is favorable for terrain slugs to form. Thus, I evaluated whether terrain slugs were initiated at the base of this first hill.

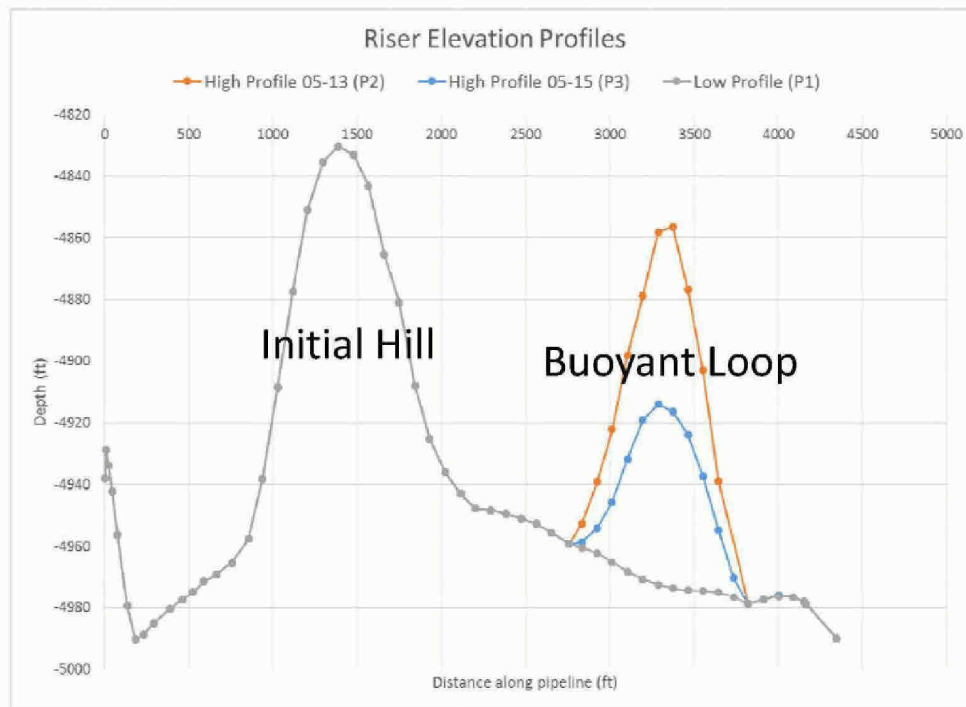


Figure 4 – Riser elevation profiles showing the buoyant loop on the sea floor (Low), and its peak position on May 13th and May 15th

Model Setup

Since the buoyant loop was not being modeled as a moving section, the terrain slugging simulations were performed using both the low profile (P1) as well as the high profile on May 13 (P2). The No-Kink model was used to investigate terrain slugging.

Simulation Matrix

Terrain slugging simulations were performed for a range of flow rates from ~800 stbpd to ~12000 stbpd. The simulations were also performed using three different inlet temperatures, namely 65 °C, 80 °C, and 95 °C. These three temperatures are the same inlet temperatures used in the sensitivity analysis of the No-Kink Model as explained in Appendix G. The simulations were performed using OLGA 5.3.2, OLGA 7.2, and LedaFlow 1.2.

Results

No terrain slugging was observable at rates above 2,500 stbpd using any of the software. Because the production rate through the RITT at certain times during May 13 to May 20 was over 2,500 stbpd, I concluded that the observed slugging from the Riser End between May 13 and May 20 could not have been terrain induced. Figure 5 through Figure 7 show the OVF bifurcation maps for terrain slugging cases.

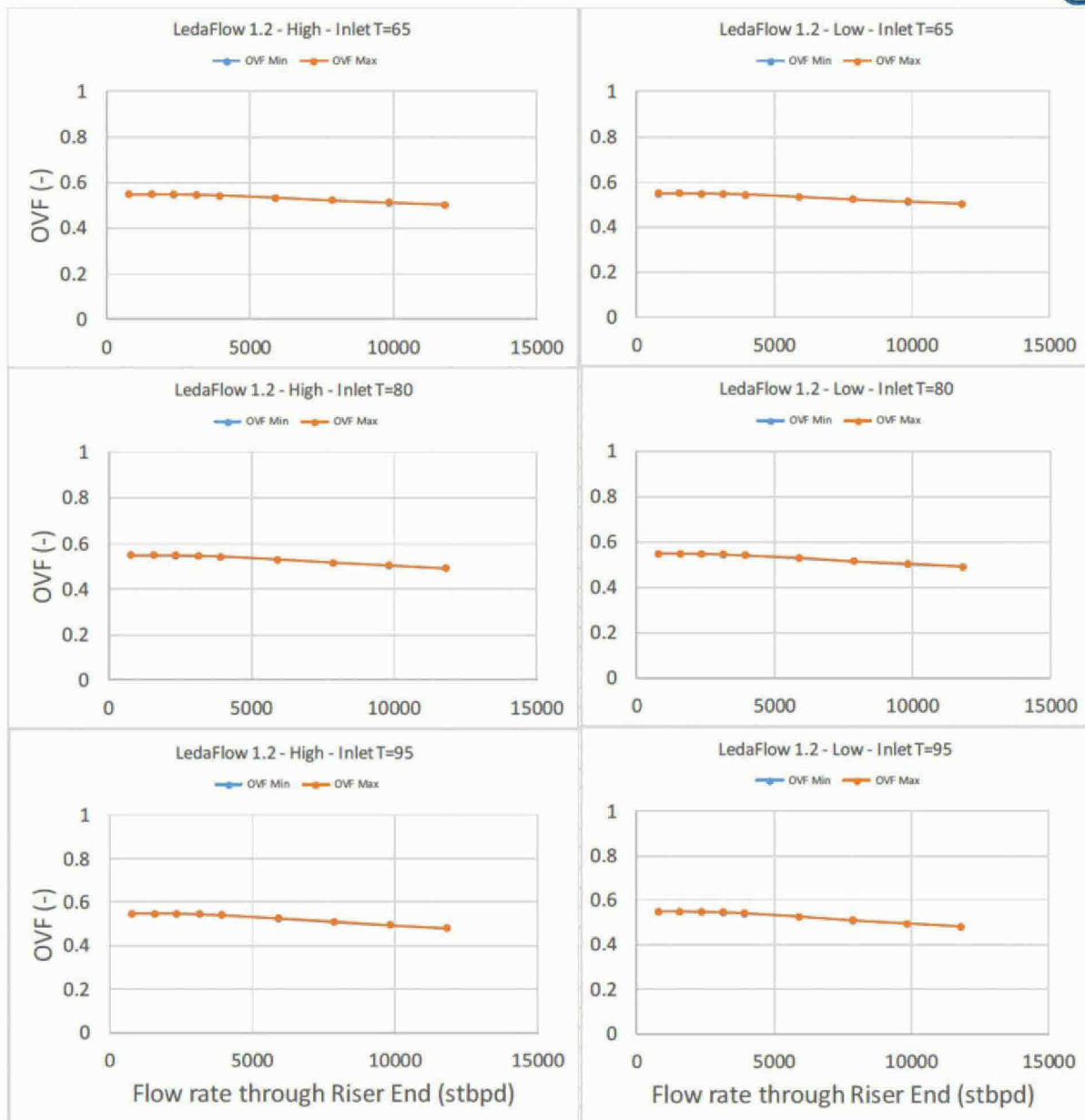


Figure 5 - OVF Bifurcation Map for LedaFlow 1.2 terrain slugging simulations all of which indicate no slug flow

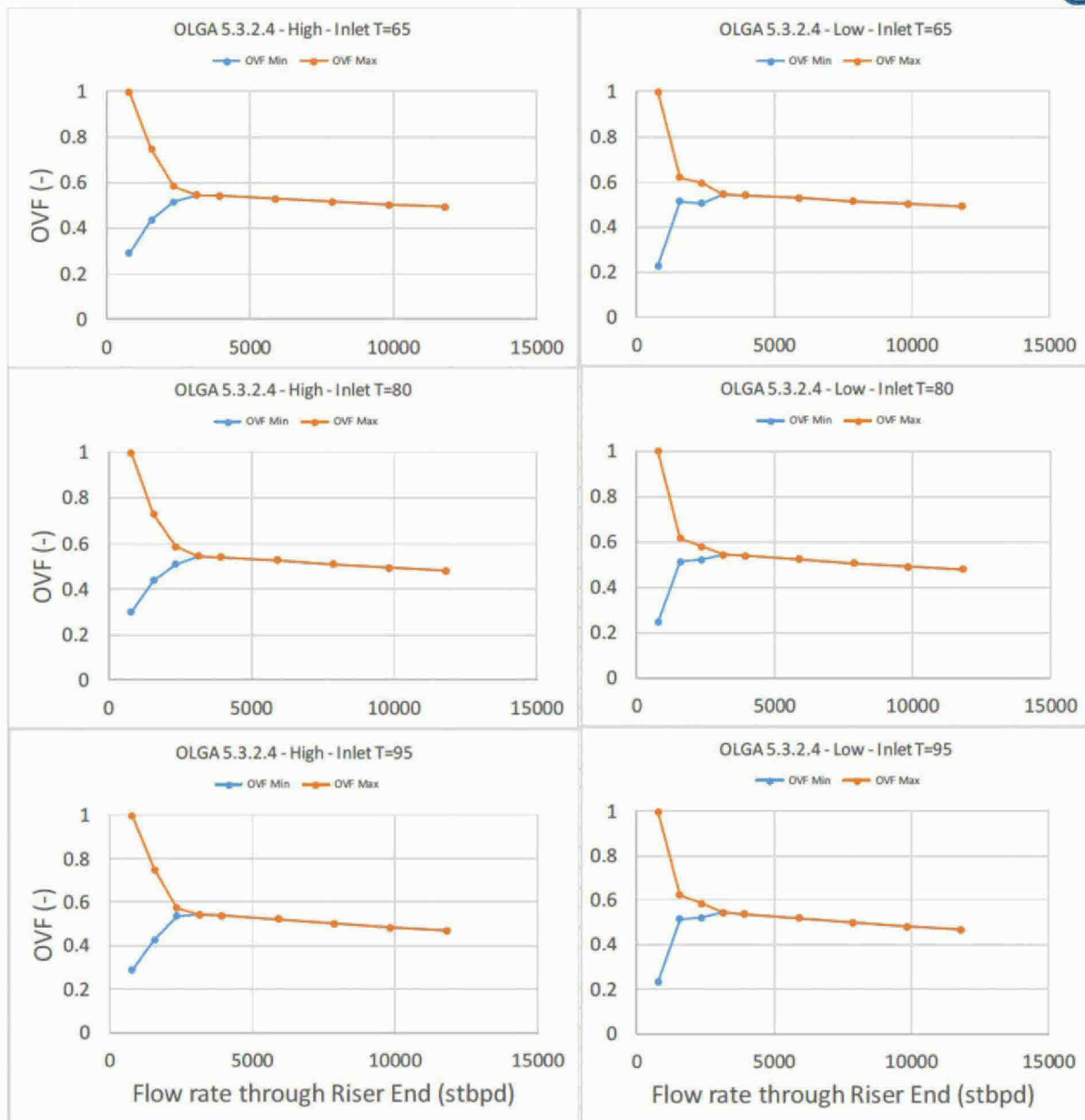


Figure 6 - OVF Bifurcation Map for OLGA 5.3.2.4 terrain slugging simulations

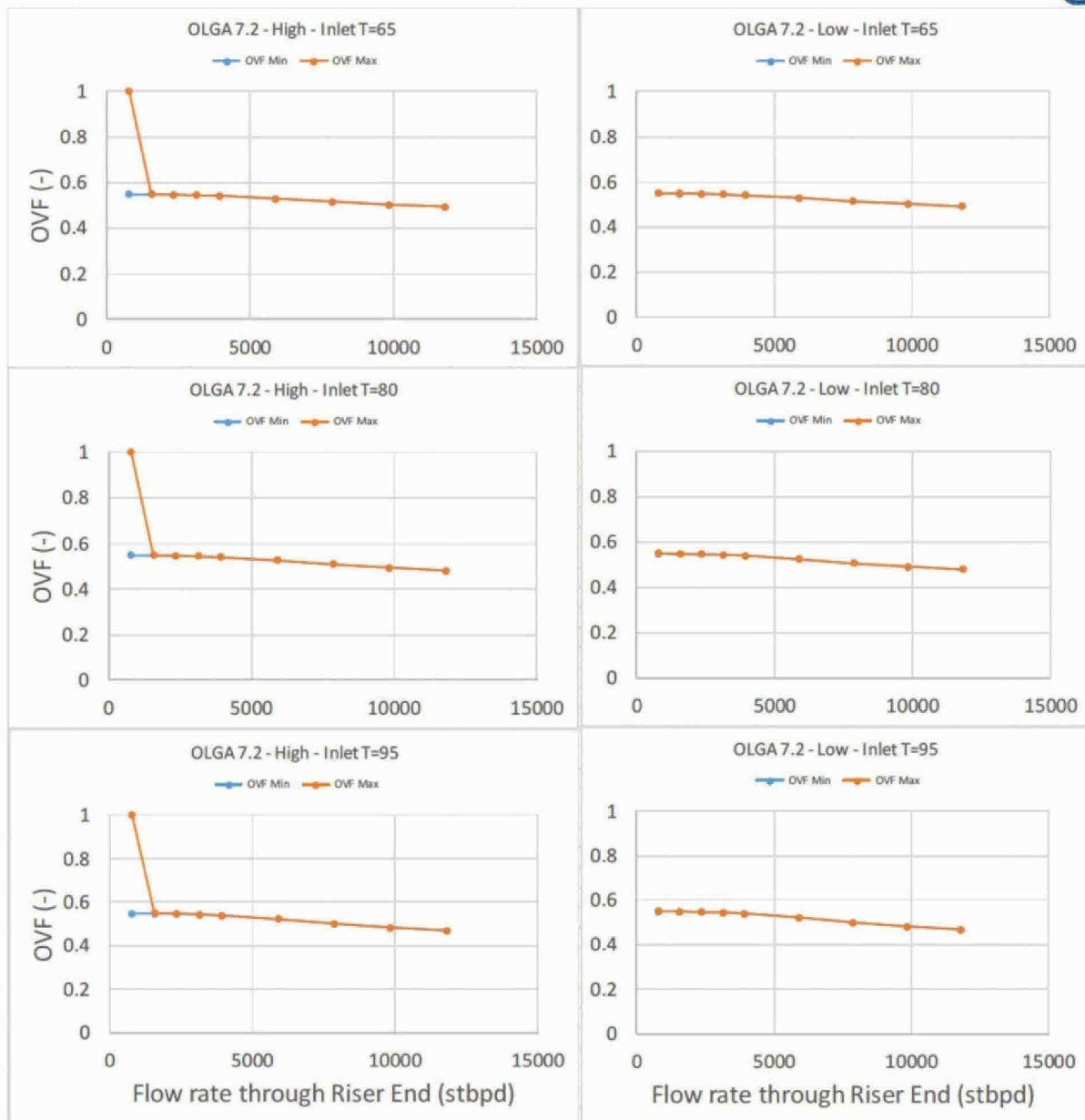


Figure 7 - OVF Bifurcation Map for OLGA 7.2 terrain slugging simulations

Hydrodynamic Slugging

Modeling Hydrodynamic Slugs

Hydrodynamic slugs form when gas flows across a wavy liquid surface⁴. As the gas rate increases, the size of the wave increases. Eventually, at higher rates of gas flow, the waves span the entire cross-sectional area of the pipe and form liquid slugs. Immediately behind these liquid slugs, gas accumulates.

⁴ Kordyban, E.S., Ranov, T., Mechanism of Slug Formation in Horizontal Two-Phase Flow, J. Fluids Eng. 92(4), 857-864 (Dec 01, 1970)

This process is called *slug formation*. Once these pockets of liquid with gas behind them, called *slug units*, are created, they are propagated through the pipeline together. This process is called *slug propagation*. In the process of a slug unit moving through the pipeline it may undergo changes as it encounters different local conditions such as the terrain and presence of other slug units.

OLGA and LedaFlow, two commercially-available software packages for transient multiphase modeling, permit the user to model slug flow but in different ways. An OLGA user can activate a module called *slug tracking* that models the physics of slug propagation, but not that of slug formation. Rather, to form slugs, OLGA requires user inputs that instruct OLGA to form a slug unit at a specified frequency.⁵ Once the slug is formed, the slug propagation model tracks the progress of the slugs as they move through the pipeline.

LedaFlow on the other hand has a module called *slug capturing* that models the physics of slug formation as well as slug propagation.⁶ In LedaFlow, however, the user merely turns the slug capturing module on or off. LedaFlow then decides, without any other user input needed, when and how to form slugs and track their propagation.⁷

Model Setup

I investigated whether or not the observed slugging between May 13 and May 20, 2010 was caused by hydrodynamic slugging using the P1 and P2 riser elevation profiles. The No-Kink model was used and the inlet flow rate was varied as the parameter in each simulation batch.

Simulation Matrix

Hydrodynamic slugging simulations were performed for a range of flow rates from 12,000 stbpd to 60,000 stbpd. The simulations were performed using an inlet temperature of 80 °C. The simulations were performed using OLGA 5.3.2, OLGA 7.2, and LedaFlow 1.2.

Results

Slug modeling using the slug tracking and slug capturing modules of OLGA and LedaFlow respectively showed that hydrodynamic slugs were able to produce discernible slugging behavior at the end of the riser. However, the slugging produced at the end of the riser based on hydrodynamic slug initiation did not have the regularity of the riser end plume as observed in ROV videos.

Figure 8 shows the OVF bifurcation maps using P1 and P2 profiles with LedaFlow 1.2, OLGA 5.3.2.4, and OLGA 7.2. LedaFlow results are more meaningful here because of its increased capability to model the physics of slug formation. Because of this, once the flow rate exceeds the point beyond which slug flow is not possible, the OVF Bifurcation Map collapses to a single line as expected.

⁵ OLGA 7.2 User Manual – Slug Tracking > Methods and Assumptions

⁶ Danielson, T.J., Bansal, K.M., Simulation of Slug Flow in Oil and Gas Pipelines Using a New Transient Simulator, Offshore Technology Conference, Houston, Texas, USA, 30 April-3 May, 2012, OTC-23353-PP

⁷ I will use the term “slug modeling” throughout the remainder of this Appendix to refer collectively to both the slug tracking feature in OLGA and the slug capturing feature in LedaFlow.

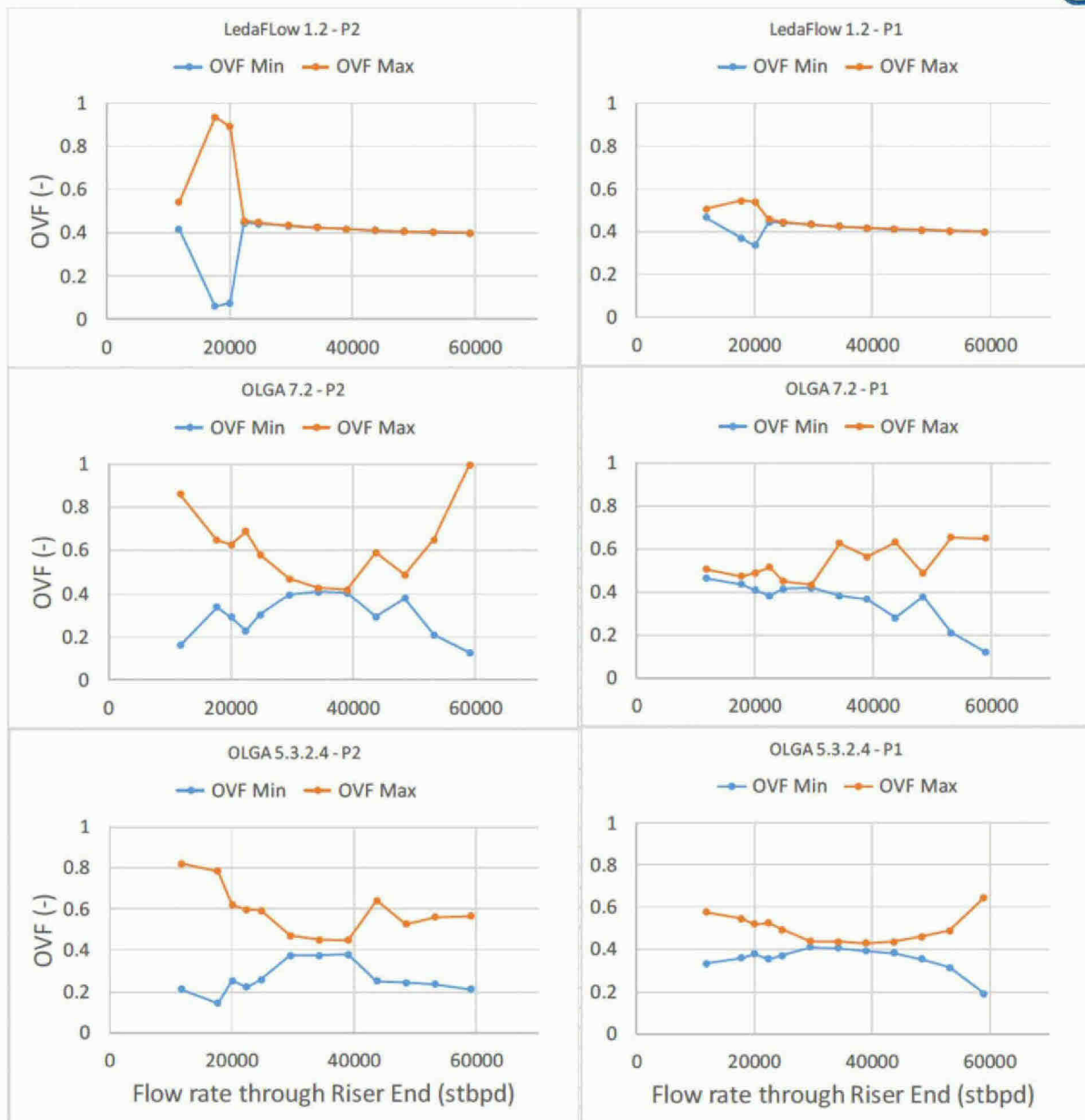


Figure 8 - OVF Bifurcation Map for hydrodynamic slug modeling using LedaFlow, OLGA 5.3.2.4, and OLGA 7.2

I further analyzed the results by calculating the time period between each successive time when the OVF goes below a value of 0.3. This is similar to using a stopwatch to calculate the time between successive gas-dominant flow periods in the ROV videos. Within a simulation the OVF goes below 0.3 several times. I calculated the period between successive excursions below 0.3 and then calculated the average and standard deviation of these periods in each simulation. I expected, if the hydrodynamic slugs were the mechanism by which the observed slugging were initiated, to see a very low standard deviation since my analysis of slug periods based on ROV footage shows very little variability. The results of this analysis are tabulated in Table 1. Empty cells indicate that the simulations did not exhibit OVF

excursions below 0.3. The most prominent feature of the values shown in the table is that the standard deviations of the slug periods are very high. The only exception is the simulation at 11,800 stbpd using OLGA 7.2 which has a standard deviation of 11. However, since these simulations used the P2 profile on May 13, I also expect the average period to be close to the period observed in the ROV footage which is over 4 minutes. Because the OLGA simulation had a period of 101 seconds this did not match the observed period.

Table 1 - Slug timing for hydrodynamic slugging simulations using the P2 profile

Flow rate (stbpd)	Profile	OLGA 5.3.2.4 Period (s)		OLGA 7.2 Period (s)		LedaFlow 1.2 Period (s)	
		Average	St. Dev.	Average	St. Dev.	Average	St. Dev.
11800	P2			101	11		
17700	P2	128	64			214	222
20100	P2	607	410			397	439
22500	P2			750	1075		
43700	P2	388	479				
53200	P2	64	37	420	1233		
59100	P2	83	141	107	261		

Conclusions

Based on my simulations, neither terrain-induced slugging nor hydrodynamic slugging were capable of producing the kind of regular slugs that were seen at the end of the DWH riser between May 13 and May 20, 2010. Terrain-induced slugging could not have caused the observed slugging because the slugs were only formed at flow rates lower than 2,500 stbpd. Because the RITT was collecting in excess of 2,500 stbpd over the period from May 16-May 20, I could eliminate terrain-induced slugging as a possible slug initiation mechanism.

Hydrodynamic slugging could not have been the cause of the slugging behavior because the slugs formed using the hydrodynamic model did not exhibit the regularity observed in the ROV videos. While I was able to measure uniform time periods between two slugs observed in the ROV videos, the modeled hydrodynamic slugs were erratic in their period and did not resemble the nature of observed slugging.